2016

Reflectance-based Calibration and Validation of the Landsat Satellite Archive

Sandeep Kumar Chittimalli

REFLECTANCE-BASED CALIBRATION AND VALIDATION OF THE LANDSAT SATELLITE ARCHIVE

BY

SANDEEP KUMAR CHITTIMALLI

A thesis submitted in partial fulfilment of the requirement for the

Master of Science

Major in Electrical Engineering

South Dakota State University

2016

REFLECTANCE-BASED CALIBRATION AND VALIDATION OF THE LANDSAT SATELLITE ARCHIVE

This thesis is approved as a creditable and independent investigation by a candidate for the Master of Science in Electrical Engineering degree and is acceptable for meeting the thesis requirements for this degree. Acceptance of this thesis does not imply that the conclusions reached by the candidate are necessarily the conclusions of the major department.

Larry Leigh
Thesis Advisor — Date

Dennis Helder, PhD
Major Advisor — Date

Steven Hietpas, PhD
Head, Electrical Engineering and Computer Science Dept. — Date

Dean, Graduate School — Date

ACKNOWLEDGEMENTS

I take this opportunity to express my deep sense of gratitude to my major advisor, Dr. Dennis Helder, who has been my driving force during this project work. This work would not have been possible without his moral support and continuous guidance. I am highly thankful to my advisor Larry Leigh, for his suggestions and constant help throughout the research work. His invaluable support and suggestions during thesis writing were of profound help in completing this thesis successfully. I would like to thank Morakot Kaewmanee for sending required MSS data on time through IAS processing system.

I would also thank Nischal Mishra, Esad Micijevic, and Obaidul Haque, currently working at USGS EROS for their continuous help in MSS data analysis.

My sincere thanks to Ashish Shrestha for building a solid base to the project. The project was the continuation of his work.

My special thanks go to Lisa Wells for her tremendous help in improving the grammar in my thesis. I would like to thank all my friends in IP lab, especially Mahesh Shrestha for his valuable suggestions and ideas for improving my thesis.

I would like to dedicate this thesis to my father Srisailam Chittimalli, mother Renuka Chittimalli, brother Shravan Kumar Chittimalli, and sister Sadhana Vuppala.

TABLE OF CONTENTS

ABBREVIATIONS

MSS	Multispectral Scanner System
RBV	Return Beam Vidicon
TM	Thematic Mapper
ETM+	Enhanced Thematic Mapper Plus
OLI	Operational Land Imaging
DCS	Data Collection System
TIRS	Thermal Infrared Sensor
FPM	Focal Plane Module
SLC	Scan Line Corrector
IC	Internal Calibrator
NIR	near Infrared
SWIR	Short Wave Infrared
PICS	Pseudo Invariant Calibration Site
TOA	Top of Atmosphere
DN	Digital Number
LUT	Look-Up Table
RSR	Relative Spectral Response
BRDF	Bidirectional Reflectance Distribution Function
ROI	Region of Interest
USGS	United States Geological Survey
ERTS	Earth Resources Technology Satellite
SBRC	Santa Barbara Research Center

LIST OF FIGURES

LIST OF TABLES

ABSTRACT

REFLECTANCE-BASED CALIBRATION AND VALIDATION OF THE LANDSAT SATELLITE ARCHIVE

SANDEEP KUMAR CHITTIMALLI

2016

The primary objective of this project was to consistently calibrate the entire Landsat series to a common reflectance scale by performing cross-calibration corrections from Landsat-8 OLI to Landsat-1 MSS. A consistent radiance-based calibration was already performed from Landsat-8 OLI through Landsat-1 MSS using bright targets and dark targets. The MSS radiance-based calibration results showed an uncertainty of about ±5%. Typically to convert from radiance to reflectance a solar model is used. Unfortunately, there are numerous solar models, all with various levels of accuracies. It was also seen that there is a data format inconsistency for different types of MSS data that impact the radiometric uncertainty of the products when compared to Landsat-8 OLI data. One of the advances Landsat-8 OLI has over to earlier missions is a solar model independent reflectance calibration. Hence, to reduce these uncertainties and remove the dependency on the solar model, direct reflectance-based calibration was performed for all previous missions using Landsat-8 OLI as the "standard".

A consistent cross-calibration of all Landsat sensors was achieved using coincident/near-coincident scene pairs. The work started from cross-calibration of Landsat-8 OLI to Landsat-7 ETM+ and continued through Landsat-1 MSS. Due to the fact each Landsat sensor measures slightly different parts of the electromagnetic spectrum, a spectral band adjustment factor (SBAF) was computed and used prior to the cross-calibration. To determine the significance of the bias derived from cross-calibration, a t-test was performed with a null hypothesis that the bias equals zero at a confidence interval of 95%. From the final calibration equations, it was found that for band 5 of Landsat-1 bias is significant. The effectiveness of these cross-calibration results is discussed by showing a significant improvement in the

observed inconsistencies in the absolute calibration of all Landsat sensors for both bright and dark targets. The results show a significant improvement in reflectance calibration, and an overall uncertainty of less than ±3%.

Chapter 1 Introduction

Remote sensing is the process of acquiring information about an object without making physical contact with it [1]. It involves the measurement of radiation of different wavelengths that are reflected from distant objects or materials. In general, Remote Sensors can be used to obtain particular information about an object, for example, the diameter of a cottonwood tree's crown and shape. The idea of looking down at the Earth's surface was introduced in the 1840s when images were taken from cameras secured to tethered balloons or observation balloons, which became famous during the American Civil War and French Revolutionary War. Observation balloons were used for intelligence gathering and topographic mapping of an area. The electromagnetic radiation (EMR) reflected or backscattered from the geographic area is observed by the sensor; this electromagnetic energy measurement must be calibrated and converted into information using visual or digital image processing techniques. Generally, continuous observation of the Earth's surface using remotely sensed data gives a temporal sequence of images that enables the scientific community to study global environmental changes, industrial growth, land surface use, and land mapping, etc.[2]. Many studies have suggested that monitoring short-term changes of a single generation of remote sensing satellite instrumentation is sufficient, but long-term monitoring requires measurements from successive generations of instrumentation (i.e. Landsat series) [3]. However, to be comparable, each generation of remotely sensed data must be persistently scaled to a consistent-calibration. In other words, a satellite should be continuously calibrated over its lifetime, and each subsequent satellite must have a cross-calibration. The quality and accuracy of the calibrated data are very important. Therefore, before the images from these satellite sensors can be used, each pixel must be consistently calibrated, and data from all pertinent sensors (i.e. Landsat series) must be conformed to a common radiometric scale.

1.1 Landsat Background and History

Landsat series of satellites provides the longest continuous record of remotely sensed-based observation data [4]. Landsat is an invaluable resource for monitoring global variation, and it is a primary source of medium spatial resolution for earth observations. In the mid-1960s, fortified by U.S. achievements in a planetary investigation, unmanned remote-detecting satellites were introduced. Thereafter, scientific groups in NASA and the National Aeronautics set forth to create and launch the first Earth-monitoring satellite. Their objective was accomplished on July 23, 1972, with the launch of Landsat-1 MSS, which was initially named Earth Resources Technology Satellite (ERTS) [5]. Later in 1975 ERTS was renamed Landsat-1 MSS. The second spacecraft in the Landsat series (Landsat-2 MSS) was launched on January 22, 1975. Subsequently, Landsat-3 MSS was launched on March 5, 1978. Henceforth, the Landsat series was declared operational [3].

Landsat satellites are arranged into three categories in terms of varying sensor designs. The first category is derived from the multispectral Scanner (MSS) sensors, all of which have similar onboard sensors with the same fundamental design. Landsat 1-3 are comprised of an MSS sensor and the Return Beam Vidicon (RBV) camera as payloads [5].

The second group includes satellites like Landsat-4 and Landsat-5, which carried the Thematic Mapper (TM) sensor and the MSS on the same spacecraft [6]. Everything was automated and computerized in this period; faster and more reliable processing systems were used. The MSS sensor was included to provide a radiometric basis to compare data with the preceding Landsat missions. Landsat-4 TM was launched on July 16, 1982, and Landsat-5 TM was launched on March 1, 1984. Landsat-5 TM was the longest satellite in operation; it was decommissioned on June 5, 2013, after serving 29 years in space. TM data from these satellites was rapidly utilized since the information was improved in spatial, radiometric, and geometric accuracy compared to the data acquired from the MSS sensor.

Finally, the third category includes Landsat-6 and Landsat-7, which used the Enhanced Thematic Mapper (ETM) and the Enhanced Thematic Mapper Plus (ETM+) sensors, separately. No MSS sensors were placed on either Landsat-6 or Landsat-7. Landsat-6 failed to reach the orbit [6]. The Landsat-7 ETM+ sensor has a spatial resolution of 30 meters (same as TM) for six bands, and 60 meters for the thermal band. ETM+ also includes a panchromatic band with a 15-meter spatial resolution. Landsat-7 ETM+ has a 378 gigabit Solid State Recorder that can hold 42 min (roughly 100 scenes) of sensor data and 29 hours of housekeeping telemetry simultaneously [7]. The latest satellite, Landsat-8, carries two sensors, the Operational Land Imager (OLI) and Thermal Infrared Sensor (TIRS). Unlike other Landsat sensors, OLI has two new bands: Coastal band and Cirrus band. At the time of this writing, there will be a Landsat image of the same target on the earth from Landsat-8 OLI and Landsat 7 ETM+ every eight days. Below, Figure 1.1 shows the time scale for Landsat missions.

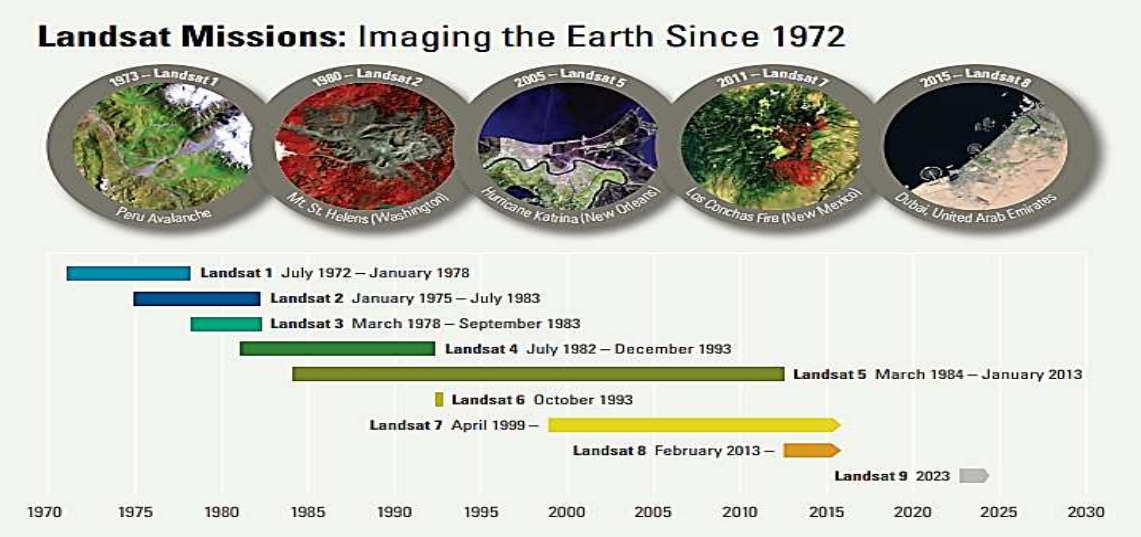

Figure 1.1. Time–scale of Landsat instrument technology introduction (Image credits: USGS).

1.2 Application of Landsat data in remote sensing field

Landsat data is used by commercial, government, industrial, civilian, military, and educational communities throughout the world. The data support a wide range of applications in areas such as agriculture, global change research, forestry, resource management, mapping, geography, water quality, and coastal studies. Furthermore, Landsat data has become a valuable resource to decision-

makers in fields such as forestry, agriculture, land-usage, and water resources. A complete Landsat archive has been documented and is maintained by the U.S. Geographical Survey (USGS) Earth Resources Observation and Science (EROS) Center. This archive holds 40 years of the Earth's surface. Clients, researchers, and scientists can access Landsat information through the Earth Explorer (EE) 3 or Global Visualization Viewer (GloVis) 4 websites.

1.3 Landsat-1 to Landsat-3 (MSS, RBV)

The sensors on-board Landsat 1-3 were the Multispectral Scanner (MSS) and Radio Beam Vidicon (RBV) as shown in Figure 1.2. Landsat-1 MSS was a whiskbroom scanner—a unidirectional operation that had scanning mirror, filters, detectors, and double reflector type telescope, and was built by Santa Barbara Research Center (SBRC).

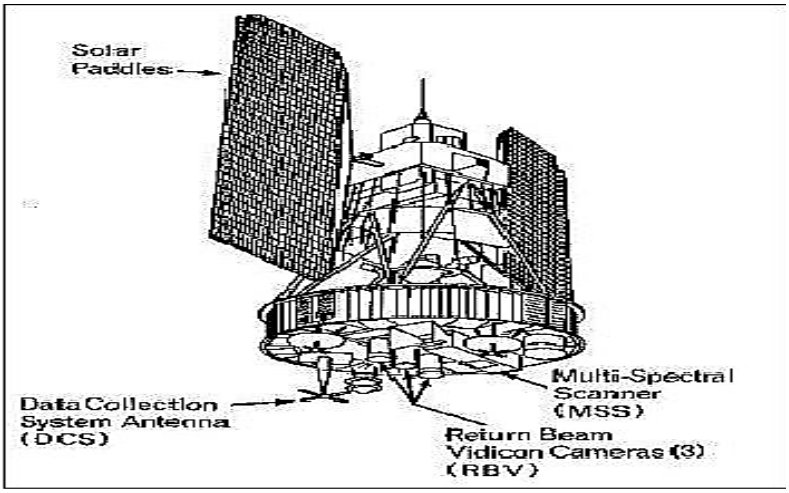

Figure 1.2. Landsat1/ERTS spacecraft [5].

The MSS has four bands as shown below in Table 1.1.

Table 1.1. Spectral Bands for Multispectral Sensor [7].

Landsat-1 through Landsat-3	**Landsat-4 and Landsat-5**	**Wavelength in μm**
band 4	band 1	0.5 – 0.6 (green) (PMT)
band 5	band 2	0.6 – 0.7 (red) (PMT)
band 6	band 3	0.7 – 0.8 (NIR1) (PMT)
band 7	band 4	0.8 – 1.1 (NIR2) (Si photodiodes)

The MSS sensor on Landsat-3 also had an extra band with a thermal infrared wavelength range from 10.4 μm to 12.6 μm, which was called band 8.

1.3.1 Scanning pattern of MSS

The MSS uses a line-scanning device, which consists of an oscillating mirror that scans continuously perpendicular to the spacecraft velocity. For MSS, six lines are scanned at the same time in each of the four spectral bands for each mirror sweep as shown in Figure 1.3. However, for Landsat 3, two detectors are used to scan in a fifth band of the MSS. The line array of six detectors was positioned in the along-track direction, thus providing parallel along-track coverage of about 480 m in one cross-track scan. Satellite motion provides the progression of the scan lines. Then, radiation is sent serially from the detectors to ground stations or sometimes stored with on-board recorders.

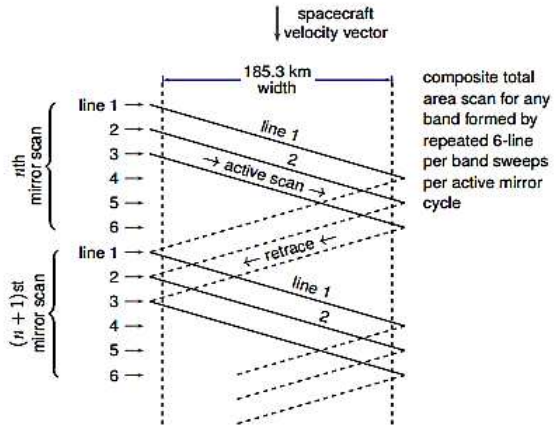

Figure 1.3. MSS active scan pattern with respect to the direction of flight [8].

The scanning system design is a whiskbroom scanner. The instrument used an oscillating mirror at a frequency rate of 13.6 Hz(74 millisecond period) that scans light reflected from the earth's surface through a ground-pointed telescope (22.9 cm diameter) where the focal length (f) is 0.82 meters. Each oscillation cycle took 33 milliseconds and had an angular displacement of ±2.89 degrees from nadir to satellite orbital track. The mirror along the track covered 11.56 degrees in a scan Angular Field of View (AFOV). This created a view of 185km (115 miles) across the orbital track from an altitude of 917km (570 miles) [8].

1.3.2 Internal calibration for band-4 to band-7 and extraction of calibration wedges

One of the two tungsten lamps, with known output radiance, was used to calibrate the detectors during every second retrace period of the scan mirror. During the retrace scan, a shutter wheel blocked the earth surface view from the optical fibers (folding mirror), and then the calibration lamp was projected into the optical fibers through a neutral density filter (NDF) which is on the shutter wheel. The shutter wheel rotated once for every two-scan mirror cycles. It produced a calibration wedge as shown in Figure 1.4. A multiplexer was included in the MSS system. The data was multiplexed with respect to time and then converted to a pulse-code modulated (PCM) signal by an analog-to-digital (A/D) converter. The data was transmitted (2229.5 MHz) directly to an acquisition station.

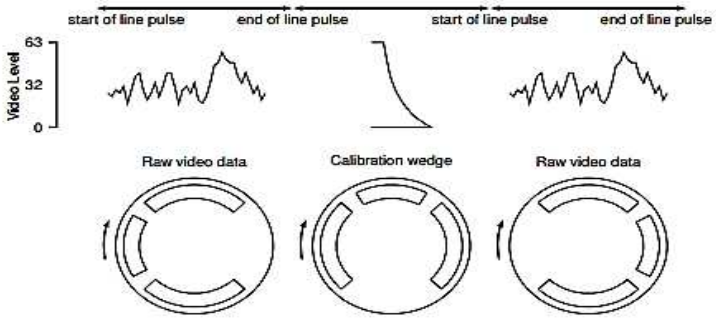

Figure 1.4. MSS video and wedge Level Timing Sequence [8].

1.3.3 MSS data formats

Because the technology was not fully developed when MSS sensors were in operation, devices lacked sufficient storage, and different data formats were used to compensate for this shortcoming. At present, MSS data at USGS EROS were archived into three different formats: MSS-X, MSS-P, and MSS-A. MSS-X data were archived from the launch of the first Landsat satellite until 1979. During this time interval, the USGS archive has MSS data from Landsat-1 to Landsat-3 [3]. The full Cal wedge was processed and stored in the MSS-X WBVT, but only six samples from the wedge are available in MSS CCT-X and MSS-A data.

MSS-X

Most of the MSS-X data format, which was collected from 1972 to 1976, is from Landsat-1 MSS and, to a lesser extent, for scenes from Landsat 2 and Landsat 3 until January 1979. These data were

divided into an MSS-X GSFC format and an MSS-X WBVT format. The main difference between these two formats, excluding the sensor, was that band-4 of the MSS-X GSFC format was not calibrated post-launch, but band 4 of the WBVT format was calibrated post-launch [8].

MSS-X WBVT

MSS-X WBVT retained the full calibration wedge. This allowed the format to characterize the calibration wedge from the historical calibration. This also provided a more accurate and precise method to calculate gains and biases [9].

MSS-X CCT-X

Bands 1-3 of the MSS CCT-X had calibration already performed, but Band-4 of the CCT-X data was never calibrated. MSS CCT-X image data is available in a band sequential format with calibration data, and they are stored in a separate file, which is called the calibration data record.

MSS-P

MSS-P data is available from January 1979 through May 1981 for MSS 2-3. Data archived in this period was the in MSS-P format. This is the only data that is both radiometrically and geometrically corrected. In recent years, the calibration information of MSS-P was lost and further processing became very difficult.

MSS-A

MSS-A data was available from 1981 onward, and all MSS data from this period were archived in this MSS-A format. The data format from Landsat-4 MSS and Landsat-5 MSS and some of the Landsat-2 MSS and Landsat-3 MSS data has MSS-A format.

MSS-X Orphans

This data had no historical calibration files, and there are no records to know how the data is calibrated. Thus, most of the data have stripes, and in some images, the data cannot be seen. The stripes are not aligned in the same direction.

1.4 Landsat-4 TM and Landsat-5 TM

The Landsat-4 and 5 TM instruments are whiskbroom scanning-based electro-mechanical-optical sensors. The scan mirror in the TM sweeps the detector across the Earth's surface from east to west

and back again, while orbital motion provided the north-to-south dimensions. The Scan Line Corrector (SLC) corrects the scan for orbital motion, which essentially produces scans that are parallel with each other. A single TM scene consists of 384 scans and is acquired in approximately 24 seconds. In TM, the mirror rotates so that the detector collects data in a line, which is perpendicular to the motion of the satellite. The scan mirror directs the signal through a telescope and sends it onto the detector as shown in Figure 1.4.1. The detector creates a weak electric signal that is amplified, sampled and recorded as bits. Then, the signal is sent or transmitted to ground stations to produce an image.

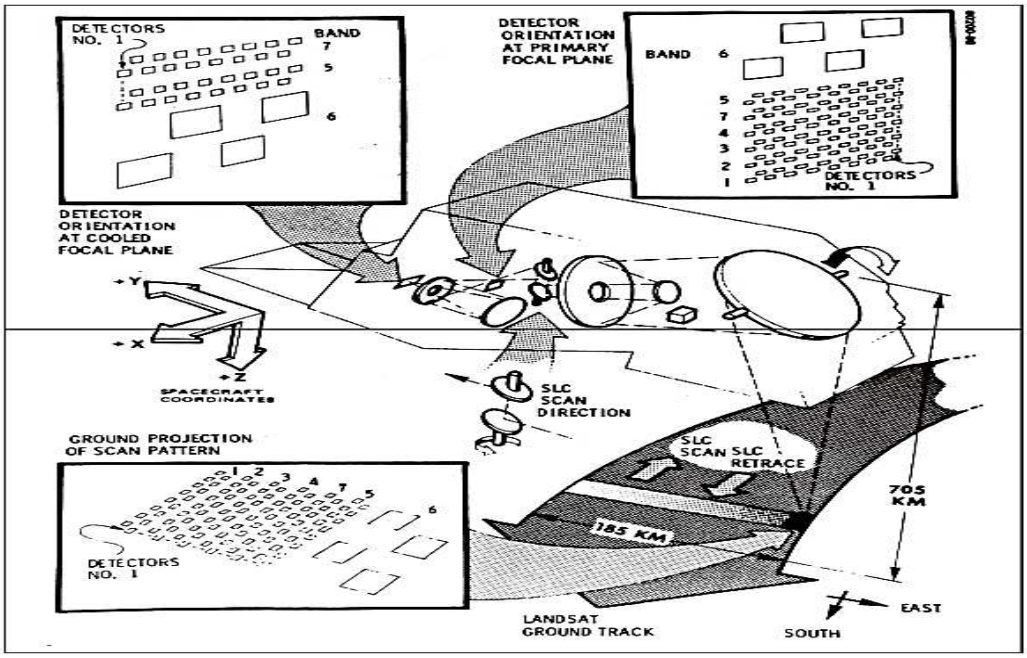

Figure 1.4.1. Landsat TM detector orientation relative to ground track [10].

Both Landsat-4 TM and Landsat-5 TM were placed at an inclination of 98 degrees and in a sun-synchronous orbit, and provide repeat coverage every 16 days [10]. Unlike the 24-detector MSS instrument, TM had 96 detectors with 16 for each band; the mirror scan produced 16 lines at once, but only four for the thermal band. It has seven spectral bands and they are Blue, Green, Red, NIR, SWIR1, Thermal, and SWIR2, which range from 0.45-12.5 μm as shown in Table 1.4.1.

Each band consists of 16 photodiode detectors where Bands 1-4 are silicon-based detectors,

and, bands 5 and 7 are indium antimonide (INSB) detectors. The sixth band had an array of four mercury cadmium telluride (HgCdTe) detectors.

Table 1.4.1. Wavelength of spectral bands and spatial resolution for TM sensor [7].

Band	**Spectral Range**
Blue	0.45-0.52 μm
Green	0.52-0.60 μm
Red	0.63-0.69 μm
NIR	0.76-0.90 μm
SWIR1	1.55-1.75 μm
Thermal	10.5-12.5 μm
SWIR2	2.05-2.35 μm

1.5 Landsat-7 (ETM+)

The main instrument on board Landsat-7 is the Enhanced Thematic Mapper Plus (ETM+). Landsat-7 also carries a Thermal Infrared Sensor (TIRS). This design offered several enhancements over Landsat-4 and Landsat-5 Thematic mappers. Landsat-7 was launched on April 15, 1999, and it is the seventh satellite of the Landsat program. The wavelengths of each band are shown in below Table 1.5.1.

Table 1.5.1. Wavelength of spectral bands and spatial resolution for ETM+ sensor [11].

Band	**Spectral Range**
Blue	0.45 - 0.52 μm
Green	0.52 - 0.60 μm
Red	0.63 - 0.69 μm
Near Infrared	0.77 - 0.90 μm
Short-wave Infrared	1.55 - 1.75 μm
Thermal Infrared	10.40 - 12.50 μm
Short-wave Infrared	2.09 - 2.35 μm
Panchromatic	0.52 - 0.90 μm

ETM+ contained a scan mirror and a scan line correction (SLC) assembly [11]. The SLC consists of a pair of small mirrors that rotate about an axis in a direction tandem with the motion of the scan mirror. The ETM+ uses two focal planes as shown in Figure 1.5.1. The Primary Focal Plane uses silicon photodiode material and detects radiation for Bands 1-8. The Cold Focal Plane uses InSb and HgCdTe detectors. Along with this, it has three on-board calibration devices. They include an

internal calibrator (IC), which consists of two lamps, a shutter, and a black body. Along with this, it has a full aperture solar calibrator, which is similar to a white painted diffuser panel, with a partial aperture solar calibrator, which serves to image the sun through small holes.

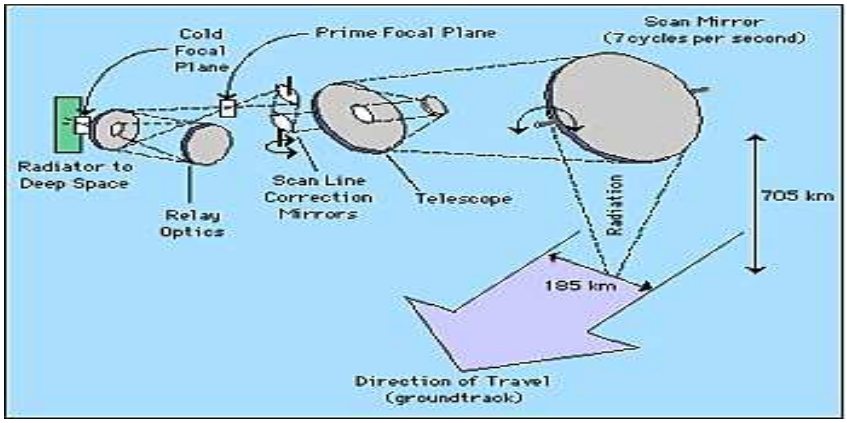

Figure 1.5.1. ETM+ Optical Path [11].

1.6 Landsat-8 (OLI,TIRS)

Landsat-8 is the most recent spacecraft, which was launched into orbit on February 11th, 2013. As Landsat-8 was being designed, scientists formed the notion that new focal plane technology might allow a new class of enhanced and improved instruments to meet the needs of the Landsat community. NASA launched Earth Observing 1 (EO-1), which carried the Advanced Land Imager (ALI), in 2000, and it proved to be a successful implementation of push broom architecture [12]. Thus, the OLI design is based on ALI architecture. Therefore, the OLI has nine spectral bands in the visible and shortwave infrared spectrum region. The TIRS measures two longwave infrared bands as shown in Table 1.6.1. Each multispectral band again has 494 detectors for each module. However, for the Pan Band, the number is doubled. The Landsat-8 spacecraft carries the Operational Land Imager (OLI) and Thermal Infrared Sensor (TIRS). The design of these two is significantly different when compared to other sensors. This instrument has the ability to look off-nadir, turn to look at the sun via a diffuser panal, and image the Moon. Landsat-8 is providing more than 700 scenes on a daily basis, each covering 185 km by 180 km on the ground [11].

Table 1.6.1. Spectral ranges of the OLI and TIRS [12].

Bands	**Wavelength (μm)**
Coastal aerosol	0.43 - 0.45
Blue	0.45 - 0.51
Green	0.53 - 0.59
Red	0.64 - 0.67
Near Infrared (NIR)	0.85 - 0.88
SWIR 1	1.57 - 1.65
SWIR 2	2.11 - 2.29
Panchromatic	0.50 - 0.68
Cirrus	1.36 - 1.38
Thermal Infrared (TIRS) 1	10.60 - 11.19
Thermal Infrared (TIRS) 2	11.50 - 12.51

The system has a push broom architecture that depends on 14 individual overlapping Focal Plane Modules (FPM) to cover the swath width. Each FPM includes nine rows of detectors, one for each band, with the intervention of filters that will provide spectral separation. The complete focal plane array (FPA) is designed so that it allows OLI's focus to be adjusted on-orbit if it is required. The focal plane array is cooled to <200K using a heat pipe that is connected to a radiator. Each FPM consists of a silicon photodiode array and an HgCdTe array that was placed on each readout chip. The focal plane digitizes the signal to 14 bits. However, due to data rate limitations, only 12 bits are sent to the ground which is the most significant of the 14 bits. This design does not require any SLC, which failed in the previous Landsat. The architecture for OLI is shown in Figure 1.6.1.

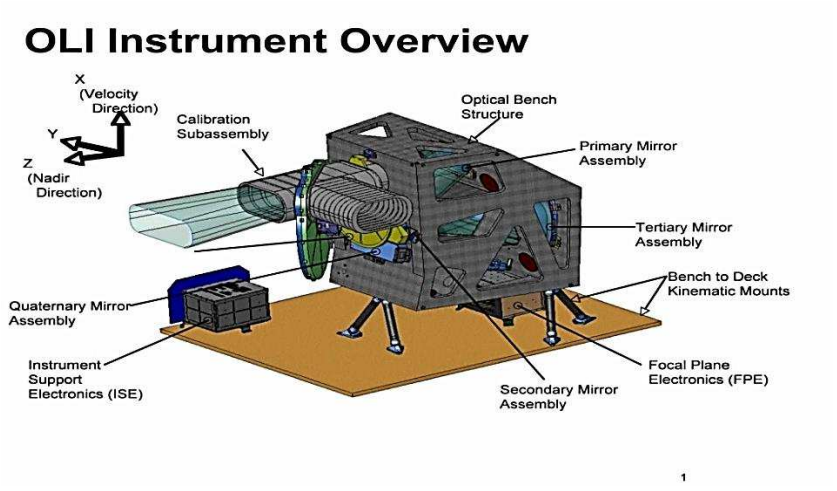

Figure 1.6.1. OLI architecture [12].

1.7 Methods of Calibration

In order to use this Landsat data record, different calibration techniques are required to ensure that data is consistent and not affected by any artifacts. The main objective of radiometric calibration is for getting good remote sensing data to create high-quality science data [13]. Sensors can be characterized by two methods: pre-launch and post-launch calibration. Pre-launch calibration is done in the lab before launching the spacecraft into space to ensure that everything works properly. Post-launch calibration is performed after launching the vehicle into space. The earlier radiometric analyses of Landsats were accomplished via many different calibration techniques.

1.7.1 Absolute Calibration

To make quantitative measurements, which represent the actual energy reflected from various targets, for comparative purposes, absolute calibration is used. Absolute calibration is required to relate the absolute value of the recorded signal strength to the actual amount of energy. To perform an absolute calibration, the voltage or digital output of a sensor for a given input radiance must be known; the design of optics between the illumination source and the sensor also must be known. This requires modeling the characteristics of the optics and electronics of the sensors [14].

1.7.2 Pre-Launch Calibration

Pre-launch calibration is done prior to the launch of the spacecraft to make sure everything is fine. Testing in the lab will be verified in multiple stages to ensure the integrity of the performance at the subsystem level. The integrating sphere used for calibration has enough brightness to measure the sensors full dynamics ranges in all bands. For example, the integrator sphere method calibration technique was applied to Landsat-8 OLI before its launch [15]. Pre-launch calibration also helps to understand any behavior or features that can appear in the orbit data.

1.7.3 Post-Launch Calibration

Post-launch calibration is generally done after the launch of satellites to check the sensor performance. The characteristics of the sensors and filters may change due to numerous reasons [16]. After launch, the sensor will be in a new environment, which may degrade its performance. Additionally, sensors

naturally degrade over time due to aging from ongoing use. Post-launch calibration includes many different techniques like Cross-Calibration, Vicarious, On-board, etc.

1.7.4 Vicarious Calibration

Over the past 20 years, vicarious calibration has become widely used. It is a technique that makes use of natural sites on the surface of the earth. The energy reflected from the ground surface is measured empirically using an accurate radiometer like Analytical Spectral Device ASD. The measured radiance is then propagated to the top of the atmosphere using an atmospheric radiative transfer model like MODTRAN. Vicarious calibration is done generally on a clear sky day.

On-Board Calibration

For on-board radiometric calibrations, many methods have been developed. On-board black bodies are also used to calibrate the thermal bands of sensors. Most sensors have a feature for post-launch checks of spectral and geometric sensor characteristics. The radiometric reference targets sometimes include the sun and moon (i.e. OLI uses the moon Measurements taken from these on-board calibrators allow radiometric gains to be calculated which can be applied to sensed data. However, sometimes degradation of on-board calibrators limits the calibration accuracy.

1.7.5 Cross-Calibration

Cross-calibration is one of the methods in vicarious calibration where the calibration of a well-calibrated sensor is transferred to another. Cross-Calibration is one of the best methods for calibrating remote sensing satellites because it is cheap, fast, and very accurate. For cross-calibration, the target can be any invariant site, like PICS. In this method, two sensors are placed in the axis of the coordinate system where calibration accuracy of the best sensor is transferred to another. This method does not require costly instruments like vicarious calibration, nor does it require atmospheric corrections. The equation (1), which transforms the response of one sensor (X) of another sensor (Y). The linear equation estimates gain and bias of the sensor.

$$\mathrm{LTOA,Y} = \mathrm{G} \cdot \mathrm{LTOA,X} + \mathrm{B} \quad (1)$$

Where: G = Sensor Gain, B = Sensor Bias.

Chapter 2 Literature review

Many articles on Landsat systematic calibrations have been published. Different calibration techniques were involved in bringing all 40-years Landsat data onto a common radiometric scale [32]. Pre-launch, post-launch, on-board, vicarious, cross-cal, and absolute-cal techniques play a vital role in the calibration of remote sensing satellites. Many of the previous calibration techniques have been based on considering only bright targets like the Sonoran Desert, Algodones Dunes, etc. The following chapter explains how consistent radiometric calibration was obtained previously from Landsat-8 OLI to Landsat-1 MSS.

2.1 Calibration of Landsat-7 ETM+

Landsat -7 ETM+ has been continuously monitored using onboard calibration devices, vicarious calibration, and PICS. ETM+ is fairly stable when compared to previous missions. PICS sites were used to detect long-term changes in Landsat-7 ETM+. An independent study using PICS sites [17] showed sub 2% for the first 10 years of life. The requirement of the ETM+ on absolute calibration was ±5%. Comparisons with different calibration techniques, and also using internal calibration of the ETM+ (i.e. solar diffusers) showed 4% or better overall and 2% in the longer wavelengths. The vicarious calibrations also showed the differences are less than 3%. However, vicarious measurement results by SDSU were slightly different in longer wavelengths [32]. All the results for ETM+ were consistent and radiometric calibration uncertainty was 5% or less, in some bands as good as 3%. In this way, radiometric calibration for ETM+ was performed. The studies suggested that ETM+ can serve as a standard reference to calibrate other sensors [18] [19].

But, some of the issues in the datasets due to SLC failure and systematic variations need to be addressed for long-term instrument monitoring.

2.2 Consistent-Calibration between Landsat-8 OLI and Landsat-7 ETM+

Landsat-7 ETM+ and Landsat-8 OLI were cross-calibrated by SDSU and USGS EROS [15]. They used simultaneous scene pairs, which were acquired during under-fly on March 22nd and 23rd, 2013.

The results suggested that the TOA reflectance between Landsat-7 ETM+ and Landsat-8 OLI had a difference of 2% for all the bands except in NIR, which showed a difference of 4%.

2.3 Calibration of Landsat-5 TM and tie to Landsat-7 ETM+

Landsat-7 ETM+ was initially placed in an orbit that was very close to that of Landsat-5 TM. So, on June 1-4, 1999, both tracks were exactly the same, and that gave the opportunity for the tandem configuration. The cross-calibration between Landsat-7 ETM+ and Landsat-5 TM was performed using three simultaneous data acquisitions from Railroad Valley, Nevada; Niobrara, Nebraska; and Washington, DC [20]. This indicated that a tandem (time coincident) cross-calibration approach is a better way to calibrate Landsat-5 TM because it is based on a well-calibrated radiometric standard, namely ETM+. Comparison with other independent methods developed by different research groups similar to SDSU and the University of Arizona indicated that the tandem based approach is within 3% in bands 1-4, compares less 3% favorably in bands 5 and 7 [32]. The gains were updated in the CPF for Landsat-5 TM in 2003 [21]. The gains were updated for all reflective bands based on vicarious, cross-calibration with ETM+ and sensor response to the IC. The study showed that changes in lifetime gains were due to the lamps and not the detectors. Thus, it provided a consistent calibration for Landsat-5 TM. However, the gains were again updated in the CPF in April 2007, based on the sensor response to PICS and cross-calibrated with ETM+ [13]. This made USGS update the Level 1 product of Landsat-5 TM. The lifetime gain model for Landsat-5 TM was developed in the USGS processing system on May 5, 2003, for reflective bands (1-5 and 7) and it was replaced by a new lifetime radiometric calibration curve in April 2007.

Based on further analysis [22], a new radiometric gain model was implemented. The studies stated that Landsat-5 TM product values would change because of a change in absolute gains determined in 2013. Gradual decay was observed since 1999 in bands 1 and 3. This was also due to a change in the cross-calibration with Landsat-7 ETM+ due to a new bias estimation. The new model provides corrected linear drift gains. The maximum change will be in the blue band at 2% and the red band at 1 % as shown in Figure 2.3.1. Adjustment of cross-calibration gain between Landsat-5 TM and Landsat-7

ETM+ showed 1% of the maximum change in the red band. SWIR1 and SWIR2 gain correction will minimize the overall correction error by 1-2%.

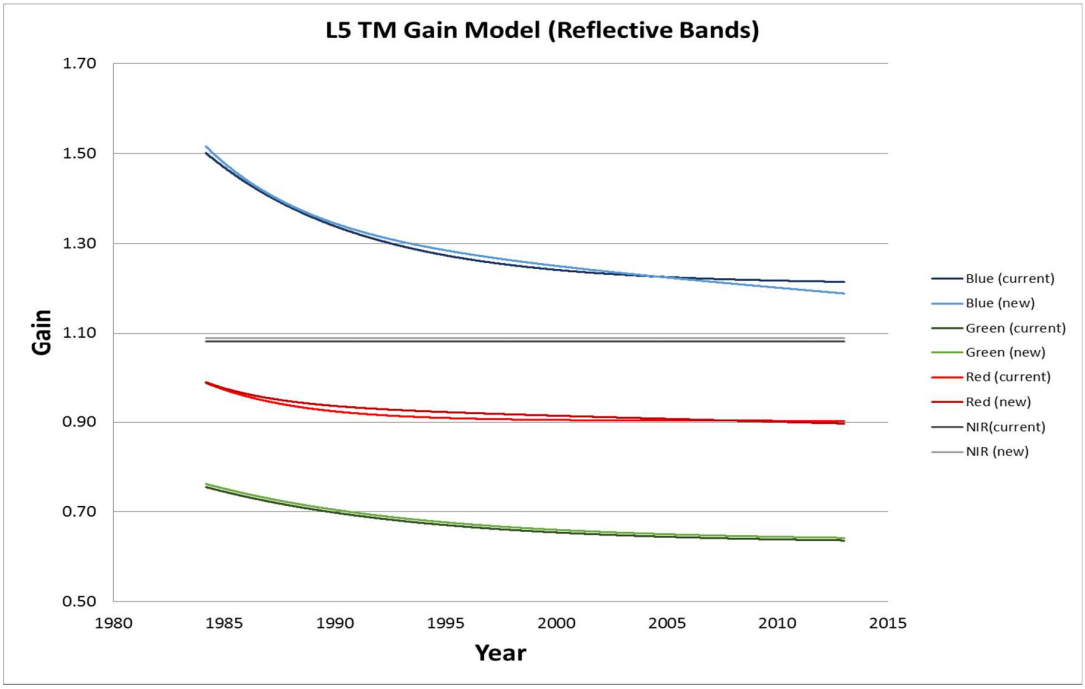

Figure 2.3.1. New gain model for Landsat-5 TM [22].

2.4 Calibration for Landsat-4 TM and tie to Landsat-5 TM

Landsat-4 TM was calibrated prior to launch using an integrating sphere that was traceable to NIST. This calibration was propagated to the onboard calibration system which was similar to Landsat-5 TM. An initial step at cross-calibration to TM-5 was taken using under-fly scenes from both sensors [23]. The results indicated the two instrument gains were within 15%. Mettler (2005) used nearly simultaneous overpasses from PICS locations – the Sonoran Desert and a location near the Kuwait/ Iraqi border - to establish a cross-calibration with Landsat-5 TM [24]. Results from the study indicated that reflective band calibration for Landsat-4 TM was within 5%. Similarly, Malla (2008) [25] used scene pairs from 1988 through 1990 and achieved the same results. To determine radiometric gains of Landsat 4 over its lifetime, time series from two locations – Libya 4 and the Sonoran Desert were developed. The results indicated that calibration for TM-4 had changed less than 5%. However, the results are quite different when compared with the on-board calibration system. So, in order to

maintain continuous calibration records for the instrument, [32] used PICS locations like the Sonoran desert and Libya 4 [26]. There was a downward trend in band 1 as shown in Figure 2.4.1, whereas there was no significant trend observed in the remaining reflective bands. Results from this work were implemented at USGS EROS and consistently calibrated data can be obtained for Landsat-4 TM similar to Landsat-5 TM and Landsat-7 ETM+.

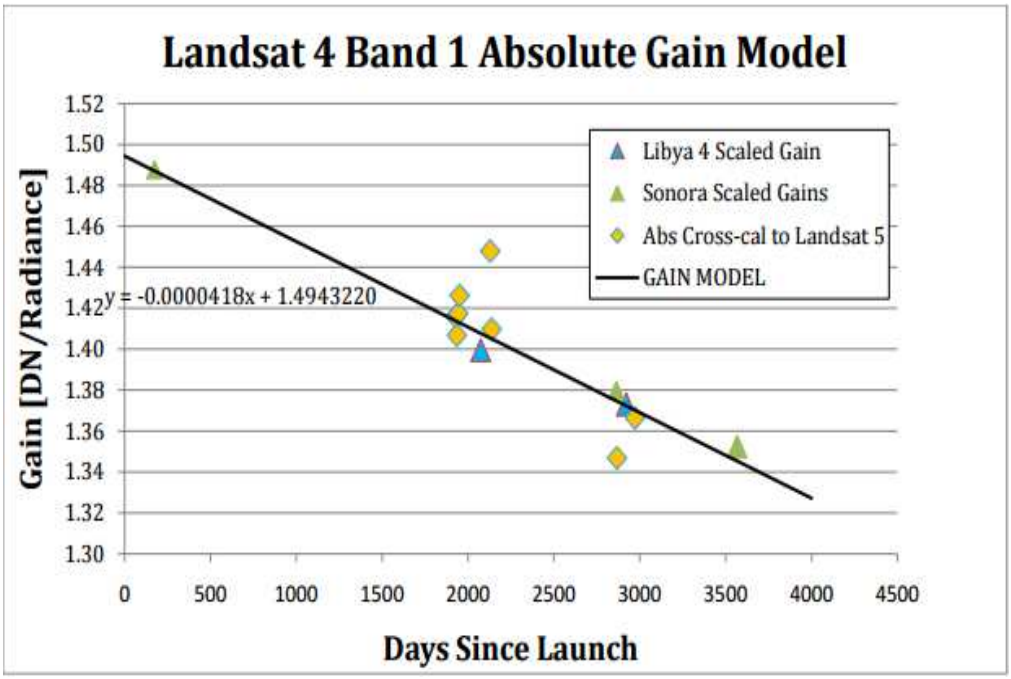

Figure 2.4.1. Calibration model for Landsat-4 TM, band 1 [26].

In this way, radiometric calibration was done from Landsat-8 to Landsat-4 TM, and all the work was implemented in the USGS processing system.

The following sections provide an explanation about previous calibrations of MSS data.

2.5 MSS Standard Interface Document

This document describes the radiometric calibration procedure for the first three satellites (i.e. Landsat-1 to Landsat-3). It was prepared by General Electric (GE) Company in July 1978 [27]. This document detailed MSS scanner optics, pre-launch testing, and calibration of MSS sensors. It also addressed some of the striping issues in the MSS imagery. The gains and offsets of sensors changed with time. This demands a calibration adjustment to reduce the striping. The correction was done

using calibration modifiers known as M and A. Detailed information about calibration wedge word locations, decompression tables, and the regression coefficients which help to determine calibration parameters were explained in this document.

The drawback of this document is that different notations were used for radiometric calibration compared to today, and sometimes this is a major source of confusion in tracking the equations.

2.6 Landsat to Ground Station Interface Description

This document covers the technical specifications and internal calibration system of MSS and TM sensors [28]. Scanning mechanisms for these instruments are different. They are separately described in a very understandable way. This document also consists of some of the information about calibration modifiers (i.e. M and A). There is not much useful information in this document regarding radiometric calibration. This document has calibration coefficients (i.e. M and A), which are very much important in addressing striping issues.

2.7 Previous work on Landsat MSS Calibration

Before 1993, R. F. Nelson scrutinized the MSS data from Landsat-1 MSS and Landsat-2 MSS [29]. Nelson investigated data acquired over spectrally stable targets between 1975 and 1977. He compared the results of the two instruments using the Top-of-Atmospheric (TOA) Reflectance scale and determined the calibration consistency over time. His analysis stated that the MSS-1 response over a 1000-day period starting January 1, 1975, decreased approximately 25-32% in all bands. However, surprisingly, the Landsat-2 MSS sensor response was stable. The time-dependent linear model for both the sensor reflectance calibrations also revealed that at the beginning of 1975 the TOA reflectance for Landsat-1 MSS would have been 14-24% higher when compared with Landsat-2 MSS TOA reflectance. This indicated an inconsistency between the calibrations of these two instruments.

Again, in 1987, post-launch cross-calibration between different MSS sensors suggested that Landsat-2 MSS to Landsat-5 MSS radiometric calibration consistency is within 12% [30]. It was also reported that the overall pre-launch calibration accuracy of the entire MSS was ±10%. However, for

Landsat-4 MSS bands, the gain was calculated using internal calibrator data over a 3-year period after launch. It showed that Landsat-4 MSS band-4 gain decreased by 15% during that period. It also showed that all the detectors in band-4 followed a decreasing pattern, which was never explained.

All the older studies about MSS showed that there was sensor degradation over time and some calibration discrepancies existed between sensors, thus the strong need for a sensor investigation of the lifetime calibration consistency on the Landsat-1 MSS to Landsat-5 MSS instruments became apparent.

2.8 Radiometric Calibration Handbook for Absolute Calibration

Helder performed the first radiometric calibration attempt in 1993 where all the details of this approach were compiled and documented in the 'MSS Radiometric Calibration Handbook' [31]. This handbook details the radiometric calibration of MSS data acquired by the first five Landsat satellites. The document mainly focused on the post-launch calibration of the older sensors. The handbook demonstrated the use of cal-wedge samples, radiometric gains, bias, and the application of smoothing techniques. The book also consists of some post-launch calibration parameters such as radiance max, radiance min, Cal-wedge information, regression coefficients and the application of these coefficients to the different MSS data sets. This document was made to extract possible information contained in the older archive to be used in future research. The handbook contained detailed instrument calibration procedures for MSS-1 to MSS-5.

As previously discussed, MSS data were stored using several different data formats, which has been a major source of confusion in the past. However, this book also explained the different MSS data formats and tape formats, detailing some of their issues. It explained what calibration information is contained in the respective tapes, where it is located, and how it is located. In the appendix of the handbook, Relative Spectral Response (RSR) profiles of spectral filters were provided – these RSR profiles were digitalized by South Dakota State University (SDSU). This study was a crucial stepping stone and has been increasingly applicable when studying the effect of spectral band differences from one sensor to another.

2.9 Systematic-Calibration of the Landsat MSS sensor

Systematic calibration of MSS data was based on the onboard calibration system [30]. Radiometric calibration of the first five MSS sensors was very difficult due to the age of MSS data - which had different formats like MSS-X, MSS-P, and MSS-A, and limited documentation. Most of the MSS data used in calibration were from the Sonoran Desert. In 2010, Helder and Karki et.al performed systematic cross-calibration of the MSS with the use of PICS where MSS-5 was considered the standard [3]. MSS1 was calibrated to MSS2, MSS2 was calibrated to MSS3, MSS3 was calibrated to MSS4, and MSS4 was calibrated to MSS5. The data from MSS-1 to MSS-5 was put on an absolute scale.

The result improved from 16% to 5% or less in some of the bands for some of the sensors. The uncertainty of 12% in band 4 was due to the presence of atmospheric water absorption features. To account for the change in sensor gain with respect to time as shown in Figure 2.9.1, a TDF (time dependent factor) was added to the final cross-calibration equation. The Landsat-5 MSS placed sensors on an absolute radiometric scale based on the Landsat-5 TM sensor with the use of PICS and Spectral Band Adjustment Factor (SBAF) correction.

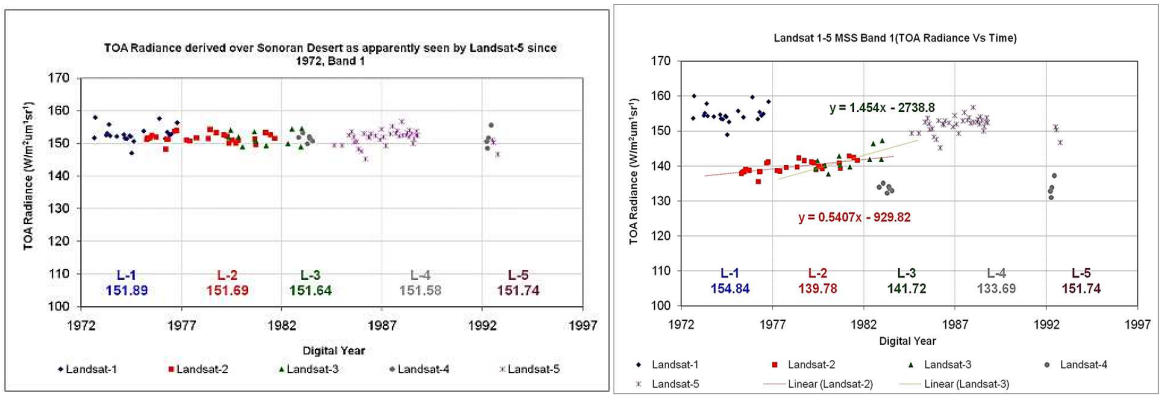

Figure 2.9.1. Consistent-Calibration of MSS data before and after applying TDF's [3].

The study showed that for bright targets like the Sonoran Desert, radiometric calibration of each sensor was stable. Thus, an absolute calibration was developed for MSS that was similar to the approach used for TM-5.

MSS-X-WBVT and MSS-X-CCT were also used in cross-calibration. But, there is a known inconsistency associated with these data formats and, hence, Time Dependent factor (TDF) derived from this calibration needs to be addressed.

2.10 Landsat MSS to Landsat-5 TM calibration

Landsat MSS to Landsat TM5 radiometric calibration was accomplished by taking advantage of the fact that Landsat TM-5 carried both an MSS and a TM sensor on board which provided many opportunities for coincident collections. Landsat-5 TM was well calibrated and it was used as a standard radiometer for the cross-calibration of Landsat-5MSS-5. SBAFs were calculated to take into account the spectral differences between the two sensors. The Sonoran Desert was used to cross-calibrate MSS-5 to TM-5 [32]. Twenty-five scene pairs were used for cross-calibration. A number of ROI's were used in order to have a large dynamic range of the sensors. For all bands, the MSS response is less than the TM response, a difference of 3%.

In this way, consistent radiometric calibration between MSS sensors was performed and, the existing MSS data calibration was based on the well-calibrated Landsat-5 TM. USGS EROS implemented this work in June 2011.

However, due to limited dataset, cross-calibration was performed using only bright targets. After cross-calibration, a negative radiance was seen in some bands of Landsat-1 MSS and Landsat-2 MSS sensors for the dark targets such as water, vegetation, and also there were inconsistencies in some of the bands as shown in Figure 2.9.2; the issue was never addressed.

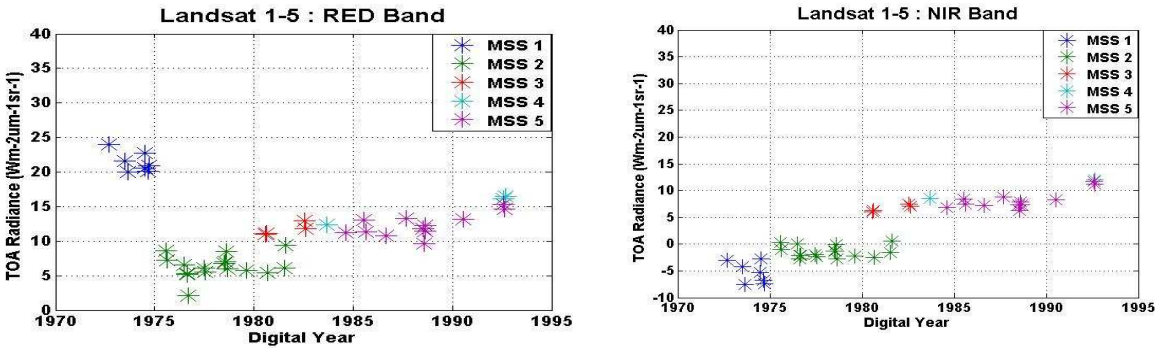

Figure 2.9.2. Temporal trend of the dark target (Crater Lake).

A new set of coefficients will be required for some bands of MSS1 and MSS2 in order to have a consistent radiometric calibration similar to other MSS sensors.

Hence, except for a few bands in MSS sensors, current USGS data has all radiometric calibration applied to the standard terrain corrected product (L1T).

2.2 Limitations of all previous calibrations

Thus, with the help of many research organizations and universities, a consistent radiometric calibration of the Landsat archive was done at USGS from Landsat-8 OLI to Landsat-1 MSS using a variety of calibration techniques. There was no paper published until now which described the overall uncertainty of radiometric calibration for the entire Landsat archive.

It was assumed that uncertainty of 5% for series of instruments i.e. TM/ETM+ for each band. The uncertainty for the Landsat-5 TM to MSS calibration process is assumed to be similar to that of MSS cross-calibration. Results indicated that TM-4 was within 9% absolute. However, MSS sensors are also within 10% absolute radiometric accuracy [32].

Hence, absolute uncertainty for the band of MSS sensors increases rapidly where Landsat-1 MSS band 4 approaches 25%.

Previous MSS calibration was performed using different data formats. The uncertainties may vary if a large set of data used in cross-calibration process. Simultaneous collections, similar data formats and use of dark targets will minimize the uncertainty for some of the bands in radiometric calibration for MSS sensors.

2.3 Need for reflectance-based calibration

Conversion from Digital number i.e. Q_{cal} in Landsat Level-1 product to at-sensor spectral radiance requires knowledge of the lower and upper limits of the original coefficients. The equation to convert Q_cal to radiance is given in equation (2)

$$L\lambda = \left(\frac{Lmax\lambda - Lmin\lambda}{Qcalmax - Qcalmin}\right) \cdot (Qcal - Qcalmin) + Lmin\lambda \quad (2)$$

Where:

L_λ = Spectral radiance at the sensor's aperture [$W/m^2/sr/\mu m$]

Q_{cal} = Quantized calibrated pixel value [DN].

Q_{calmin} = Minimum quantized calibrated pixel value corresponding to Lminλ [DN].

Q_{calmax} = Maximum quantized calibrated pixel value corresponding to Lmaxλ [DN].

$L_{min\lambda}$ = Spectral at–sensor radiance that is scaled to Qcalmin [$W/m^2/sr/\mu m$].

$L_{max\lambda}$ = Spectral at–sensor radiance that is scaled to Qcalmin [$W/m^2/sr/\mu m$].

For Landsat to measure reflectance initially the DNs must be converted to radiance and then converting to reflectance can be done easily using Exoatmospheric Solar irradiance (ESUN (λ)). At-sensor spectral radiance is converted to TOA reflectance using the equation below

$$\rho_\lambda = \frac{\pi \cdot L_\lambda \cdot d^2}{Esun_\lambda \cdot Cos\theta_S} \quad (1)$$

Where

ρ_λ = TOA reflectance [unitless].

L_λ = Spectral radiance at the sensors aperture [$W/m^2 sr\ \mu m$].

$Cos\theta_S$ = Cosine of solar zenith angle in degrees.

d^2 = Earth−sun distance (d), available in the Landsat-7 ETM+ handbook [11].

$Esun_\lambda$ = Mean exoatmospheric solar irradiance [$W/m^2 \mu m$].

To convert Landsat L1T products to reflectance products, many application scientists use Thuillier solar models or the ChKur solar model (MODTRAN5) [33]. Currently, all Landsat products produced at EROS are calibrated using ChKur-Modtran 5, but the Committee on Earth Observation Satellites (CEOS) recommends using the Thuillier solar model to generate reflectance for the L1T product.

The Neckel and Lab (Neckel & Labs, 1984) solar spectrum was used for MSS and TM solar irradiance values (Markham & Barker, 1986).

Hence, there are numerous solar models, all with various levels of accuracies. To, reduce the uncertainties due to solar model and also to address the inconsistency in the data format for

different types of MSS data, direct reflectance based calibration was needed for all previous missions using Landsat-8 OLI as the baseline. The approach will be explained in the following chapters.

Chapter 3 Cross-Calibration methodology implemented on the Landsat archive

As discussed in previous sections, reflectance-based calibration is highly desirable for Landsat-8 OLI to Landsat-1 MSS. The previous study suggested that a well-calibrated sensor (i.e. Landsat-8 OLI) could be used to provide a consistent calibration across all the Landsat sensors. It was already known that Landsat-8 OLI has minimum uncertainty in both radiance and reflectance calibration that is traceable to the National Institute of Standards and Technology (NIST). OLI was radiometrically calibrated before its launch in terms of spectral radiance using an integrating sphere source. The results all showed an uncertainty of ~3% in radiance and an uncertainty of ~2% in reflectance. Additionally, on-orbit comparisons and vicarious calibration techniques have shown similar radiance and reflectance uncertainties (i.e. not more than ~3% and ~2% respectively) [12]. Hence, Landsat-8 is known to be the best-calibrated Landsat sensor to date, and it provided a basis for a transfer of the OLI reflectance calibration to data generated by the previous Landsat sensors. Reflectance-based calibration is better than radiance-based calibration it terms of uncertainty and will, therefore, be used in the following cross-calibration analysis. This cross-calibration method connects the reflectance space of one sensor to the DN space of another sensor in order to determine the gain and bias of the linear equations that relates the two sensors.

Due to the need to get to the most fundamental measurement made by sensors, an effort to undo all of the radiometric calibration needed to be performed to convert back to DN's. Some of the previously modeled detector degradation corrections are maintained, resulting in what is termed normalized DN's. To determine the normalized DN's, the current radiance is scaled by un-correcting the radiance gain that changed with time. Then a "two-point" reflectance cross-calibration approach is used to determine the new reflectance bias and gain. The "two-point" cross calibration approach refers to an approach where both darker PICS (i.e. lakes) and brighter PICS (i.e. deserts), are used to better understand the behavior across the entire dynamic range of the sensor. PICS [34] are commonly used to calibrate optical imaging satellites because of the properties of having low uncertainty, high uniformity, and brighter intensity.

The following Steps explain how reflectance cross-calibration is implemented:

- In the first step, two or more scenes are identified, preferably from known PICS, taken by different sensors over the same geographical region of interest (ROI) with the minimal time difference. For stable regions, non-coincident image pairs are also allowed but can have an only minimal time difference.
- A well-calibrated sensor treated as the 'known' is used to transfer its radiometric calibration to the preceding sensor using the mathematical expression shown at the bottom of Figure 3.1.1
- To find the original or Normalized DNs for a particular sensor, using the USGS radiometrically corrected L1T product, the current radiance is scaled by un-correcting the radiance gain. As an example, to get uncorrected radiance for MSS sensors, cross-calibration coefficients available in Calibration parameter File (CPF) (i.e. cross-calibration gains and TDF's) were removed. Then, the uncorrected radiance is scaled by absolute gains available in the CPF to generate original or Normalized DNs. More details are described in the following sections.
- To get an accurate regression line, a wide range of ROIs with differing intensity levels are selected manually from a given scene. This includes studying the spatial and temporal properties of each selected ROI to validate that these sites are of high enough quality to meet the needs of cross-calibration. A linear regression line is then fitted as shown in Figure 3.1.1. Then the gains and biases are determined. A statistical test is performed to check their significance.

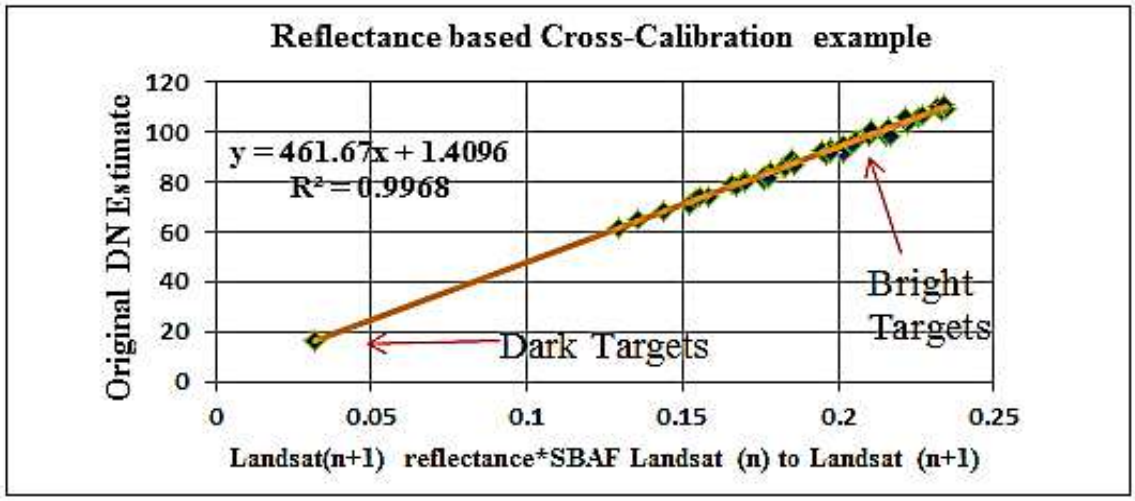

Figure 3.1.1. An example of reflectance-based cross-calibration approach.

- Validation of the cross-calibration gains and biases is performed using PICS. A statistical test is done to check the significance of any potential difference between the means of TOA reflectance as measured by different sensors. To evaluate the consistency between the sensors, lifetime trending of all the sensors is plotted on an absolute scale.

3.1 Invariant ROI's selection from scenes

Most often, errors in calibration occur when the site does not behave as expected, which requires a focused effort to evaluate and validate each ROI. A number of parameters need to be considered with choosing an ROI.

There exists a "trade space" when evaluating ROIs, i.e. good spatial uniformity, temporal stability, and atmospheric stability are needed. To achieve all three of these is tough; so, there is a need to balance each of the criteria to generate optimal ROIs. For example, an ROI may have good spatial uniformity but is affected by varying atmospheric effects, this would lead to a site that might be usable for coincident scene cross-calibration, but is not useable for non-coincident scenes. On the other hand, it may have good temporal stability, but be less spatially uniform. Under these conditions, it might be more suitable for non-coincident scene pairs because it has high geometric precision. Calibration sites like Libya are temporally stable and spatially uniform such that even small changes in time and pointing error will have small effects on the calibration results [35].

In this project, in order to cover a wide dynamic range of the sensor, a number of ROIs were selected that varied from dark to bright. A big goal of the cross-calibration research was to do a nearly exhaustive search for viable ROIs. This tends to lead towards a better understanding of the behavior of the instrument across the entire dynamic range and, therefore, a better linear regression line fit which minimizes uncertainty. An optimal size (3km to 5km) was chosen for cross-calibration to overcome potential registration problems which had been a problem with some of the earlier Landsat instruments. Preference was given towards using scenes containing PICS. Due to existing knowledge and experience of these sites, the work for choosing ROIs was simplified.

3.2 Relative Spectral analysis between sensors (RSR profiles)

It is already known that the response from two sensors of the same series can be significantly different, even if they are looking at the same target. This is due to the difference in RSR. So, the difference between RSRs of any two sensors must be compensated for by using an SBAF [37]. This adjustment is an important step to compensate for the differences and reduce the uncertainties in final cross-calibrations. RSR mismatches can be compensated for by using a target-based SBAF [36], which is based on the spectral signature of the respective target as shown in Figure 3.2.1 In this work, a hyperspectral sensor like E01 Hyperion launched on November 21, 2000, [38] was used to find the spectral signature of the target.

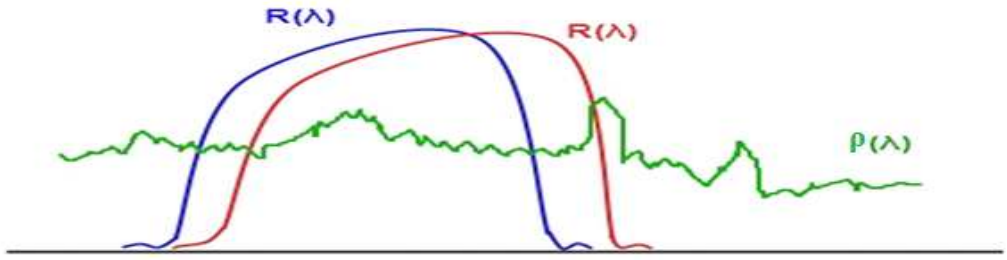

Figure 3.2.1. Spectral signature and SBAF representation.

The simulated TOA reflectance in this work refers to the reflectance that is corrected by integrating the RSRs of the multispectral sensor using a hyperspectral profile of the target, which is generated by

Hyperion. The generated TOA reflectance for any of the sensors can be measured by integrating the RSRs of the sensors with the Hyperion TOA reflectance profiles at each sampled wavelength and weighted by the respective RSR.

The spectrally banded reflectance of one sensor is given by the following equation

$$\rho'_{\lambda,(\text{sensor1})} = \frac{\int \rho_\lambda \cdot \text{RSR}_{\lambda,(\text{sensor1})}\ d_\lambda}{\int \text{RSR}_{\lambda,(\text{sensor1})}\ d_\lambda} \quad (4)$$

Similarly, the spectrally banded band reflectance of another sensor is given by using the following equation

$$\rho'_{\lambda,(\text{sensor2})} = \frac{\int \rho_\lambda \cdot \text{RSR}_{\lambda,(\text{sensor2})}\ d_\lambda}{\int \text{RSR}_{\lambda,(\text{sensor2})}\ d_\lambda} \quad (5)$$

Dividing the equations (5) & (6) gives the factor SBAF

$$\text{SBAF} = \frac{\rho'_{\lambda,(\text{sensor1})}}{\rho'_{\lambda,(\text{sensor2})}} = \frac{\frac{\int \rho_\lambda \cdot \text{RSR}_{\lambda,(\text{sensor1})}\ d_\lambda}{\int \text{RSR}_{\lambda,(\text{sensor1})}\ d_\lambda}}{\frac{\int \rho_\lambda \cdot \text{RSR}_{\lambda,(\text{sensor2})}\ d_\lambda}{\int \text{RSR}_{\lambda,(\text{sensor2})}\ d_\lambda}} \quad (6)$$

Where:

RSR_λ = RSR of the sensor (unitless).

ρ_λ = Hyperspectral TOA reflectance profile (unitless).

$\rho'_{\lambda,(\text{sensor1})}$ = Simulated TOA reflectance for sensor1 (unitless).

$\rho'_{\lambda,(\text{sensor2})}$ = Simulated TOA reflectance for sensor2 (unitless).

Relative spectral responses (RSR) for each pair of sensors are given in Appendix A.

In general, this is the approach for doing a cross-calibration. Specific steps for each cross-calibration combination will be explained in the following sections.

3.3 Cross-Calibration approach from Landsat-8 OLI to Landsat-7 ETM+

Due to Landsat-8 having minimal uncertainty, it is used as the cross-calibration reference to transfer reflectance from Landsat-8 OLI to Landsat-7 ETM+. The Landsat-8 OLI reflectance calculation used

metadata file parameters. Radiance or reflectance can be directly generated from DNs. For Landsat-8 OLI, the following equation (7) is used to find the DN:

$$DN_{8,\lambda} = g_{8,\rho,\lambda} \cdot \rho_{8,\lambda} + b_{8,\rho,\lambda} \quad (7)$$

Where:

$\rho_{8,\lambda}$ = Band specific Reflectance as seen by Landsat-8 OLI.

$g_{8,\rho,\lambda}$ = Band specific Landsat-8 OLI reflectance – gain to convert from reflectance to DN.

$b_{8,\rho,\lambda}$ = Band specific Landsat-8 OLI additive bias in DN.

To find the Landsat-8 OLI Reflectance from DN, equation (8) is used:

$$\rho_{8,\lambda} = M_{8,\rho,\lambda} \cdot DN_{8,\lambda} + A_{8,\rho,\lambda} \quad (8)$$

Where:

$\rho_{8,\lambda}$ = Band specific Reflectance as seen by Landsat-8 OLI.

$M_{8,\rho,\lambda}$ = Band specific Landsat-8 OLI multiplicative term to convert from DN to reflectance.

$A_{8,\rho,\lambda}$ = Band specific Additive rescaling factor from the metadata.

Now, the corresponding Landsat-8 OLI reflectance was transferred to Landsat-7 ETM+ using equation (9).

$$DN_{7,\lambda} = g_{7,\rho,\lambda} \cdot \left(SBAF_{\frac{7}{8},\rho,\lambda,ROI} \cdot \rho_{8,\lambda} \cdot \frac{1}{d^2{}_7} \cdot \frac{\cos\alpha_7}{\cos\alpha_8} \right) + b_{7,\rho,\lambda} \quad (9)$$

Where:

$\rho_{8,\lambda}$ = Band specific Reflectance as seen by Landsat-8 OLI.

$b_{7,\rho,\lambda}$ = Band specific Landsat-7 ETM+ additive bias in DN units.

$g_{7,\rho,\lambda}$ = Band specific Landsat-7 ETM+ reflectance – gain to convert from reflectance to DN.

$SBAF_{\frac{7}{8},\rho,\lambda,ROI}$ = Landsat-8 OLI to Landsat-7 ETM+ reflectance based adjustment factor for a specific region of interest.

$d^2{}_7$ = Earth–Sun distance for Landsat-7 ETM+ found in Landsat-7 ETM+ handbook [11].

$d^2{}_8$ is already included in Landsat -8 OLI Reflectance calculation equation.

$\frac{\cos\alpha_7}{\cos\alpha_8}$ = Normalization using cosine angle correction.

α = Sun zenith angle in degrees derived from sun elevation angle, which is provided in MTL file.

In order to find the original DN estimates for Landsat-7 ETM+, the current radiance is scaled by the average of each detector post-launch low gains taken from the first generated CPF. As there is no change in radiance gain of Landsat-7 ETM+, day1 CPF coefficients were used to generate normalized DN's or original DN estimates. The following equation (10) provides the DN estimate equation for Landsat-7 ETM+

$$DN_{7,\lambda} = \left(L_{7,\lambda} \cdot G_{7,\lambda,Avg}\right) \quad (10)$$

$L_{7,\lambda}$ = Landsat-7 ETM+ Radiance in $W/m^2/sr/\mu m$ calculated using the equation (2)

$G_{7,\lambda,Avg}$ are the average of each detector post–launch low gains for each band taken from the first CPF of Landsat-7 ETM+ and they are shown in Table 3.3.1

Table 3.3.1. Average of each detector post-launch low gains (i.e. $G_{7,\lambda,Avg}$) for each band from the first CPF of Landsat-7 ETM+ [38].

Blue	Green	Red	NIR	SWIR1	SWIR2	Pan
0.8163225	0.793825	1.02446125	0.9969375	5.0594825	14.5321381	0.98854

Then, Landsat-7 ETM+ reflectance (11) was derived by dividing the original estimate of DNs (from (10)) with Landsat-8 to Landsat-7 ETM+ reflectance cross–calibration gains that are obtained using linear regression. Notably, no bias is required to convert DNs to reflectance because the Landsat-8 OLI to Landsat-7 ETM+ reflectance-based linear regression had no bias.

$$\rho_{7,\lambda} = \left(\frac{DN_{7,\lambda}}{G_{\frac{8,\lambda}{7,\lambda}}}\right) \quad (11)$$

Where:

$\rho_{7,\lambda}$ = Band specific Reflectance as seen by Landsat-7 ETM+.

$DN_{7,\lambda}$ = Original DN estimate of Landsat-7 ETM+ calculated using equation (10).

$G_{\frac{8,\lambda}{7,\lambda}}$ = Band specific Landsat-8 OLI to Landsat-7 ETM+ Reflectance cross-cal gains.

3.4 Cross-Calibration approach from Landsat-7 ETM+ to Landsat-5 TM

To find the original DN estimates for Landsat-5 TM, the current radiance is scaled by correcting the radiance gain that changed with time. The newly obtained radiance is then normalized by some reference gain values. The studies suggested that a cross–calibration gain with ETM+ obtained on June 1, 1999, provides a good reference.

The equation below, (12), provides the original DN estimates after applying the entire gain model including normalized gains (i.e. reference gains to current radiance)

$$DN_{5,\lambda} = L_{5,\lambda} \cdot \left(\left(\frac{G_{5,\lambda,\text{Current-CPF\_gains(t)}}}{G_{5,\lambda,\text{Corrected linear drift\_ gains(t)}} \right) \cdot G_{\frac{L7}{L5},\lambda,\text{June1,1999}} \right) \quad (12)$$

Where:

$DN_{5,\lambda}$ = Original DN estimate of Landsat-5 TM.

$L_{5,\lambda}$ = Landsat-5 TM Radiance in $W/m^2/sr/\mu m$ calculated using the equation (2).

Current–CPF_gains (t) (i.e. current gains given in the Landsat-5 TM CPF) are calculated using

$$G_{5,\lambda,\text{Current-CPF\_ gains(t)}} = a_0 \cdot \exp(a_1 \cdot (t - 1984.2082)) + a_2 \quad (13)$$

Model parameters a_0, a_1, a_2 are provided in [40].

Corrected–linear drift_gains (t) are based on a double degree exponential model used to correct the drift in Landsat-5 TM radiance gain.

$$G_{5,\lambda,\text{Corrected linear drift gains(t)}} = a0 \cdot \exp(-a1 \cdot (t - 1984.2082)) + a2 \cdot \exp(-a3 \cdot (t - 1984.2082)) \quad (14)$$

Model parameters a_0, a_1, a_2, a_3 are provided in [22].

$G_{\frac{L7}{L5},\lambda,\text{June1,1999}}$ are the Landsat-7 ETM+ to Landsat-5 TM cross-calibration gains, which are obtained on June1,1999 when both sensors looking the same target and are shown in Table 3.4.1.

Table 3.4.1. Cross-Calibration gains (i.e. $\mathbf{G}_{\frac{L7}{L5},\lambda,\mathbf{June1,1999}}$) using tandem datasets between Landsat-7 ETM+ and Landsat-5 TM [20].

DSL	YEAR	DOY	BLUE	GREEN	RED	NIR	SWIR1	SWIR2
5571	1999.4164	152	1.2531	0.6619	0.9150	1.0896	8.20910	14.6950

In order to cross-calibrate Landsat-7 ETM+ to Landsat-5 TM, Landsat-7 ETM+ reflectance was transferred to Landsat-5 TM using (15)

$$DN_{5,\lambda} = g_{5,\rho,\lambda} \cdot \left(SBAF_{\frac{5}{7},\rho,\lambda,ROI} \cdot \rho_{7,\lambda} \cdot \frac{d^2{}_7}{d^2{}_5} \cdot \frac{\cos\alpha_5}{\cos\alpha_7} \right) + b_{5,\rho,\lambda} \quad (15)$$

Where:

$\rho_{7,\lambda}$ = Band specific reflectance as seen by Landsat-7 ETM+ calculated using (11).

$b_{5,\rho,\lambda}$ = Band specific Landsat-5 TM additive bias in DN units.

$g_{5,\rho,\lambda}$ = Band specific Landsat-5 TM reflectance – gain to convert from reflectance to DN.

$SBAF_{\frac{5}{7},\rho,\lambda,ROI}$ = Landsat-7 ETM+ to Landsat-5 TM reflectance based adjustment factor for a specific region of interest.

$\frac{d^2{}_7}{d^2{}_5}$ = Normalization using Earth–Sun distance found in Landsat-7 ETM+ handbook [11].

$\frac{\cos\alpha_5}{\cos\alpha_7}$ = Normalization using cosine angle correction.

α = Sun zenith angle in degrees derived from sun elevation angle, which is provided in MTL file.

Then, Landsat-5 TM reflectance (16) was derived by dividing the original estimate of DNs (from (12)) with Landsat-7 ETM+ to Landsat-5 reflectance cross–calibration gains that are obtained using linear regression. Notably, no bias is required to convert DNs to reflectance because the Landsat-7 ETM+ to Landsat-5 TM reflectance-based linear regression had no bias.

$$\rho_{5,\lambda} = \left(\frac{DN_{5,\lambda}}{G_{\frac{7,\lambda}{5,\lambda}}} \right) \quad (16)$$

Where:

$\rho_{5,\lambda}$ = Band specific Reflectance as seen by Landsat-5 TM.

$DN_{5,\lambda}$ = Original DN estimate of Landsat-5 TM calculated using equation (12).

$G_{\frac{7,\lambda}{5,\lambda}}$ = Band specific Landsat-7 ETM+ to Landsat-5 TM Reflectance cross-cal gains.

3.5 Cross-Calibration approach from Landsat-5 TM to Landsat-4 TM

The Landsat-4 TM calibration of reflective bands is achieved by PICS analysis [24]. The PICS model improved the calibration consistency to less than 6% in band 1, to nearly 2% in bands 2, 3, and 4, and to within 4% in bands 5 and 7 respectively. So, the results showed that there was no change in the radiance gain model of Landsat- 4 TM, resulting in an easy way to implement a cross-calibration equation from Landsat-5 TM to Landsat-4 TM.

To get original DN estimates (17) for Landsat-4 TM, the current radiance of Landsat-4 TM was normalized to the band average day1 gains, as there was no change in the lifetime radiance gain of Landsat-4 TM for all bands.

$$DN_{4,\lambda} = \left(L_{4,\lambda} \cdot G_{4,\lambda,\text{band\_Avg day1 gains}} \right) \quad (17)$$

Where:

$DN_{4,\lambda}$ = Original DN estimate for Landsat-4 TM.

$L_{4,\lambda}$ = Landsat-4 TM Radiance in $W/m^2/sr/\mu m$ calculated using the equation (2).

$G_{4,\lambda,\text{band\_Avg day1 gains}}$ are the average of each detector day1 gains for each band obtained from 1st CPF of Landsat-4 TM and shown in Table 3.5.1.

Table 3.5.1 Band average Day1 gains (i.e. $\mathbf{G_{4,\lambda,band\_Avg\ day1\ gains}}$) obtained from Landsat-4 TM CPF [39].

BLUE	GREEN	RED	NIR	SWIR1	SWIR2
1.4890	0.7190	0.9540	1.0730	7.7080	14.6500

Cross-Calibration of Landsat-5 TM to Landsat-4 TM was achieved successfully by transferring Landsat-5 TM reflectance to Landsat-4 TM using the equation (18)

$$DN_{4,\lambda} = g_{4,\rho,\lambda} \cdot \left(SBAF_{\frac{4}{5},\rho,\lambda,ROI} \cdot \rho_{5,\lambda} \cdot \frac{d^2{}_5}{d^2{}_4} \cdot \frac{\cos\alpha_4}{\cos\alpha_5} \right) + b_{4,\rho,\lambda} \quad (18)$$

Where

$\rho_{5,\lambda}$ = Band specific reflectance as seen by Landsat-5 TM calculated using (16).

$b_{4,\rho,\lambda}$ = Band specific Landsat-4 TM additive bias in DN units.

$g_{4,\rho,\lambda}$ = Band specific Landsat-4 TM reflectance – gain to convert from reflectance to DN.

$SBAF_{\frac{4}{5},\rho,\lambda,ROI}$ = Landsat-5 TM to Landsat-4 TM reflectance based adjustment factor for a specific region of interest.

$\frac{d^2{}_5}{d^2{}_4}$ = Normalization using Earth– Sun distance found in Landsat-7 ETM+ handbook [11].

$\frac{\cos\alpha_4}{\cos\alpha_5}$ = Normalization using cosine angle correction.

α = Sun zenith angle in degrees derived from sun elevation angle, which is provided in MTL file.

Then, Landsat-4 TM reflectance (19) was derived by dividing the original estimate of DNs in (from (17)) with Landsat-5 TM to Landsat-4 TM reflectance cross-calibration gains that are obtained using linear regression. Notably, no bias is required to convert DNs to reflectance because the Landsat-5 TM to Landsat-4 TM reflectance-based linear regression had no bias.

$$\rho_{4,\lambda} = \left(\frac{DN_{4,\lambda}}{G_{\frac{5,\lambda}{4,\lambda}}} \right) \quad (19)$$

Where:

$\rho_{4,\lambda}$ = Band specific Reflectance as seen by Landsat-4 TM.

$DN_{4,\lambda}$ = Original DN estimate of Landsat-4 TM calculated using equation (17).

$G_{\frac{5,\lambda}{4,\lambda}}$ = Band specific Landsat-5 TM to Landsat-4 TM Reflectance cross–cal gains.

3.6 Cross-Calibration approach from Landsat-5 TM to Landsat-5 MSS

Cross-calibration of MSS sensors is a little bit different when compared to the previous sensors. When cross-calibrating from Landsat-5 TM to Landsat-5 MSS all the calibration factors of MSS were removed to get uncorrected radiance. The uncorrected radiance was scaled by the coefficients in the CPF to get archive radiance (i.e. original DN estimation). Bias mapped to Landsat-5 MSS was also removed. The same procedure was followed for all MSS sensors. To estimate original DNs, uncorrected radiance was divided by absolute gains as shown below:

$$DN_{5M,\lambda} = \left(\frac{\left(\frac{L_{5M,\lambda}}{G_{5M,\lambda,rad\_cross-cal} \cdot TDF_{\lambda}} \right)}{G_{5M,\lambda,absolute\ gains}} \right) - bias_{(5M,\lambda)} \quad (20)$$

Where:

$DN_{5M,\lambda}$ = Original DN estimate for Landsat-5 MSS.

$L_{5M,\lambda}$ = Landsat-5 MSS Radiance in $W/m^2/sr/\mu m$ calculated using the equation (2).

$bias_{(5M,\lambda)}$ = Band specific bias with respective to Landsat-5 MSS and it is '0' for all bands.

TDF_{λ} = Time-dependent factor was calculated to consider the change in radiance gain for some bands of MSS sensors. It is given by

$$TDF_{\lambda} = \frac{C}{A \cdot (T - T_{launch}) + B} \quad (21)$$

Where:

T = Scene acquisition date (units: Decimal years).

T launch = Satellite launch date (units: Decimal years).

Coefficient's C, A, and B are provided in Landsat 1-5 MSS CPF's.

$G_{5M,\lambda,absolute\ gains}$ are band specific absolute gains to convert Landsat-5 MSS uncorrected radiance to original DN estimates and they are shown in Table 3.6.1 for each band.

$G_{5M,\lambda,rad\_cross-cal}$ are radiance cross–cal gains obtained from Landsat-5 MSS CPF and are

shown in Table 3.6.2.

Table 3.6.1. Absolute gains ($\mathbf{i.e.}\ \mathbf{G_{MSS5,\lambda,absolute\ gains}}$) obtained from Landsat-5 MSS CPF [39].

GREEN	RED	NIR1	NIR2
0.824	0.914	0.948	0.955

Table 3.6.2. Radiance cross-calibration ($\mathbf{i.e.}\ \mathbf{G_{5M,\lambda,rad\_cross-cal}}$) gains for each band obtained from Landsat-5 MSS CPF [39].

GREEN	RED	NIR1	NIR2
1	1	1	1

Landsat-5 TM reflectance was transferred to Landsat-5 MSS using equation below

$$DN_{5M,\lambda} = g_{5M,\rho,\lambda} \cdot \left(SBAF_{\frac{5M}{5},\rho,\lambda,ROI} \cdot \rho_{5,\lambda} \cdot \frac{d^2{}_5}{d^2{}_{5M}} \cdot \frac{\cos\alpha_{5M}}{\cos\alpha_5} \right) + b_{5M,\rho,\lambda} \qquad (22)$$

Where:

$\rho_{5,\lambda}$ = Band specific reflectance as seen by Landsat-5 TM and calculated using (16)

$b_{5M,\rho,\lambda}$ = Band specific Landsat-5 MSS additive bias in DN units.

$g_{5M,\rho,\lambda}$ = Band specific Landsat-5 MSS reflectance – gain to convert from reflectance to DN.

$SBAF_{\frac{5M}{5},\rho,\lambda,ROI}$ = Landsat-5 TM to Landsat-5 MSS reflectance based adjustment factor for a specific region of interest.

$\frac{d^2{}_5}{d^2{}_{5M}}$ = Normalization using Earth− Sun distance found in Landsat-7 ETM+ handbook [11].

$\frac{\cos\alpha_{5M}}{\cos\alpha_5}$ = Normalization using cosine angle correction.

α = Sun zenith angle in degrees derived from sun elevation angle, which is provided in MTL file.

Then, Landsat-5 MSS reflectance (23) was derived by dividing the original estimate of DNs, in (from (20)), with Landsat-5 TM to Landsat-5 MSS reflectance cross-calibration gains that are obtained using linear regression. Notably, no bias is required to convert DNs to reflectance because the Landsat-5 TM to Landsat-5 MSS reflectance-based linear regression had no bias.

$$\rho_{5M,\lambda} = \left(\frac{DN_{5M,\lambda}}{G_{\frac{5,\lambda}{5M,\lambda}}} \right) \quad (23)$$

Where:

$\rho_{5M,\lambda}$ = Band specific Reflectance as seen by Landsat-5 MSS.

$DN_{5M,\lambda}$ = Original DN estimate of Landsat-5 MSS calculated using equation (20).

$G_{\frac{5,\lambda}{5M,\lambda}}$ = Band specific Landsat-5 TM to Landsat-5 MSS Reflectance cross–cal gains.

3.7 Cross-Calibration approach from Landsat-5 MSS to Landsat-4 MSS

The same method was followed to cross-calibrate Landsat-5 MSS to Landsat-4 MSS. When cross–calibrating from Landsat-5 MSS to Landsat-4MSS all the calibration factors of MSS were removed to get uncorrected radiance. The uncorrected radiance was scaled by the coefficients in the CPF to get archive radiance (i.e. original DN estimation). Bias mapped to Landsat-5 MSS was also removed to calculate original DN estimates as shown in equation (24).

$$DN_{4M,\lambda} = \left(\frac{\left(\frac{L_{4M,\lambda}}{G_{4M,\lambda,rad\_cross-cal} \cdot TDF_{\lambda}} \right)}{G_{4M,\lambda,absolute\ gains}} \right) - bias_{(5M,\lambda)} \quad (24)$$

Where:

$DN_{4M,\lambda}$ = Original DN estimate for Landsat-4 MSS.

$L_{4M,\lambda}$ = Landsat-4 MSS Radiance in $W/m^2/sr/\mu m$ calculated using the equation (2).

$bias_{(5M,\lambda)}$ = Band specific bias with respective to Landsat-5 MSS and it is '0' for all bands.

$G_{4M,\lambda,absolute\ gains}$ are band specific absolute gains to convert Landsat-4 MSS uncorrected radiance to original DN estimates and they are shown in Table 3.7.1 for each band.

$G_{4M,\lambda,rad\_cross-cal}$ are radiance cross–cal gains to Landsat-5 MSS obtained from Landsat-4 MSS CPF and are shown in Table 3.7.2

The Time-dependent factor is '1' for all bands of Landsat-4 MSS.

Table 3.7.1 Absolute gains (**i. e.** $\mathbf{G_{MSS4,\lambda,absolute\ gains}}$) obtained from Landsat-4 MSS CPF [39].

GREEN	RED	NIR1	NIR2
0.824	0.914	0.948	0.955

Table 3.7.2 Radiance cross–calibration gains (**i. e.** $\mathbf{G_{4M,\lambda,rad\_cross-cal}}$) to Landsat-5 MSS for each band obtained from Landsat-4 MSS CPF [39].

GREEN	RED	NIR1	NIR2
1.1338	1.0803	1.0517	1.0349

Landsat-5 MSS reflectance was transferred to Landsat-4 MSS using equation below

$$DN_{4M,\lambda} = g_{4M,\rho,\lambda} \cdot \left(SBAF_{\frac{4M}{5M},\rho,\lambda,ROI} \cdot \rho_{5M,\lambda} \cdot \frac{d^2{}_{5M}}{d^2{}_{4M}} \cdot \frac{\cos\alpha_{4M}}{\cos\alpha_{5M}} \right) + b_{4M,\rho,\lambda} \quad (25)$$

Where:

$\rho_{5M,\lambda}$ = Band specific reflectance as seen by Landsat-5 MSS and calculated using (23).

$b_{4M,\rho,\lambda}$ = Band specific Landsat-4 MSS additive bias in DN units.

$g_{4M,\rho,\lambda}$ = Band specific Landsat-4 MSS reflectance – gain to convert from reflectance to DN.

$SBAF_{\frac{4M}{5M},\rho,\lambda,ROI}$ = Landsat-5 MSS to Landsat-4 MSS reflectance based adjustment factor for a specific region of interest.

$\frac{d^2{}_{5M}}{d^2{}_{4M}}$ = Normalization using Earth– Sun distance found in Landsat-7 ETM+ handbook [11].

$\frac{\cos\alpha_{4M}}{\cos\alpha_{5M}}$ = Normalization using cosine angle correction.

α = Sun zenith angle in degrees derived from sun elevation angle, which is provided in MTL file.

Then, Landsat-4 MSS reflectance (26) was derived by dividing the original estimate of DNs, in (from (24)) with Landsat-5 MSS to Landsat-4MSS reflectance cross-calibration gains that are obtained using linear regression. Notably, no bias is required to convert DNs to reflectance because the Landsat-5 MSS to Landsat-4 MSS reflectance-based linear regression had no bias.

$$\rho_{4M,\lambda} = \left(\frac{DN_{4M,\lambda}}{G_{\frac{5M,\lambda}{4M,\lambda}}} \right) \quad (26)$$

Where:

$\rho_{4M,\lambda}$ = Band specific Reflectance as seen by Landsat-4 MSS.

$DN_{4M,\lambda}$ = Original DN estimate of Landsat-4 MSS calculated using equation (24).

$G_{\frac{5M,\lambda}{4M,\lambda}}$ = Band specific Landsat-5 MSS to Landsat-4 MSS Reflectance cross–cal gains.

3.8 Cross-Calibration approach from Landsat-4 MSS to Landsat-3 MSS

The same method was followed to cross-calibrate Landsat-4 MSS to Landsat-3 MSS. When cross–calibrating from Landsat-4 MSS to Landsat-3 MSS all the calibration factors of MSS were removed to get uncorrected radiance. The uncorrected radiance was scaled by the coefficients in the CPF to get archive radiance (i.e. original DN estimation). Bias mapped to Landsat-5 MSS was also removed to calculate original DN estimates as shown in equation (27). A TDF factor was seen in some bands of Landsat-3 MSS. Landsat-4 MSS to Landsat-3 MSS are in different orbits and a view angle correction was done for each ROI selected.

$$DN_{3M,\lambda} = \left(\frac{\left(\frac{L_{3M,\lambda}}{G_{3M,\lambda,rad\_cross-cal} \cdot TDF_{\lambda}} \right)}{G_{3M,\lambda,absolute\ gains}} \right) - bias_{(5M,\lambda)} \quad (27)$$

Where:

$DN_{3M,\lambda}$ = Original DN estimate for Landsat-3 MSS.

$L_{3M,\lambda}$ = Landsat-3 MSS Radiance in $W/m^2/sr/\mu m$ calculated using the equation (2)

$bias_{(5M,\lambda)}$ = Band specific bias with respective to Landsat-5 MSS and it is ‘0’ for all bands.

$G_{3M,\lambda,absolute\ gains}$ are band specific absolute gains to convert Landsat-3 MSS uncorrected radiance to original DN estimates and they are shown in Table 3.8.1 for each band.

$G_{3M,\lambda,rad\_cross-cal}$ are radiance cross–cal gains to Landsat-5 MSS obtained from Landsat-3 MSS CPF and are shown in Table 3.8.2

A time-dependent factor was present in the Green band and shown by equation (28)

For green band:

$$\frac{151.55}{(1.5251 \cdot (T - T_{Launch}) + 144.10} \quad (28)$$

Table 3.8.1 Absolute gains($\mathbf{i.e.}\ \mathbf{G_{MSS3,\lambda,absolute\ gains}}$) obtained from Landsat-3 MSS CPF [39].

GREEN	RED	NIR1	NIR2
0.824	0.914	0.948	0.955

Table 3.8.2. Radiance cross–calibration gains ($\mathbf{i.e.}\ \mathbf{G_{3M,\lambda,rad\_cross\_cal}}$) to Landsat-5 MSS for each band obtained from Landsat-3 MSS CPF [39].

GREEN	RED	NIR1	NIR2
1.0489	1.0035	1.0353	0.9952

Landsat-4 MSS reflectance was transferred to Landsat-3 MSS using the equation below

$$DN_{3M,\lambda} = g_{3M,\rho,\lambda} \cdot \left(SBAF_{\frac{3M}{4M},\rho,\lambda,ROI} \cdot \rho_{4M,\lambda} \cdot \frac{d^2{}_{4M}}{d^2{}_{3M}} \cdot \frac{\cos\alpha_{3M}}{\cos\alpha_{4M}} \right) + b_{3M,\rho,\lambda} \quad (29)$$

Where:

$\rho_{4M,\lambda}$ = Band specific reflectance as seen by Landsat-4 MSS and calculated using (26).

$b_{3M,\rho,\lambda}$ = Band specific Landsat-3 MSS additive bias in DN units.

$g_{3M,\rho,\lambda}$ = Band specific Landsat-3 MSS reflectance – gain to convert from reflectance to DN.

$SBAF_{\frac{3M}{4M},\rho,\lambda,ROI}$ = Landsat-4 MSS to Landsat-3 MSS reflectance based adjustment factor for a specific region of interest.

$\frac{d^2{}_{4M}}{d^2{}_{3M}}$ = Normalization using Earth– Sun distance found in Landsat-7 ETM+ handbook [11].

$\frac{\cos\alpha_{3M}}{\cos\alpha_{4M}}$ = Normalization using cosine angle correction.

α = Sun zenith angle in degrees derived from sun elevation angle, which is provided in MTL file.

Then, Landsat-3 MSS reflectance (30) was derived by dividing the original estimate of DNs in (from (27)), with Landsat-4 MSS to Landsat-3 MSS reflectance cross-calibration gains that are obtained

using linear regression. Notably, no bias is required to convert DNs to reflectance because the Landsat-4 MSS to Landsat-3 MSS reflectance-based linear regression had no bias.

$$\rho_{3M,\lambda} = \left(\frac{DN_{3M,\lambda}}{G_{\frac{4M,\lambda}{3M,\lambda}}} \right) \tag{30}$$

Where:

$\rho_{3M,\lambda}$ = Band specific Reflectance as seen by Landsat-3 MSS.

$DN_{3M,\lambda}$ = Original DN estimate of Landsat-4 MSS calculated using equation (27).

$G_{\frac{4M,\lambda}{3M,\lambda}}$ = Band specific Landsat-4 MSS to Landsat-3 MSS Reflectance cross – cal gains.

3.9 Cross-Calibration approach from Landsat-3 MSS to Landsat-2 MSS

The same method was followed to cross-calibrate Landsat-3 MSS to Landsat-2 MSS. When cross–calibrating from Landsat-3 MSS to Landsat-2 MSS all the calibration factors of MSS were removed to get uncorrected radiance. Then, the uncorrected radiance of Landsat-2 MSS was scaled by the absolute gains available in CPF to estimate the original DN's. A TDF factor and significant bias were determined in the previous radiance calibration for some bands of Landsat-2 MSS and they were taken into account in the final cross-calibration equation as shown in (31).

$$DN_{2M,\lambda} = \left(\frac{\left(\frac{L_{2M,\lambda}}{G_{2M,\lambda,rad\_cross-cal} \cdot TDF_{\lambda}} \right)}{G_{2M,\lambda,absolute\ gains}} \right) - bias_{(5M,\lambda)} \tag{31}$$

Where:

$DN_{2M,\lambda}$ = Original DN estimate for Landsat-2 MSS.

$L_{2M,\lambda}$ = Landsat-2 MSS Radiance in $W/m^2/sr/\mu m$ calculated using the equation (2).

$bias_{(5M,\lambda)}$ = Band specific bias with respective to Landsat-5 MSS shown in Table 3.9.1.

$G_{2M,\lambda,absolute\ gains}$ are band specific absolute gains to convert Landsat-2 MSS uncorrected radiance to original DN estimates and they are shown in Table 3.9.2 for each band.

$G_{2M,\lambda,rad\_cross-cal}$ are radiance cross–cal gains to Landsat-5 MSS obtained from Landsat-2 MSS CPF and are shown in Table 3.9.3.

A Time-dependent factor was suggested for some bands and it is shown by equation (32) & (33)

For Green band

$$\frac{147.72}{(0.567092 \cdot (T - T_{Launch}) + 144.85} \quad (32)$$

For Red band

$$\frac{170.85}{(0.53916 \cdot (T - T_{Launch}) + 168.11} \quad (33)$$

Table 3.9.1. Cross-Calibration bias (**i.e.** $\mathbf{bias_{(5M,\lambda)}}$) to Landsat-5 MSS for each band obtained from Landsat-2 MSS CPF [39].

GREEN	RED	NIR1	NIR2
0	-7.2141	-8.9049	0

Table 3.9.2. Absolute gains($\mathbf{i.e.\ G_{2M,\lambda,absolute\ gains}}$) obtained from Landsat-2 MSS CPF [39].

GREEN	RED	NIR1	NIR2
0.824	0.914	0.948	0.955

Table 3.9.3. Radiance cross-calibration gains (**i.e.** $\mathbf{G_{2M,\lambda,rad\_cross\_cal}}$) to Landsat-5 MSS for each band obtained from Landsat-2 MSS CPF [39].

GREEN	RED	NIR1	NIR2
1.0806	1.0737	1.0552	1.0134

Landsat-3 MSS reflectance was transferred to Landsat-2 MSS using the equation (34)

$$DN_{2M,\lambda} = g_{2M,\rho,\lambda} \cdot \left(SBAF_{\frac{2M}{3M},\rho,\lambda,ROI} \cdot \rho_{3M,\lambda} \cdot \frac{d^2{}_{3M}}{d^2{}_{2M}} \cdot \frac{\cos\alpha_{2M}}{\cos\alpha_{3M}} \right) + b_{2M,\rho,\lambda} \quad (34)$$

Where

$\rho_{3M,\lambda}$ = Band specific reflectance as seen by Landsat-3 MSS and calculated using (30).

$b_{2M,\rho,\lambda}$ = Band specific Landsat-2 MSS additive bias in DN units.

$g_{2M,\rho,\lambda}$ = Band specific Landsat-2 MSS reflectance – gain to convert from reflectance to DN.

$SBAF_{\frac{2M}{3M},\rho,\lambda,ROI}$ = Landsat-3 MSS to Landsat-2 MSS reflectance based adjustment factor for a specific region of interest.

$\frac{d^2{}_{3M}}{d^2{}_{2M}}$ = Normalization using Earth– Sun distance found in Landsat-7 ETM+ handbook [11].

$\frac{\cos\alpha_{2M}}{\cos\alpha_{3M}}$ = Normalization using cosine angle correction.

α = Sun zenith angle in degrees derived from sun elevation angle, which is provided in MTL file.

Then, Landsat-2 MSS reflectance (35) was derived by dividing the original estimate of DNs in (from (31)), with Landsat-3 MSS to Landsat-2 MSS cross–calibration gains that are obtained using linear regression. Notably, no bias is required to convert DNs to reflectance because the Landsat-3 MSS to Landsat-2 MSS reflectance-based linear regression had no bias.

$$\rho_{2M,\lambda} = \left(\frac{DN_{2M,\lambda}}{G_{\frac{3M,\lambda}{2M,\lambda}}} \right) \tag{35}$$

Where:

$\rho_{2M,\lambda}$ = Band specific Reflectance as seen by Landsat-2 MSS.

$DN_{2M,\lambda}$ = Original DN estimate of Landsat-2 MSS calculated using equation (31).

$G_{\frac{3M,\lambda}{2M,\lambda}}$ = Band specific Landsat-3 MSS to Landsat-2 MSS Reflectance cross–cal gains.

3.10 Cross-Calibration approach from Landsat-2 MSS to Landsat-1 MSS

The same method was followed to cross-calibrate Landsat-2 MSS to Landsat-1 MSS. When cross–calibrating from Landsat-2 MSS to Landsat-1 MSS all the calibration factors of MSS were removed to get uncorrected radiance. Then, the uncorrected radiance of Landsat-1 MSS was scaled by the absolute gains available in CPF to estimate the original DN's. A significant bias was seen in radiance calibration for some bands of Landsat-1MSS and they were taken into the final cross-calibration expression.

$$DN_{1M,\lambda} = \left(\frac{\left(\frac{L_{1M,\lambda}}{G_{1M,\lambda,rad\_cross-cal} \cdot TDF_{\lambda}} \right)}{G_{1M,\lambda,absolute\ gains}} \right) - bias_{(5M,\lambda)} \quad (36)$$

Where:

$DN_{1M,\lambda}$ = Original DN estimate for Landsat-1 MSS.

$L_{1M,\lambda}$ = Landsat-1 MSS Radiance in $W/m^2/sr/\mu m$ calculated using the equation (2)

$bias_{(5M,\lambda)}$ = Band specific bias with respective to Landsat-5 MSS shown in Table 3.10.1.

$G_{1M,\lambda,absolute\ gains}$ are band specific absolute gains to convert Landsat-1 MSS uncorrected radiance to original DN estimates and they are shown in Table 3.10.2 for each band.

$G_{1M,\lambda,rad\_cross-cal}$ are radiance cross–cal gains to Landsat-5 MSS obtained from Landsat-1 MSS CPF and are shown in Table 3.10.3.

The time-dependent factor is '1' for all the bands of Landsat-1 MSS.

Table 3.10.1 Cross-Calibration bias (**i.e. $bias_{(5M,\lambda)}$**) to Landsat-5 MSS for each band obtained from Landsat-1 MSS CPF [39].

GREEN	RED	NIR1	NIR2
0	9.9635	-8.9049	0

Table 3.10.2. Absolute gains (**i.e.$G_{1M,\lambda,absolute\ gains}$**) obtained from Landsat-1 MSS CPF [39].

GREEN	RED	NIR1	NIR2
0.824	0.914	0.948	0.955

Table 3.10.3. Radiance cross-calibration gains (**i.e.$G_{1M,\lambda,rad\_cross-cal}$**) to Landsat-5 MSS for each band obtained from Landsat-1 MSS CPF [39].

GREEN	RED	NIR1	NIR2
0.9837	0.8951	1.0193	1.0883

Landsat-2 MSS reflectance was transferred to Landsat-1 MSS using equation (37)

$$DN_{1M,\lambda} = g_{1M,\rho,\lambda} \cdot \left(SBAF_{\frac{1M}{2M},\rho,\lambda,ROI} \cdot \rho_{2M,\lambda} \cdot \frac{d^2{}_{2M}}{d^2{}_{1M}} \cdot \frac{\cos\alpha_{1M}}{\cos\alpha_{2M}} \right) + b_{1M,\rho,\lambda} \quad (37)$$

$\rho_{2M,\lambda}$ = Band specific reflectance as seen by Landsat-2 MSS and calculated using (35).

$b_{1M,\rho,\lambda}$ = Band specific Landsat-1 MSS additive bias in DN units.

$g_{1M,\rho,\lambda}$ = Band specific Landsat-1 MSS reflectance – gain to convert from reflectance to DN.

$SBAF_{\frac{1M}{2M},\rho,\lambda,ROI}$ = Landsat-2 MSS to Landsat-1 MSS reflectance based adjustment factor for a specific region of interest.

$\frac{d^2{}_{2M}}{d^2{}_{1M}}$ = Normalization using Earth– Sun distance found in Landsat-7 ETM+ handbook [11].

$\frac{\cos\alpha_{1M}}{\cos\alpha_{2M}}$ = Normalization using cosine angle correction.

α = Sun zenith angle in degrees derived from sun elevation angle, which is provided in MTL file.

Then, Landsat-1 MSS reflectance (38) was derived by dividing the original estimate of DNs in (from (36)) with Landsat-2 MSS to Landsat-1 MSS reflectance cross-calibration gains that are obtained using linear regression. A bias is required to convert DNs to reflectance because the Landsat-2 MSS to Landsat-1 MSS reflectance – based linear regression had a statistically significant bias.

$$\rho_{1M,\lambda} = \left(\frac{DN_{1M,\lambda} + b_{\frac{2M,\lambda}{1M,\lambda}}}{G_{\frac{2M,\lambda}{1M,\lambda}}} \right) \quad (38)$$

Where:

$\rho_{1M,\lambda}$ = Band specific Reflectance as seen by Landsat-1 MSS.

$DN_{1M,\lambda}$ = Original DN estimate of Landsat-1 MSS calculated using equation (36).

$G_{\frac{2M,\lambda}{1M,\lambda}}$ = Band specific Landsat-2 MSS to Landsat-1 MSS Reflectance cross–cal gains.

$b_{\frac{2M,\lambda}{1M,\lambda}}$ = Reflectance cross-calibration bias in DN units.

Chapter 4 Cross-Calibration from Landsat-8 OLI to Landsat-1 MSS

Consistent cross-calibration from Landsat-8 OLI to Landsat-1 MSS was done in reflectance space. Cloud-free scenes from bright targets and dark targets were chosen to complete the Landsat calibration. The calibration process was started with Landsat-8 OLI and continued to Landsat-1MSS. A systematic cross-calibration process was followed. Landsat-8 OLI was cross-calibrated to Landsat-7 ETM+. Landsat-7 ETM+ was cross-calibrated to Landsat-5 TM. Landsat-5 TM was cross-calibrated to Landsat-4 TM and Landsat-5 MSS. Landsat-5 MSS was cross-calibrated to Landsat-4 MSS. Landsat-4 MSS was cross-calibrated to Landsat-3 MSS. Landsat-3 MSS was cross-calibrated to Landsat-2 MSS. Finally, Landsat-2 MSS was cross-calibrated to Landsat-1 MSS. The figure below shows the cross-calibration path from Landsat-8 OLI back to Landsat-1 MSS.

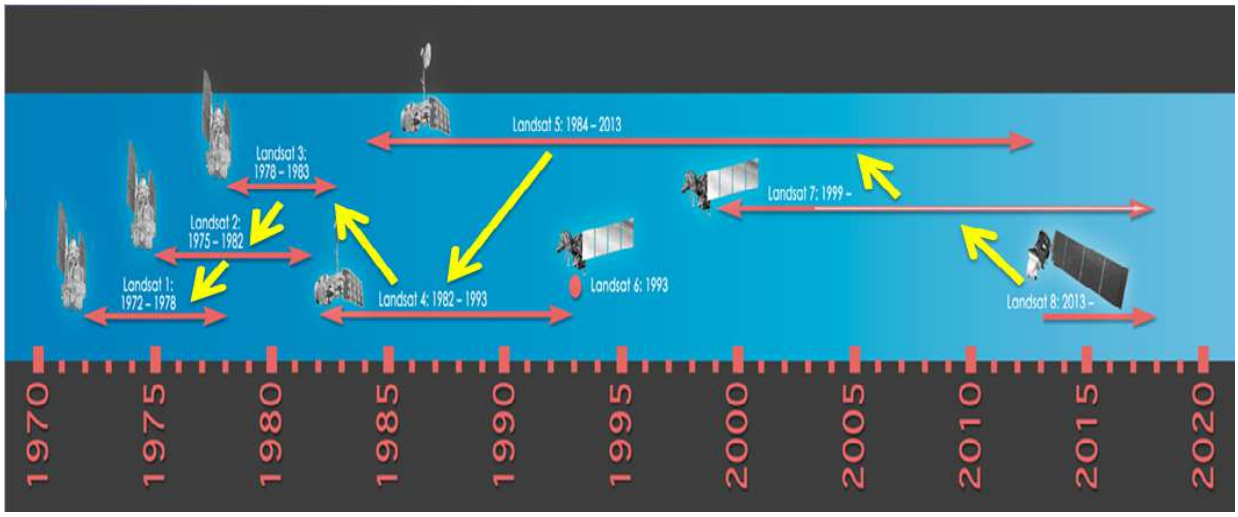

Figure 4.1. Systematic cross-calibration from Landsat-8 OLI to Landsat-1 MSS.

4.1 Landsat-8 OLI to Landsat-7 ETM+

Landsat-8 OLI to Landsat-7 ETM+ cross-calibration was accomplished by using eight scene pairs from the Sonoran Desert and four scene pairs from Lake Tahoe. Initially, Landsat-8 OLI and Landsat-7 ETM+ RSRs were compensated using SBAFs; they are included in Appendix C. For cross-calibration altogether, eight ROIs were used. Among those ROIs, seven are from the Sonoran Desert, and the remaining one is from Lake Tahoe as shown in Figure 4.2. Corner coordinates of all ROIs are given in Appendix A.

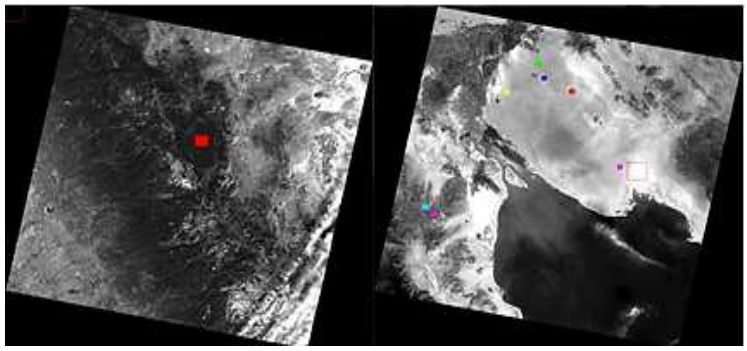

Figure 4.2. ROIs used in Landsat-8 OLI to Landsat-7 ETM cross-calibration.

4.1.1 Scene Pairs

Cross-Calibration of the Landsat-8 OLI to the Landsat-7 ETM+ sensor was achieved using 12 scene pairs. Out of the 12, eight good quality and cloud-free scene pairs were chosen from the Sonoran Desert, and four from Lake Tahoe. All of the scene pairs are nearly coincident scenes with a difference of 8 days in acquisition as shown in Table 4.1; full ROI coordinates are given in appendix A.

Table 4.1. Scene Pairs used in Landsat-8 OLI to Landsat-7 ETM+ cross-calibration.

Number of Scene Pair Used	Scene pair IDs	Time Differences	ROI Info
Scene Pair-1	LE70380382013120EDC00	8 days	Refer Table A1 L-8 to L-7 Sonoran ROI 1-7 in Appendix A.
	LC80380382013112LGN01		
Scene Pair-2	LE70380382013136EDC00	8 days	Refer Table A1 L-8 to L-7 Sonoran ROI 1-7 in Appendix A.
	LC80380382013144LGN00		
Scene Pair-3	LE70380382013168EDC00	8 days	Refer Table A1 L-8 to L-7 Sonoran ROI 1-7 in Appendix A.
	LC80380382013176LGN00		
Scene Pair-4	LE70380382014075EDC00	8 days	Refer Table A1 L-8 to L-7 Sonoran ROI 1-7 in Appendix A.
	LC80380382014067LGN00		

Scene Pair-5	LE70380382014235EDC00	8 days	Refer Table A1 L-8 to L-7 Sonoran ROI 1-7
	LC80380382014243LGN00		in Appendix A.
Scene Pair-6	LE70380382014267EDC00	8 days	Refer Table A1 L-8 to L-7 Sonoran ROI 1-7 in Appendix A.
	LC80380382014275LGN00		
Scene Pair-7	LE70380382014283EDC00	8 days	Refer Table A1 L-8 to L-7 Sonoran ROI 1-7 in Appendix A.
	LC80380382014291LGN00		
Scene Pair-8	LE70380382014315EDC00	8 days	Refer Table A1 L-8 to L-7 Sonoran ROI 1-7 in Appendix A.
	LC80380382014307LGN00		
Scene Pair-9	LE70430332013267EDC00	8 days	Refer Table A1 L-8 to L-7 Lake Tahoe ROI 1 in Appendix A.
	LC80430332013275LGN00		
Scene Pair-10	LE70430332013299EDC00	8 days	Refer Table A1 L-8 to L-7 Lake Tahoe ROI 1 in Appendix A.
	LC80430332013291LGN00		
Scene Pair-11	LE70430332014174EDC00	8 days	Refer Table A1 L-8 to L-7 Lake Tahoe ROI 1 in Appendix A.
	LC80430332014182LGN00		
Scene Pair-12	LE70430332014190EDC02	8 days	Refer Table A1 L-8 to L-7 Lake Tahoe ROI 1 in Appendix A.
	LC80430332014182LGN00		

4.1.2 Results

The response of Landsat-8 OLI was plotted against Landsat-7 ETM+ for the best matching band pairs by accounting for their spectral differences. A linear regression line, shown in orange, was fitted to determine the cross-calibration gain and bias term as shown in Figure 4.3.

$$\mathrm{X-axis} = \mathrm{SBAF}_{\frac{7}{8},\rho,\lambda,\mathrm{ROI}} \cdot \rho_{8,\lambda} \cdot \frac{1}{d^2{}_7} \cdot \frac{\cos\alpha_7}{\cos\alpha_8}$$

$$\mathrm{Y-axis} = \mathrm{DN}_{7,\lambda} = \left(\mathrm{L}_{7,\lambda} \cdot \mathrm{G}_{7,\lambda,\mathrm{Avg}}\right)$$

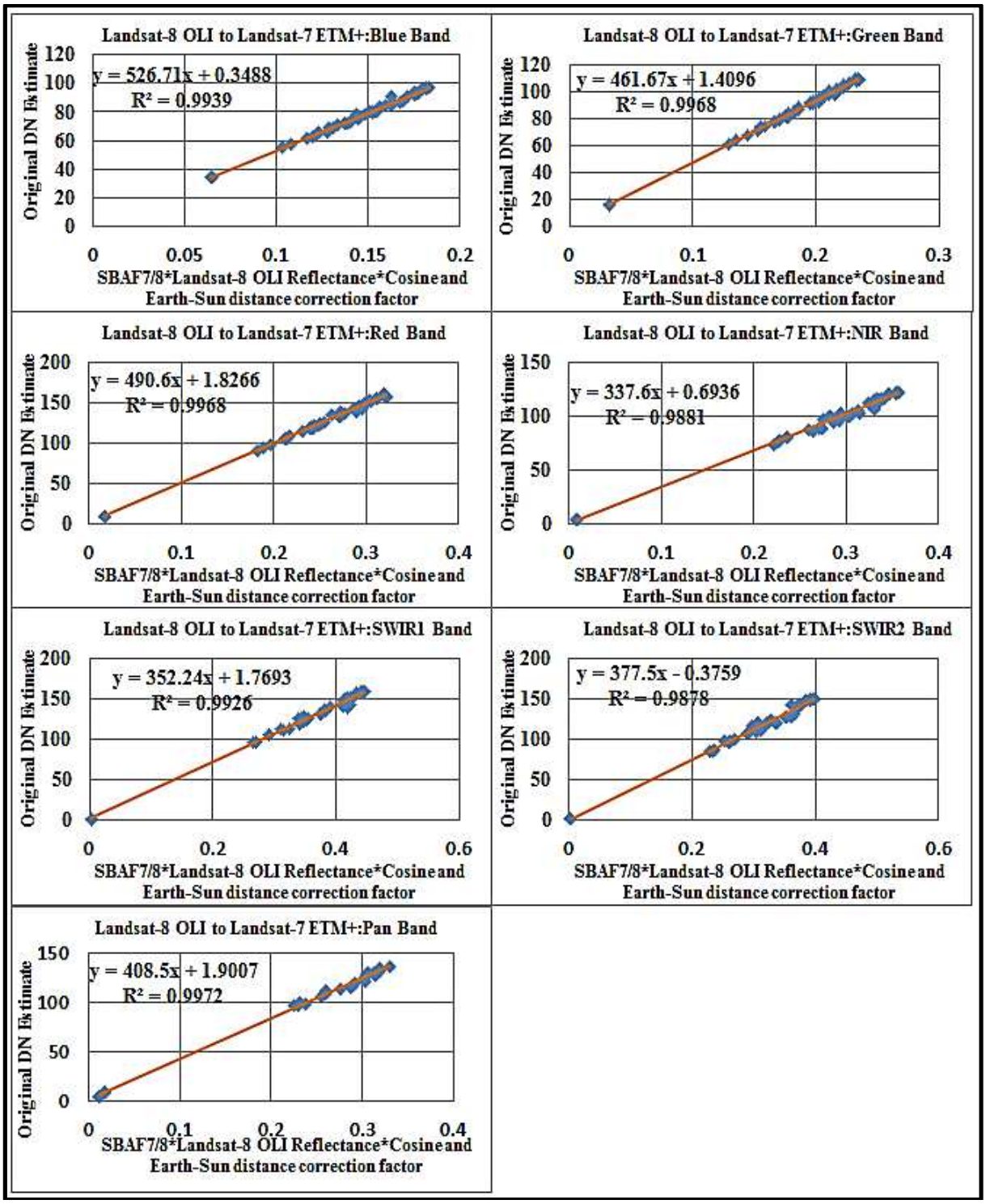

Figure 4.3. Cross-Calibration result for Landsat-8 OLI to Landsat-7 ETM+.

In order to validate if the bias term is significant, a t-test was performed at a confidence interval of 95% and the results were shown in Table 4.2.

Table 4.2. Statistical t-test for cross-calibration of Landsat-8 OLI to Landsa-7 ETM+.

		Blue Band					Green band		
	Cofficients	Std Error	t stat	P-Value		Cofficients	Std Error	t stat	P-Value
Bias	0.349	0.964	0.997	0.719	Bias	1.410	0.785	1.796	0.08
Slope	526.714	6.500	81.033	0.000	Slope	461.67	4.157	111.068	0.000
		Red Band					NIR Band		
	Cofficients	Std Error	t stat	P-Value		Cofficients	Std Error	t stat	P-Value
Bias	1.827	1.148	1.591	0.119	Bias	0.694	1.745	0.397	0.693
Slope	490.6	4.387	111.83	0.000	Slope	337.6	5.864	57.575	0
		SWIR1 Band					SWIR2 Band		
	Coefficients	Std Error	t stat	P-Value		Coefficients	Std Error	t stat	P-Value
Bias	1.769	1.774	0.997	0.325	Bias	-0.376	2.133	-0.176	0.861
Slope	352.239	4.818	73.11	0.000	Slope	377.499	6.63	56.942	0.000
		Pan Band							
	Coefficients	Std Error	t stat	P-Value					
Bias	1.901	1.136	1.674	0.106					
Slope	408.499	4.268	95.716	0.000					

At a 95% confidence interval, the result of the test shows p-values for bias in all the bands are greater than a significance level of 0.05. Hence, bias was forced through zero to find the gains and the final equation is shown below with Gain and Bias values listed in Table 4.3.

$$DN_{7,\lambda} = g_{7,\rho,\lambda} \cdot \left(SBAF_{\frac{7}{8},\rho,\lambda,ROI} \cdot \rho_{8,\lambda} \cdot \frac{1}{d^2{}_7} \cdot \frac{\cos\alpha_7}{\cos\alpha_8} \right) \tag{39}$$

Table 4.3. Reflectance cross-calibration coefficients from Landsat-OLI 8 to Landsat-7 ETM+ after forcing bias through zero.

Bands	Gain ($g_{7,\rho,\lambda}$)	Bias ($b_{7,\rho,\lambda}$)
Blue	529.02	0
Green	468.93	0
Red	497.36	0
NIR	339.86	0
SWIR1	356.88	0
SWIR2	376.37	0
PAN	415.13	0

These cross-calibration gains can be used to generate the TOA reflectance Landsat-7 ETM+ 'DN'. The equation is shown below.

$$\rho_{7,\lambda} = \frac{DN_{7,\lambda+b_{7,\rho,\lambda}}}{g_{7,\rho,\lambda}} \quad (40)$$

4.2 Landsat-7 ETM+ to Landsat-5 TM

Landsat ETM+ to TM cross-calibration was accomplished by using seven scene pairs from the Sonoran Desert and three scene pairs from Lake Tahoe. Initially, Landsat ETM+ and Landsat-5 TM RSRs are compensated using SBAFs. For cross-calibration, eight ROIs were used. Among them, seven ROIs were from the Sonoran Desert and one from Lake Tahoe as shown in Figure 4.4. Full ROI coordinates are given in appendix A.

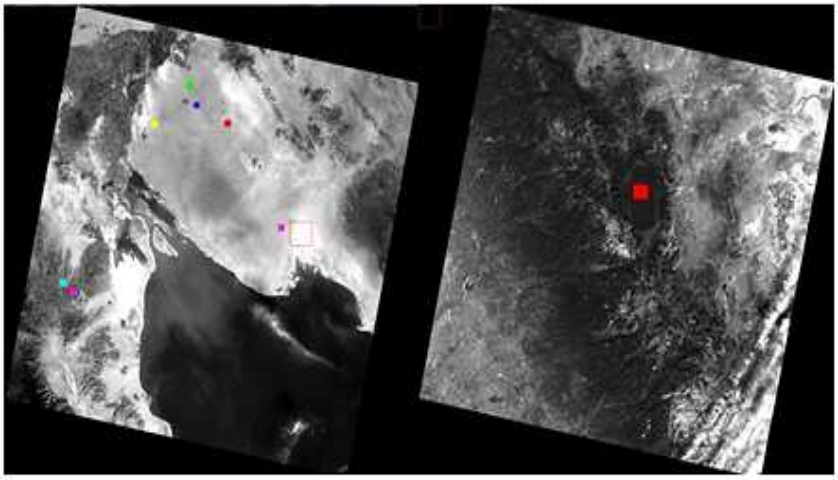

Figure 4.4. ROIs used in Landsat-7 ETM to Landsat-5 TM cross-calibration.

4.2.1 Scene Pairs

Cross-Calibration of the Landsat-7 ETM+ to the Landsat-5 TM sensor was achieved using eight scene pairs. Out of the eight, six good quality, cloud-free scene pairs were from the Sonoran Desert and three were from Lake Tahoe. All of the scene pairs are nearly coincident collections with a time difference of eight days in acquisition as shown in Table 4.4.

Table 4.4. Scene pairs used in Landsat-7 ETM+ to Landsat-5 TM cross-calibration.

Number of Scene Pair Used	Scene pair IDs	Time Differences	ROI Info
Scene Pair-1	LT50380381999250XXX04	8 days	Refer Table A2 L-7 to L-5 Sonoran ROI 1-7 in Appendix A.
	LE70380381999258EDC00		
Scene Pair-2	LT50380381999282XXX01	8 days	Refer Table A2 L-7 to L-5 Sonoran ROI 1-7 in Appendix A.
	LE70380381999290EDC00		
Scene Pair-3	LT50380382000125XXX01	8 days	Refer Table A2 L-7 to L-5 Sonoran ROI 1-7 in Appendix A.
	LE70380382000117EDC00		
Scene Pair-4	LT50380382000269XXX02	8 days	Refer Table A2 L-7 to L-5 Sonoran ROI 1-7 in Appendix A.
	LE70380382000261EDC00		
Scene Pair-5	LT50380382001159XXX02	8 days	Refer Table A2 L-7 to L-5 Sonoran ROI 1-7 in Appendix A.
	LE70380382001167EDC00		
Scene Pair-6	LT50380382002226LGS01	8 days	Refer Table A2 L-7 to L-5 Sonoran ROI 1-7 in Appendix A.
	LE70380382002234EDC00		
Scene Pair-7	LT50380382003117LGS01	8 days	Refer Table A2 L-7 to L-5 Sonoran ROI

	LE70380382003013EDC00		1-7 in Appendix A.
Scene Pair-8	LT50430331999269XXX01	8 days	Refer Table A2 L-7 to L-5 Lake Tahoe ROI1 in Appendix A.
	LE70430331999277EDC00		
Scene Pair-9	LT50430332000208XXX02	8 days	Refer Table A2 L-7 to L-5 Lake Tahoe ROI1 in Appendix A
	LE70430332000200EDC00		
Scene Pair-10	LT50430332001226LGS02	8 days	Refer Table A2 L-7 to L-5 Lake Tahoe ROI1 in Appendix A
	LE70430332001218EDC00		
Scene Pair-11	LT50430332002245LGS01	8 days	Refer Table A2 L-7 to L-5 Lake Tahoe ROI1 in Appendix A
	LE70430332002237EDC00		

4.2.2 Results

The response of Landsat-7 ETM+ was plotted against Landsat-5 TM for the matching band pairs by accounting for their spectral differences, and a linear regression line, shown in orange, was fitted to determine the cross-calibration gain and bias term as shown in Figure 4.5.

$$X - \text{axis} = \text{SBAF}_{\frac{5}{7},\rho,\lambda,\text{ROI}} \cdot \rho_{7,\lambda} \cdot \frac{d^2{}_7}{d^2{}_5} \cdot \frac{\cos\alpha_5}{\cos\alpha_7}$$

$$Y - \text{axis} = \text{DN}_{5,\lambda} = L_{5,\lambda} \cdot \left(\left(\frac{G_{5,\lambda,\text{Current}-\text{CPF\_gains(t)}}}{G_{5,\lambda,\text{Corrected linear drift\_ gains(t)}}} \right) \cdot G_{\frac{L7}{L5},\lambda,\text{June1,1999}} \right)$$

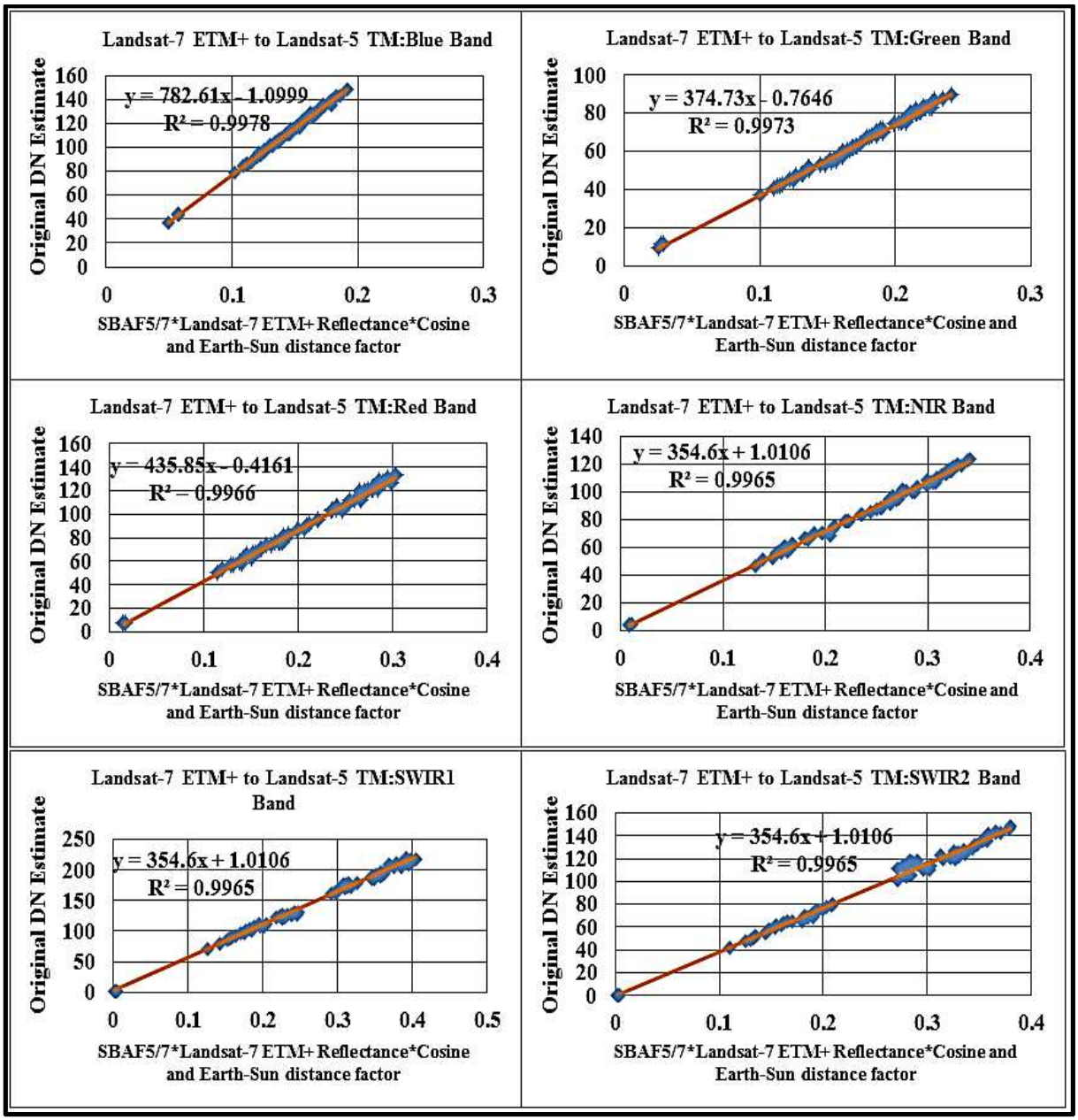

Figure 4.5. Cross-Calibration result for Landsat-7 ETM+ to Landsat-5 TM.

In order to validate if the bias term is significant, a t-test was performed at a confidence interval of 95% and the results were shown in Table 4.5.

Table 4.5. Statistical t-test for cross-calibration of Landsat-7 ETM+ to Landsat-5 TM.

		Blue Band					Green Band		
	Coefficients	Std Error	t Stat	P-value		Coefficients	Std Error	t Stat	P-value
Bias	-1.100	0.634	-1.735	0.087	Bias	-0.765	0.408	-1.872	0.065
Slope	782.614	4.300	182.009	0.000	Slope	374.732	2.299	162.976	0.000
		Red Band					NIR Band		
	Coefficients	Std Error	t Stat	P-value		Coefficients	Std Error	t Stat	P-value
Bias	-0.416	0.669	-0.622	0.536	Bias	1.011	0.617	1.638	0.106
Slope	435.848	2.996	145.485	0.000	Slope	354.603	2.465	143.862	0.000
		SWIR1 Band					SWIR2 Band		
	Coefficients	Std Error	t Stat	P-value		Coefficients	Std Error	t Stat	P-value
Bias	2.240	1.145	1.957	0.054	Bias	-0.295	1.000	-0.295	0.769
Slope	540.364	3.943	137.036	0.000	Slope	385.694	3.762	102.514	0.000

At a 95% confidence interval, the result of the test shows p-values for bias in all the bands are greater than a significance level of 0.05. Hence, bias was forced through zero to find the gains and the final equation is shown below with Gain and Bias values listed in Table 4.6.

$$DN_{5,\lambda} = g_{5,\rho,\lambda} \cdot \left(SBAF_{\frac{5}{7},\rho,\lambda,ROI} \cdot \rho_{7,\lambda} \cdot \frac{d^2{}_7}{d^2{}_5} \cdot \frac{\cos\alpha_5}{\cos\alpha_7} \right) \tag{41}$$

Table 4.6. Reflectance cross-calibration coefficients from Landsat-7 ETM+ to Landsat-5TM after forcing bias through Zero.

Bands	Gain ($g_{5,\rho,\lambda}$)	Bias ($b_{5,\rho,\lambda}$)
Blue	775.30	0
Green	370.59	0
Red	434.08	0
NIR	358.43	0
SWIR1	547.57	0
SWIR2	384.66	0

These cross-calibration gains can be used to generate the TOA reflectance Landsat-5 TM 'DN'. The equation is shown below.

$$\rho_{5,\lambda} = \frac{DN_{5,\lambda+b_{7,\rho,\lambda}}}{g_{5,\rho,\lambda}} \tag{42}$$

4.3 Landsat-5 TM to Landsat-4 TM

Initially, Landsat-5 TM and Landsat-4 TM RSRs are compensated using SBAFs. All the SBAFs are given in Appendix C. A total of 44 ROIs were selected from 11 locations as shown in Figure 4.6, and full ROI coordinates are in appendix A.

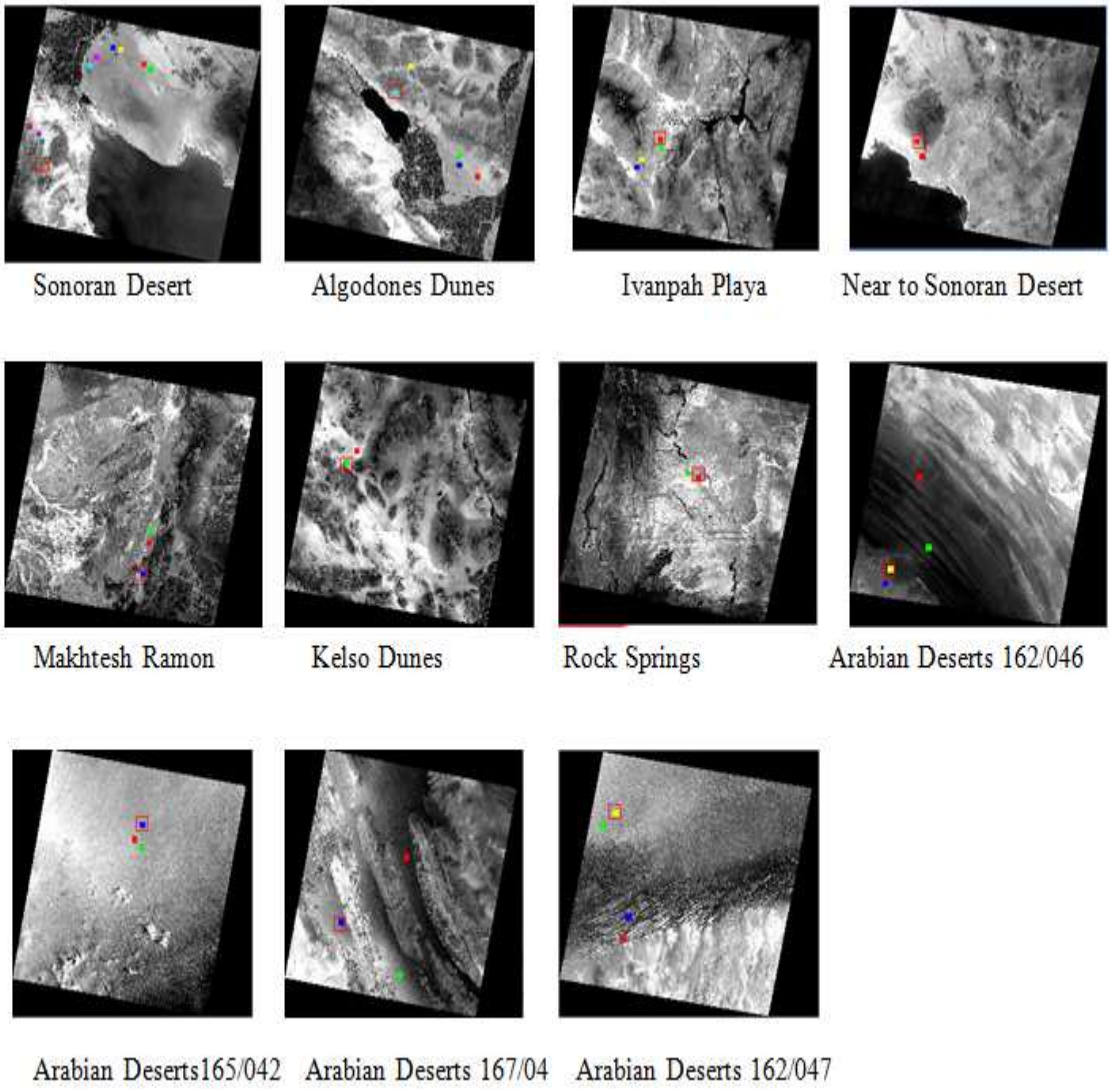

Figure 4.6. ROIs used in Landsat-5 TM to Landsat-4 TM cross-calibration.

4.3.1 Scene Pairs

Landsat-5 TM to Landsat-4 TM cross-calibration was accomplished using 31 scene pairs from the following locations: one from the Sonoran Desert, eight from near the Sonoran Desert, one from Makhtesh Ramon, four are from Ivanpah Playa, eight from the Arabian Deserts, one from Algodones,

two from near Algodones Dunes, two from Rocksprings, and four from Kelso Dunes. All the scenes used for cross-calibration are cloud free, and the time difference between any two scenes is eight days, as shown in Table 4.7.

Table 4.7. Scene Pairs used in Landsat-5 TM to Landsat-4 TM cross-calibration.

Number of Scene Pair Used	Scene pair IDs	Time Differences	ROI Info
Scene Pair-1	LT41740391990242XXX03	8 days	Refer Table A3 L-5 to L-4 Makhtesh Ramon ROI 1-3 in Appendix A.
	LT51740391990234XXX03		
Scene Pair-2	LT40390351989157XXX01	8 days	Refer Table A3 L-5 to L-4 Ivanpah Playa ROI 1-4 in Appendix A.
	LT50390351989149XXX02		
Scene Pair-3	LT40390351989157XXX01	8 days	Refer Table A3 L-5 to L-4 Ivanpah Playa ROI 1-4 in Appendix A.
	LT50390351989165XXX02		
Scene Pair-4	LT40390351990144XXX01	8 days	Refer Table A3 L-5 to L-4 Ivanpah Playa ROI 1-4 in Appendix A.
	LT50390351990136XXX03		
Scene Pair-5	LT40390351990144XXX01	8 days	Refer Table A3 L-5 to L-4 Ivanpah Playa ROI 1-4 in Appendix A.
	LT50390351990152XXX04		
Scene Pair-6	LT41620461990254XXX03	8 days	Refer Table A3 L-5 to L-4 Arabia 162/046 ROI 1-3 in Appendix A.
	LT51620461990246AAA03		
Scene Pair-7	LT41620461990254XXX03	8 days	Refer Table A3 L-5 to L-4 Arabia 162/046 ROI 1-3 in Appendix A.
	LT51620461990262XXX03		
	LT40380381992079XXX02	8 days	Refer Table A3 L-5 to L-4 Sonoran ROI 1-11 in

Scene Pair-8	LT50380381992071XXX02		Appendix A.
Scene Pair-9	LT40390371990144XXX03	8 days	Refer Table A3 L-5 to L-4 Algodones Dunes ROI 1-5 in Appendix A.
	LT50390371990152XXX03		
Scene Pair-10	LT40390361988155XXX01	8 days	Refer Table A3 L-5 to L-4 Kelso Dunes ROI 1-2 in Appendix A.
	LT50390361988147XXX03		
Scene Pair-11	LT40390361989157XXX02	8 days	Refer Table A3 L-5 to L-4 Kelso Dunes ROI 1-2 in Appendix A.
	LT50390361989149XXX02		
Scene Pair-12	LT40390361989157XXX02	8 days	Refer Table A3 L-5 to L-4 Kelso Dunes ROI 1-2 in Appendix A
	LT50390361989165XXX02		
Scene Pair-13	LT40390361990144XXX02	8 days	Refer Table A3 L-5 to L-4 Kelso Dunes ROI 1-2 in Appendix A.
	LT50390361990136XXX03		
Scene Pair-14	LT40380371990137XXX01	8 days	Refer Table A3 L-5 to L-4 Algodones Dunes ROI 1-5 in Appendix A.
	LT50380371990145AAA03		
Scene Pair-15	LT40380371990153XXX04	8 days	Refer Table A3 L-5 to L-4 Algodones Dunes ROI 1-5 in Appendix A.
	LT50380371990145AAA03		
Scene Pair-16	LT41620471990254XXX03	8 days	Refer Table A3 L-5 to L-4Arabia 162/046 ROI 1-2 in Appendix A.
	LT51620471990262XXX03		
Scene Pair-17	LT41650421990227XXX04	8 days	Refer Table A3 L-5 to L-4 Arabia 165/042 ROI 1-2 in Appendix A.
	LT51650421990219ISP00		
Scene Pair-18	LT41650421990227XXX04	8 days	Refer Table A3 L-5 to L-4 Arabia 165/042 ROI 1-2 in

	LT51650421990235ISP00		Appendix A.
Scene Pair-19	LT41650421990243XXX04	8 days	Refer Table A3 L-5 to L-4 Arabia 165/042 ROI 1-2 in Appendix A.
	LT51650421990235ISP00		
Scene Pair-20	LT41670421990225XXX01	8 days	Refer Table A3 L-5 to L-4 Arabia 167/042 ROI 1-3 in Appendix A.
	LT51670421990233XXX04		
Scene Pair-21	LT41670421990241AAA03	8 days	Refer Table A3 L-5 to L-4 Arabia 167/042 ROI 1-3 in Appendix A.
	LT51670421990233XXX04		
Scene Pair-22	LT40370311989207XXX02	8 days	Refer Table A3 L-5 to L-4 Rock Springs 037/031 ROI 1-2 in Appendix A.
	LT50370311989199AAA02		
Scene Pair-23	LT40370311989207XXX02	8 days	Refer Table A3 L-5 to L-4 Rock Springs 037/031 ROI 1-2 in Appendix A.
	LT50370311989215XXX02		
Scene Pair-24	LT40370381989175XXX01	8 days	Refer Table A3 L-5 to L-4 Near Sonoran Deserts ROI 1-2 in Appendix A.
	LT50370381989167XXX02		
Scene Pair-25	LT40370381989175XXX01	8 days	Refer Table A3 L-5 to L-4 Near Sonoran Deserts ROI 1-2 in Appendix A.
	LT50370381989183XXX04		
Scene Pair-26	LT40370381989207XXX02	8 days	Refer Table A3 L-5 to L-4 Near Sonoran Deserts ROI 1-2 in Appendix A.
	LT50370381989199AAA04		
Scene Pair-27	LT40370381989223XXX02	8 days	Refer Table A3 L-5 to L-4 Near Sonoran Deserts ROI 1-2 in Appendix A.
	LT50370381989231XXX02		
Scene Pair-28	LT40370381989239XXX02	8 days	Refer Table A3 L-5 to L-4 Near Sonoran Deserts ROI

	LT50370381989231XXX02		1-2 in Appendix A.
Scene Pair-29	LT40370381989239XXX02		Refer Table A3 L-5 to L-4 Near Sonoran Deserts ROI 1-2 in Appendix A.
	LT50370381989247XXX03	8 days	
Scene Pair-30	LT40370381989271XXX07		Refer Table A3 L-5 to L-4 Near Sonoran Deserts ROI 1-2 in Appendix A.
	LT50370381989263XXX03	8 days	
Scene Pair-31	LT40370381990146XXX03		Refer Table A3 L-5 to L-4 Near Sonoran Deserts ROI 1-2 in Appendix A.
	LT50370381990154XXX01	8 days	

4.3.2 Results

The response of Landsat-5 TM was plotted against Landsat-4 TM for matching band pairs by accounting for their spectral differences, and a linear regression line, shown in orange, was fitted to determine the cross-calibration gain and bias term as shown in Figure 4.7.

$$X - \text{axis} = \text{SBAF}_{\frac{4}{5},\rho,\lambda,\text{ROI}} \cdot \rho_{5,\lambda} \cdot \frac{d^2{}_5}{d^2{}_4} \cdot \frac{\cos\alpha_4}{\cos\alpha_5}$$

$$Y - \text{axis} = \text{DN}_{4,\lambda} = \left(L_{4,\lambda} \cdot G_{4,\lambda,\text{band\_Avg day1 gains}} \right)$$

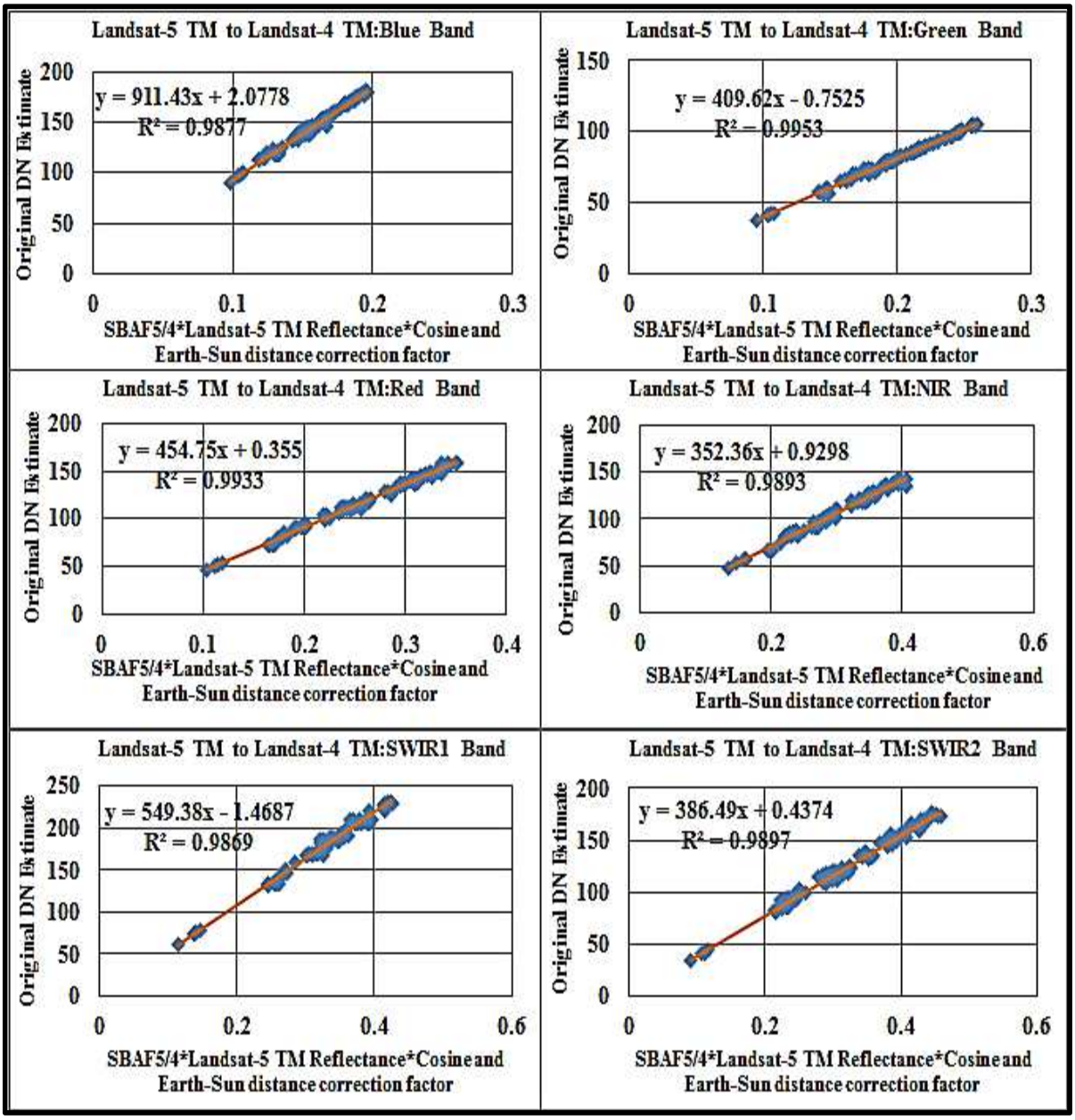

Figure 4.7. Cross-Calibration result for Landsat-5 TM to Landsat-4 TM.

In order to validate if the bias term is significant, a t-test was performed at a confidence interval of 95% and the results were shown in Table 4.8.

Table 4.8. Statistical t-test for cross-calibration of Landsat-5 TM to Landsat-4 TM.

		Blue Band					Green band		
	Coefficients	Std Error	t Stat	P-value		Coefficients	Std Error	t Stat	P-value
Bias	2.078	1.664	1.249	0.215	Bias	-0.753	0.576	-1.306	0.195
Slope	911.429	10.430	87.381	0.000	Slope	409.623	2.881	142.185	0.000
		Red Band					NIR Band		
	Coefficients	Std Error	t Stat	P-value		Coefficients	Std error	t Stat	P-value
Bias	0.355	1.004	0.354	0.724	Bias	0.930	1.151	0.808	0.421
Slope	454.748	3.828	118.805	0.000	Slope	352.362	3.768	93.520	0.000
		SWIR1 Band					SWIR2 Band		
	Coefficients	Std Error	t Stat	P-value		Coefficients	Std Error	t Stat	P-value
Bias	-1.469	2.569	-0.572	0.570	Bias	0.437	1.348	0.324	0.746
Slope	549.384	7.736	71.021	0.000	Slope	386.491	4.054	95.329	0.000

At a 95% confidence interval, the result of the test shows p-values for bias in all the bands are greater than a significance level of 0.05. Hence, bias was forced through zero to find the gains and the final equation is shown below with Gain and Bias values listed in Table 4.9.

$$DN_{4,\lambda} = g_{4,\rho,\lambda} \cdot \left(SBAF_{\frac{4}{5},\rho,\lambda,ROI} \cdot \rho_{5,\lambda} \cdot \frac{d^2{}_5}{d^2{}_4} \cdot \frac{\cos\alpha_4}{\cos\alpha_5} \right) \tag{43}$$

Table 4.9. Reflectance cross-calibration coefficients from Landsat-5 TM to Landsat-4 TM after forcing bias through zero.

Bands	Gain($g_{4,\rho,\lambda}$)	Bias($b_{4,\rho,\lambda}$)
Blue	924.32	0
Green	405.93	0
Red	456.06	0
NIR	355.33	0
SWIR1	545.07	0
SWIR2	387.76	0

These cross-calibration gains can be used to generate the TOA reflectance Landsat-4 TM 'DN'. The equation is shown below.

$$\rho_{4,\lambda} = \frac{DN_{4,\lambda+b_{4,\rho,\lambda}}}{g_{4,\rho,\lambda}} \tag{44}$$

4.4 Landsat-5 TM to Landsat-5 MSS

Landsat-5 TM and Landsat-5 MSS are spectrally different. Hence, direct band-to-band cross-comparison was not possible. Spectral band adjustment factors (SBAFs) were derived for spectrally best matching bands of Landsat-5 MSS and TM sensors using hyperspectral data acquired over the Sonoran Desert and Lake Tahoe by the Hyperion sensor on EO-1.

All the SBAFs are mentioned in Appendix C. Eight ROIs were used, seven from the Sonoran Desert and one from Lake Tahoe as shown in Figure 4.8 and full ROI coordinates are giving in appendix A.

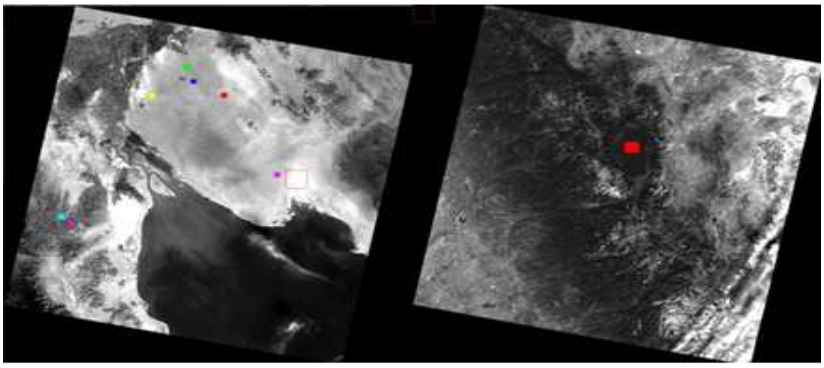

Figure 4.8. ROIs from the Sonoran Desert and Lake Tahoe.

4.4.1 Scene Pairs

Ten scene pairs were used to cross-calibrate from Landsat-5 TM to Landsat-5 MSS. Among them, seven belong to the Sonoran Desert and three belong to Lake Tahoe. All are a simultaneous collection as shown in Table 4.10.

Table 4.10. Scene pairs used in Landsat-5 TM and Landsat-5 MSS cross-calibration.

Number of Scene Pair Used	Scene pair IDs	Time Differences	ROI Info
Scene Pair-1	LM50430331984180AAA03	1 sec apart	Refer Table A4 L-5 to L-4 MSS Lake Tahoe ROI 1in Appendix A.
	LT50430331984180XXX16		
Scene Pair-2	LM50430331985214AAA03	1 sec apart	Refer Table A4 L-5

	LT50430331985214XXX05		to L-4 MSS Lake Tahoe ROI 1in Appendix A.
Scene Pair-3	LM50430331987188AAA03	1 sec apart	Refer Table A4 L-5 to L-4 MSS Lake Tahoe ROI1in Appendix A.
	LT50430331987188XXX02		
Scene Pair-4	LM50380381985275AAA03	1 sec apart	Refer Table A4 L-5 to L-4 MSS Sonoran Deserts ROI1-6 in Appendix A.
	LT50380381985275XXX04		
Scene Pair-5	LM50380381986166AAA03	1 sec apart	Refer Table A4 L-5 to L-4 MSS Sonoran Deserts ROI1-6 in Appendix A.
	LT50380381986166XXX03		
Scene Pair-6	LM50380381986326AAA03	1 sec apart	Refer Table A4 L-5 to L-4 MSS Sonoran Deserts ROI1-6 in Appendix A.
	LT50380381986326XXX04		
Scene Pair-7	LM50380381986358AAA03	1 sec apart	Refer Table A4 L-5 to L-4 MSS Sonoran Deserts ROI1-6 in Appendix A.
	LT50380381986358XXX03		
Scene Pair-8	LM50380381987281AAA03	1 sec apart	Refer Table A4 L-5 to L-4 MSS Sonoran Deserts ROI1-6 in Appendix A.
	LT50380381987281XXX03		
Scene Pair-9	LM50380381988204AAA03	1 sec apart	Refer Table A4 L-5 to L-4 MSS Sonoran Deserts ROI1-6 in Appendix A.
	LT50380381988204XXX03		
Scene Pair-10	LM50380381992199AAA03	1 sec apart	Refer Table A4 L-5 to L-4 MSS Sonoran Deserts ROI1-6 in Appendix A.
	LT50380381992199XXX02		

4.4.2 Results

The response of Landsat-5 TM was plotted against Landsat-5 MSS for the best matching band pairs by accounting for their spectral differences, and a linear regression line in orange was fitted to find gain and bias terms as shown in Figure 4.9.

$$\text{X-Axis} = \text{SBAF}_{\frac{5M}{5},\rho,\lambda,ROI} \cdot \rho_{5,\lambda} \cdot \frac{d^2{}_5}{d^2{}_{5M}} \cdot \frac{\cos\alpha_{5M}}{\cos\alpha_5}$$

$$\text{Y-Axis} = DN_{5M,\lambda} = \left(\frac{\left(\frac{L_{5M,\lambda}}{G_{5M,\lambda,\text{rad\_cross-cal}} \cdot TDF_\lambda} \right)}{G_{5M,\lambda,\text{absolute gains}}} \right) - \text{bias}_{(5M,\lambda)}$$

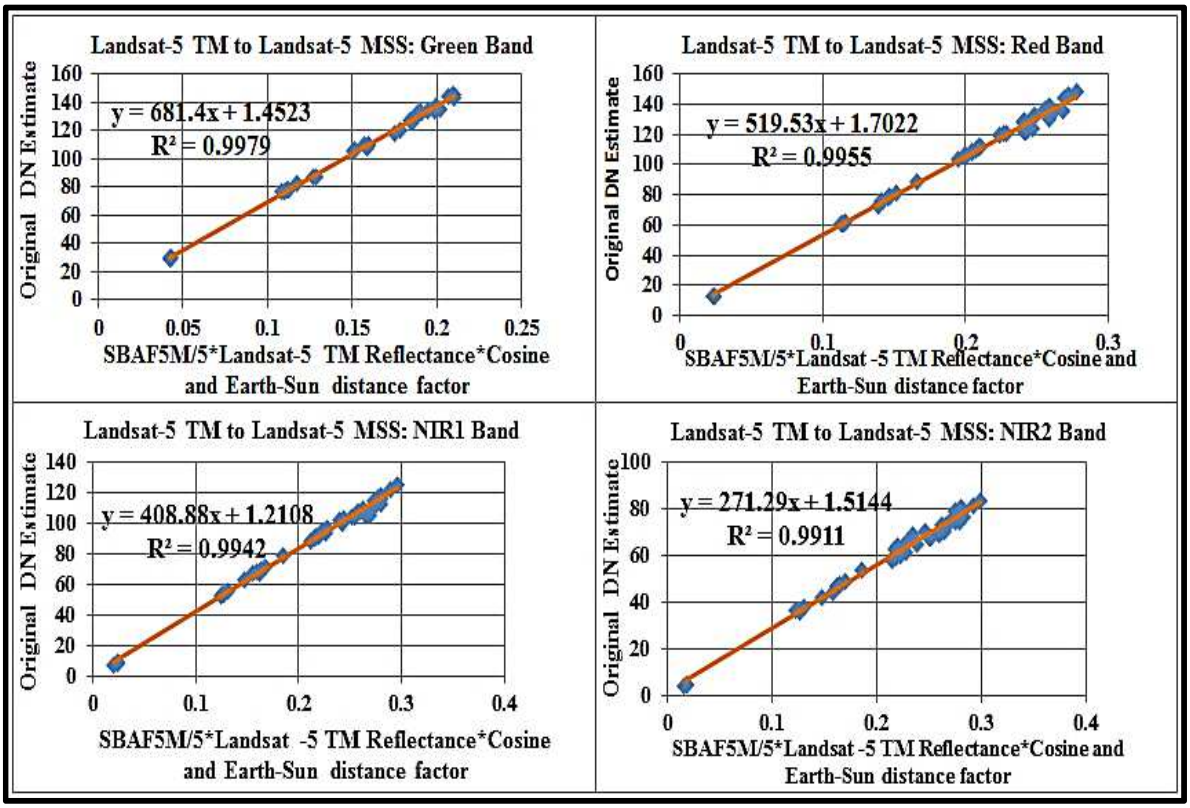

Figure 4.9. Cross-Calibration result for Landsat-5 TM to Landsat-5 MSS.

In order to validate if the bias term is significant, a t-test was performed at a confidence interval of 95% and the results were shown in Table 4.11.

Table 4.11. Statistical t-test for cross-calibration of Landsat-5 TM and Landsat-5 MSS.

		Green Band					Red Band		
	Coefficients	Std Error	t Stat	P-value		Coefficients	Std Error	t Stat	P-value
Bias	1.452	0.864	1.681	0.102	Bias	1.702	1.103	1.544	0.130
Slope	681.402	5.247	129.858	0.000	Slope	519.534	5.323	97.602	0.000
		NIR1 Band					NIR2 Band		
	Coefficients	Std Error	t Stat	P-value		Coefficients	Std Error	t Stat	P-value
Bias	1.211	1.053	1.149	0.257	Bias	1.514	0.873	1.735	0.090
Slope	408.880	4.747	86.126	0.000	Slope	271.292	3.922	69.165	0.000

At a 95% confidence interval, the result of the test shows p-values for bias in all the bands are greater than a significance level of 0.05. Hence, bias was forced through zero to find the gains and the final equation is shown below with Gain and Bias values listed in Table 4.12.

$$DN_{5M,\lambda} = g_{5M,\rho,\lambda} \cdot \left(SBAF_{\frac{5M}{5},\rho,\lambda,ROI} \cdot \rho_{5,\lambda} \cdot \frac{d^2{}_5}{d^2{}_{5M}} \cdot \frac{\cos\alpha_{5M}}{\cos\alpha_5} \right) \quad (45)$$

Table 4.12. Reflectance cross-calibration coefficients from Landsat-5 TM to Landsat-5 MSS after forcing bias through zero.

Bands	Gain ($g_{5M,\rho,\lambda}$)	Bias($b_{5M,\rho,\lambda}$)
Green	689.93	0
Red	527.31	0
NIR1	414.05	0
NIR2	277.73	0

These cross-calibration gains can be used to generate the TOA reflectance Landsat-5 MSS 'DN'. The equation is shown below.

$$\rho_{5M,\lambda} = \frac{DN_{5M,\lambda+b_{5M,\rho,\lambda}}}{g_{5M,\rho,\lambda}} \quad (46)$$

4.5 Landsat-5 MSS to Landsat-4 MSS

Initially, spectral band adjustment factors (SBAFs) were derived for spectrally best matching bands of Landsat-4 MSS and Landsat-5 MSS sensors using hyperspectral data acquired by Hyperion. All SBAFs are given in Appendix C. 21 ROIs were chosen to cross-calibrate from Landsat-5 MSS and Landsat-4 MSS. Among them, 11 are from the Sonoran Desert, four from Ivanpah Playa, one from

Lake Tahoe, one from Crater Lake, and the remaining four from White Sands as shown in Figure 4.10. Full ROI coordinates are giving in appendix A.

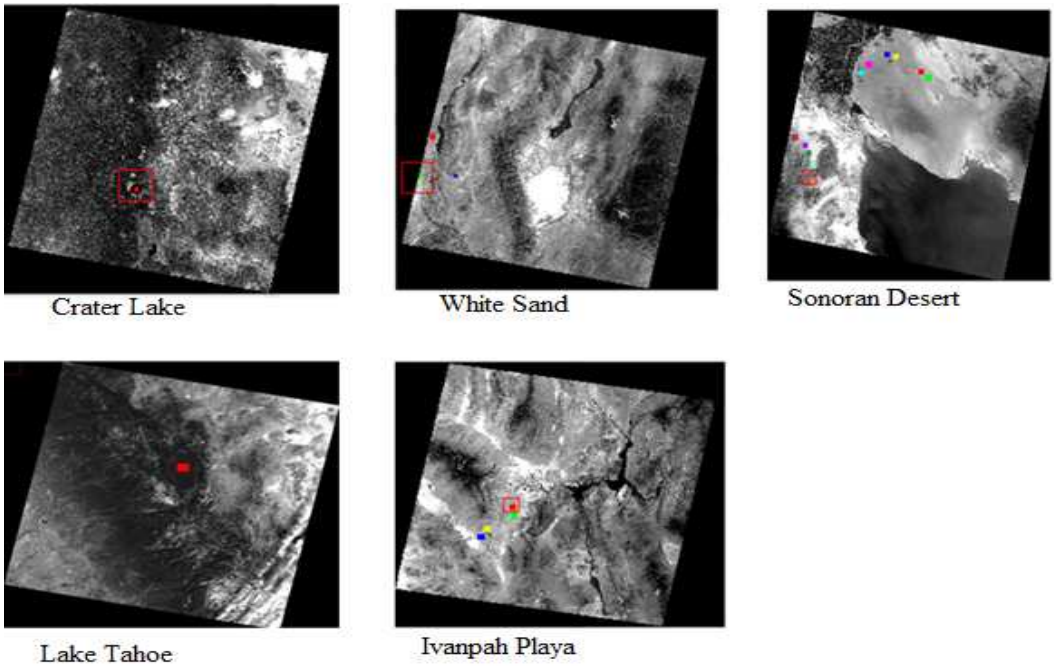

Figure 4.10. ROIs used in Landsat-5 MSS to Landsat-4 MSS cross-calibration.

4.5.1 Scene Pairs

Eight scene pairs were selected to cross-calibrate from Landsat-5 MSS to Landsat-4 MSS as shown in Table 4.13. Among them one the Sonoran Desert, two from Lake Tahoe, two from Crater Lake, one from White Sand, and two from Ivanpah Playa.

Table 4.13. Scene pairs used in Landsat-5 MSS to Landsat-4 MSS cross-calibration**.**

No. of Scene Pairs Used	Scene pairs IDs	Time Difference	ROI Info
Scene Pair-1	LM40380381992095AAA03	1 sec	Refer Table A5 L-5MSS to L-4MSS Sonoran Deserts ROI 1-11 in Appendix A.
	LM50380381992103PAC00		
Scene pair-2	LM40430331992210AAA03	1 sec	Refer Table A5 L-5MSS to L-4MSS Lake Tahoe ROI 1in Appendix A.
	LM50430431992202AAA03		
	LM40430331992210AAA03		Refer Table A5 L-5MSS

Scene pair-3	LM50430331992218AAA03	1 sec	to L-4MSS Lake Tahoe ROI 1in Appendix A.
Scene pair-4	LM40450301992208AAA03 LM50450301992216PAC04	1 sec	Refer Table A5 L-5MSS to L-4MSS Crater Lake ROI 1in Appendix A.
Scene pair-5	LM40450301992240AAA03 LM50450301992232AAA03	1 sec	Refer Table A5 L-5MSS to L-4MSS Crater Lake ROI 1in Appendix A.
Scene pair-6	LM40330371992188AAA03 LM50330371992196AAA03	1 sec	Refer Table A5 L-5MSS to L-4MSS White Deserts ROI 1-4 in Appendix A.
Scene pair-7	LM40390351986277AAA03 LM50390351986285AAA03	1 sec	Refer Table A5 L-5MSS to L-4MSS Ivanpah Playa ROI 1-4 in Appendix A.
Scene pair-8	LM40390351986309AAA03 LM50390351986317AAA03	1 sec	Refer Table A5 L-5MSS to L-4MSS Ivanpah Playa ROI 1-4 in Appendix A.

4.5.2 Results

The response of Landsat-5 MSS was plotted against Landsat-4 MSS for the best matching band pairs by accounting for their spectral differences, and a linear regression line, shown in orange, was fitted to determine the cross-calibration gain and bias terms as shown in Figure 4.11.

$$\text{X-Axis} = \text{SBAF}_{\frac{4M}{5M},\rho,\lambda,\text{ROI}} \cdot \rho_{5M,\lambda} \cdot \frac{d^2{}_{5M}}{d^2{}_{4M}} \cdot \frac{\cos\alpha_{4M}}{\cos\alpha_{5M}}$$

$$\text{Y-Axis} = \text{DN}_{4M,\lambda} = \left(\frac{\left(\frac{L_{4M,\lambda}}{G_{4M,\lambda,\text{rad\_cross-cal}} \cdot \text{TDF}_{\lambda}} \right)}{G_{4M,\lambda,\text{absolute gains}}} \right) - \text{bias}_{(5M,\lambda)}$$

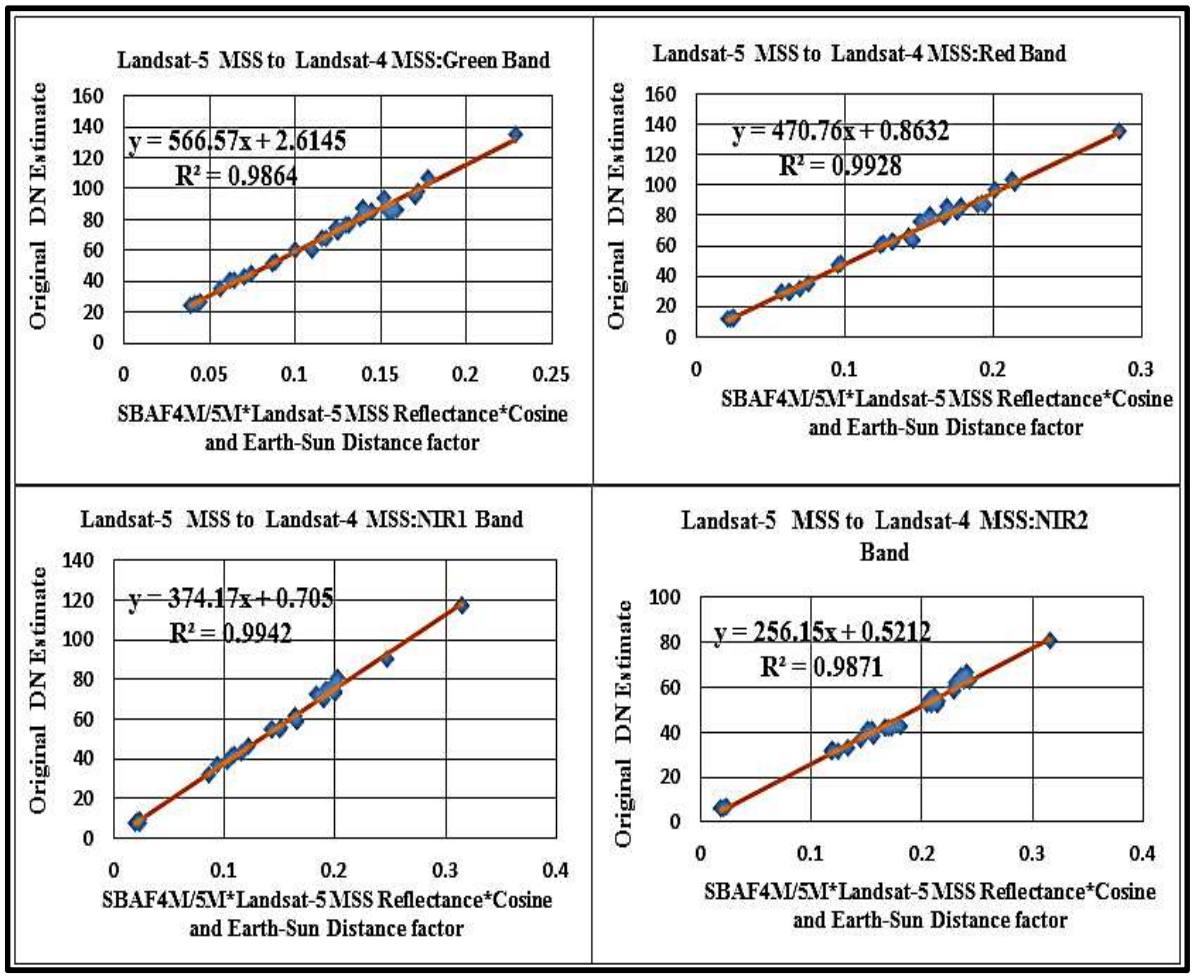

Figure 4.11. Cross-Calibration result for Landsat-5 MSS to Landsat-4 MSS.

In order to validate if the bias term is significant, a t-test was performed at a confidence interval of 95% and the results were shown in Table 4.14.

Table 4.14. Statistical t-test for cross-calibration of Landsat-5 MSS and Landsat-4 MSS.

		Green Band					Red Band		
	Coefficients	Std Error	t Stat	P-value		Coefficients	Std Error	t Stat	P-value
Bias	2.615	1.451	1.802	0.081	Bias	0.863	1.037	0.833	0.411
Slope	566.571	11.596	48.857	0.000	Slope	470.758	6.979	67.453	0.000
		NIR1 Band					NIR2 Band		
	Coefficients	Std Error	t Stat	P-value		Coefficients	Std Error	t Stat	P-value
Bias	0.705	0.849	0.830	0.412	Bias	0.521	0.937	0.556	0.582
Slope	374.171	4.973	75.234	0.000	Slope	256.146	5.087	50.349	0.000

At a 95% confidence interval, the result of the test shows p-values for bias in all the bands are greater than a significance level of 0.05. Hence, bias was forced through zero to find the gains and the final equation is shown below with Gain and Bias values listed in Table 4.15.

$$DN_{4M,\lambda} = g_{4M,\rho,\lambda} \cdot \left(SBAF_{\frac{4M}{5M},\rho,\lambda,ROI} \cdot \rho_{5M,\lambda} \cdot \frac{d^2{}_{5M}}{d^2{}_{4M}} \cdot \frac{\cos\alpha_{4M}}{\cos\alpha_{5M}} \right) \quad (472)$$

Table 4.15. Reflectance cross-calibration coefficients from Landsat-5 MSS to Landsat-4 MSS after forcing bias through Zero.

Bands	Gain ($g_{4M,\rho,\lambda}$)	Bias ($b_{4M,\rho,\lambda}$)
Green	586.08	0
Red	476.03	0
NIR1	377.94	0
NIR2	258.77	0

These cross-calibration gains can be used to generate the TOA reflectance from Landsat-4 MSS 'DN'. The equation is shown below.

$$\rho_{4M,\lambda} = \frac{DN_{4M,\lambda+b_{4,\rho,\lambda}}}{g_{4M,\rho,\lambda}} \quad (48)$$

4.6 Landsat MSS4 to Landsat MSS3

Because significant bias and stripes were seen in MSS–R and MSS–X data of Landsat-3 MSS, and due to the unavailability of MSS–P data, only MSS–A imagery was used to cross-calibrate from Landsat -4 to Landsat-3 MSS. Overall 20 ROIs were used to cross-calibrate Landsat-4 MSS to Landsat-3 MSS as shown in Figure 4.12 and full ROI coordinates are given in appendix A. SBAFs were derived from best matching bands, using Hyperion, and they are provided in Appendix C.

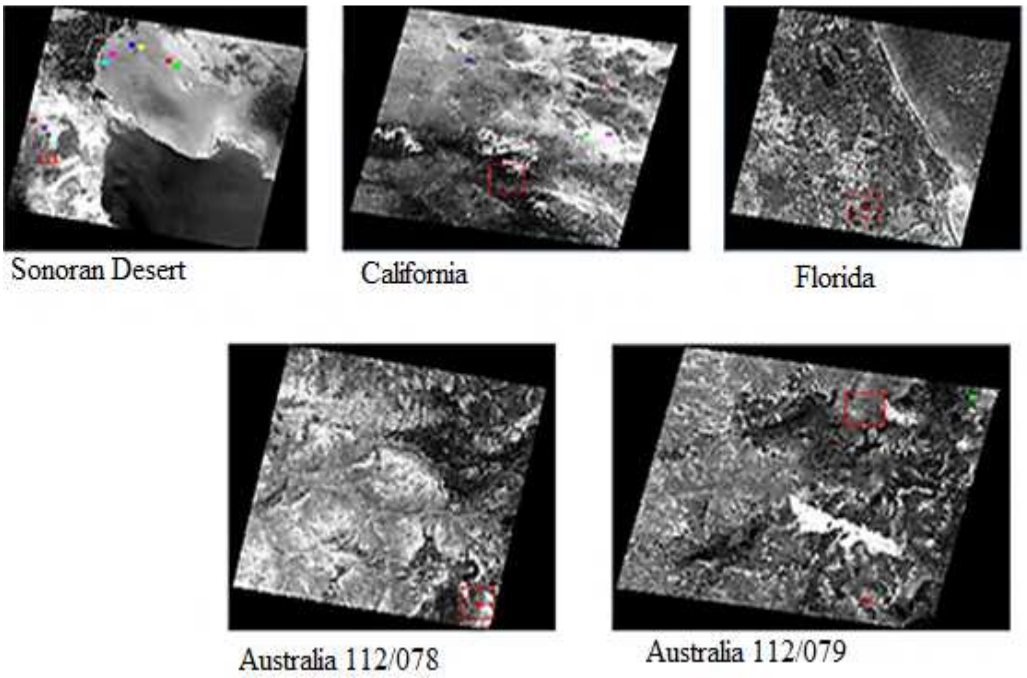

Figure 4.12. ROIs used in Landsat-4 MSS to Landsat-3 MSS cross-calibration.

4.6.1 Scene Pairs

Cross-Calibration of the Landsat-4 MSS to the Landsat-3 MSS sensor was accomplished by using six scenes as shown in Table 4.12. Out of the six, good quality, cloud-free, and near-coincident scene pairs were selected. One, from the Sonoran Desert, had a time difference of 21 days. The remaining two were near simultaneous scenes. On January 20, 1983, both MSS3 and MSS4 followed nearly synchronous orbital paths with a difference of a few seconds. This allowed the collection of simultaneous scene pairs. Among those scene pairs, two good quality scenes with no cloud cover were selected: California with Path 043/Row 036 and Florida with Path 017/Row 040. The other three scene pairs are simultaneous scenes that were selected from Australia, which had a time difference of 10 minutes. As both the sensors were in different orbits, a view angle correction was done. All the Landsat-3 MSS data belonged to a WRS1 path, whereas Landsat data belonged to a WRS2 path.

Table 4.16. Scene Pairs used for Landsat-4 MSS to Landsat-3 MSS cross-calibration**.**

Number of Scene pairs used	Scene pairs IDs	Data Type	Time Difference	ROI Info
Scene pair-1	LM30410381982365AAA03	MSSA	21 Days	Refer Table A6 L-4 MSS to L-3 MSS Sonoran Desert ROI 1-11 in Appendix A
	LM40380381983022AAA03			
Scene pair-2	LM30170401983012AAA03	MSSA	4 Seconds	Refer Table A6 L-4 MSS to L-3 MSS Florida ROI 1in Appendix A
	LM40160401983012AAA03			
Scene pair-3	LM30430361983020AAA03	MSSA	4 Seconds	Refer Table A6 L-4 MSS to L-3 MSS California ROI 1-4 in Appendix A
	LM40400361983020AAA03			
Scene pair-4	LM31190791982282AAA03	MSSA	10 Minutes	Refer Table A6 L-4 MSS to L-3 MSS Australia 112/078 , 119/078 ROI 1in Appendix A
	LM41120781982282AAA03			
Scene pair-5	LM31190801982282AAA03	MSSA	10 Minutes	Refer Table A6 L-4 MSS to L-3 MSS Australia 112/079 , 119/079 ROI 1-2 in Appendix A
	LM41120791982282AAA03			
Scene pair-6	LM31190801982282AAA03	MSSA	10 Minutes	Refer Table A6 L-4 MSS to L-3 MSS Australia 112/079 , 119/079 ROI 1-2in Appendix A
	LM41120801982282AAA03			

4.6.2 Results

The response of Landsat-4 MSS was plotted against Landsat-3 MSS for the best matching band pairs by accounting for their spectral differences, and a linear regression line, shown in orange was fitted to determine the cross-calibration gain and bias term as shown in Figure 4.13.

$$\text{X-Axis} = SBAF_{\frac{3M}{4M},\rho,\lambda,ROI} \cdot \rho_{4M,\lambda} \cdot \frac{d^2{}_{4M}}{d^2{}_{3M}} \cdot \frac{\cos\alpha_{3M}}{\cos\alpha_{4M}}$$

$$\text{Y-Axis} = DN_{3M,\lambda} = \left(\frac{\left(\frac{L_{3M,\lambda}}{G_{3M,\lambda,rad\_cross-cal} \cdot TDF_{\lambda}} \right)}{G_{3M,\lambda,absolute\ gains}} \right) - bias_{(5M,\lambda)}$$

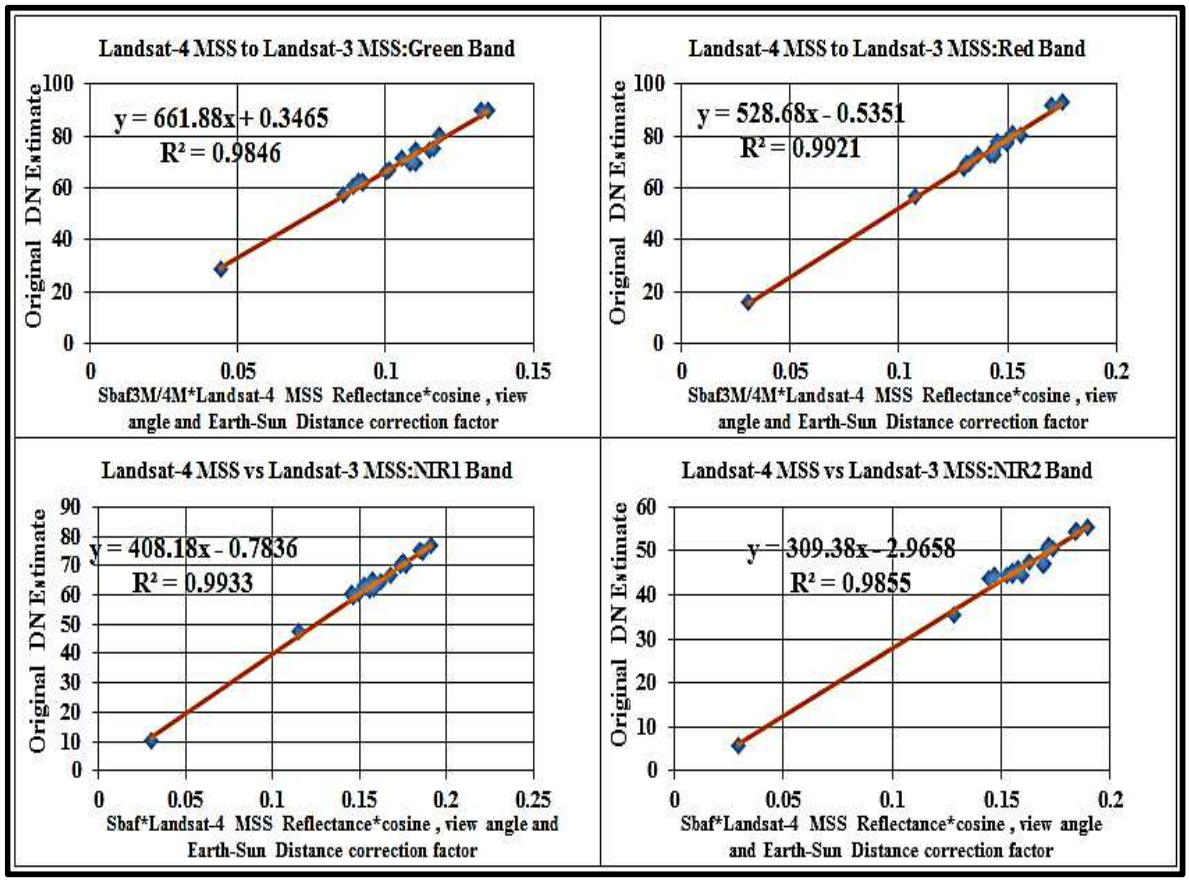

Figure 4.13. Cross-Calibration result for Landsat-4 MSS to Landsat-3 MSS.

In order to validate if the bias term is significant, a t-test was performed at a confidence interval of 95% and the results were shown in Table 4.17.

Table 4.17. Statistical test for cross-calibration of Landsat-4 MSS and Landsat-3 MSS.

		Green Band					Red Band		
	Coefficients	Std Error	t Stat	P-value		Coefficients	Std Error	t Stat	P-value
Bias	0.347	2.108	0.164	0.871	Bias	-0.535	1.621	-0.330	0.745
Slope	661.876	20.072	32.974	0.000	Slope	528.683	11.465	46.112	0.000
		NIR1 Band					NIR2 Band		
	Coefficients	Std Error	t Stat	P-value		Coefficients	Std Error	t Stat	P-value
Bias	-0.784	1.289	-0.608	0.551	Bias	-2.966	1.448	-2.048	0.056
Slope	408.184	8.121	50.264	0.000	Slope	309.383	9.100	33.998	0.000

At a 95% confidence interval, the result of the test shows p-values for bias in all the bands are greater than a significance level of 0.05. Hence, bias was forced through zero to find the gains and the final equation is shown below with Gain and Bias values listed in Table 4.18.

$$DN_{3M,\lambda} = g_{3M,\rho,\lambda} \cdot \left(SBAF_{\frac{3M}{4M},\rho,\lambda,ROI} \cdot \rho_{4M,\lambda} \cdot \frac{d^2{}_{4M}}{d^2{}_{3M}} \cdot \frac{\cos\alpha_{3M}}{\cos\alpha_{4M}} \right) \quad (49)$$

Table 4.18. Reflectance cross-calibration coefficients from Landsat-4 MSS to Landsat-3 MSS after forcing bias through Zero.

Bands	Gain ($g_{3M,\rho,\lambda}$)	Bias ($b_{3M,\rho,\lambda}$)
Green	665.12	0
Red	524.98	0
NIR1	403.36	0
NIR2	291.16	0

These cross-calibration gains can be used to generate the TOA reflectance from Landsat-3 MSS 'DN'. The equation is shown below.

$$\rho_{3M,\lambda} = \frac{DN_{3M,\lambda+b_{3M,\rho,\lambda}}}{g_{3M,\rho,\lambda}} \quad (50)$$

4.7 Landsat-3 MSS to Landsat-2 MSS

There are thousands of scenes pairs are available from Landsat-3MSS to Landsat-2 MSS, but, unfortunately, most of them belong to MSSX and MSSX-orphans. However, MSSX data has a known inconsistency. Therefore, only MSSA and MSSP data were used for cross-calibrating Landsat-3MSS to Landsat-2 MSS. Also, some Landsat-2 MSS data had stripes. Hence, ROIs are selected from non-stripy regions. 11 ROIs are from the Sonoran Desert, one from Crater Lake, four are from Ivanpah Playa, three are from Railroad Valley, two from near the Sonoran Desert, two from Algodones Dunes, and four from White Sands, 2 from Kelso Dunes were chosen and are shown in Figure 4.14. Full ROI coordinates are giving in appendix A. Spectral band adjustment factors (SBAFs) were derived for

spectrally best matching bands of Landsat-3 MSS and Landsat-2 MSS sensors using the Hyperion sensor on EO-1. All the SBAFs are given in Appendix C.

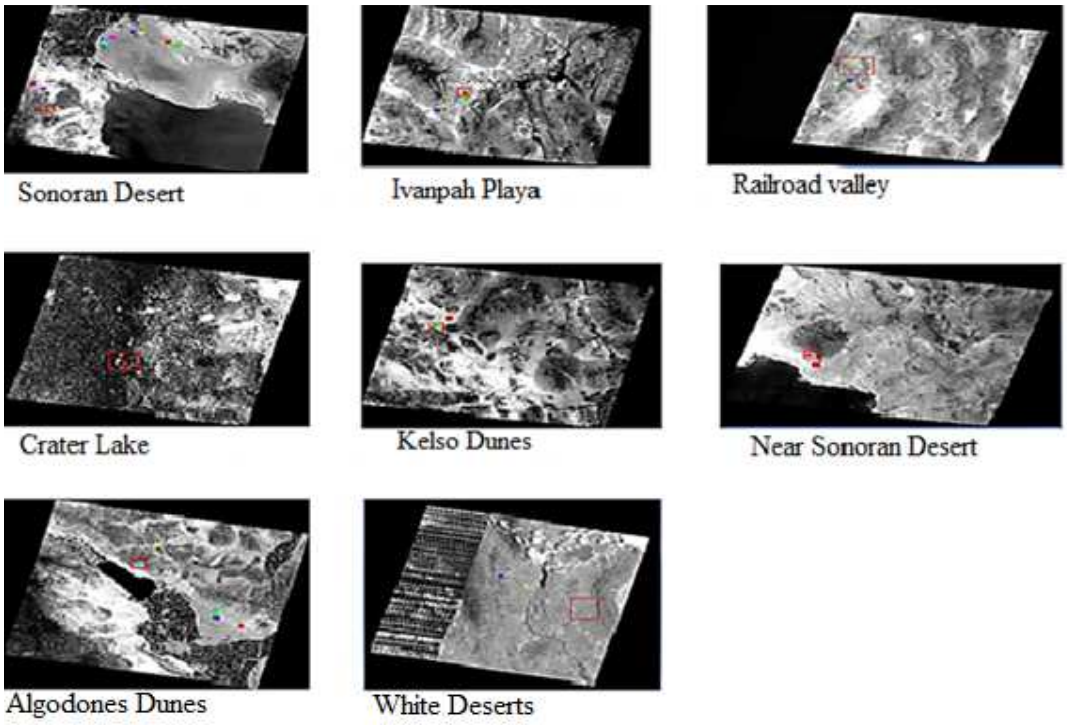

Figure 4.14. ROIs used for Landsat-3 MSS to Landsat-2 MSS cross-calibration.

4.7.1 Scene Pairs

After an exhaustive search, 10 scene pairs were found. Among them, eight belong to MSSP data type and two from Railroad valley belong to MSSA datatype as shown in Table 4.19.

Table 4.19. Scene Pairs used in Landsat-3 MSS to Landsat-2 MSS cross-calibration.

Number of Scene pairs used	Scene pairs IDs	Data Type	Time Difference	ROI Info
Scene pair-1	LM20410381980151AAA03	MSSP	9 days	Refer Table A7 L-3 MSS to L-2 MSS Sonoran Desert ROI 1-11 in Appendix A
	LM30410381980142AAA03			
Scene pair-2	LM20420351981074AAA03	MSSP	9 days	Refer Table A7 L-3 MSS to L-2 MSS Ivanpah Playa ROI 1-4 in Appendix A
	LM3420351981083AAA03			

Scene pair-3	LM20430331981237AAA03 LM30430331981246AAA03	MSSA	9 days	Refer Table A7 L-3 MSS. to L-2 MSS Rail Road valley Desert ROI 1-5 in Appendix A.
Scene pair-4	LM20430331981273AAA03 LM30430331981264AAA03	MSSA	9 days	Refer Table A7 L-3 MSS to L-2 MSS Rail Road valley Desert ROI 1-5 in Appendix A.
Scene pair-5	LM20490301980195AAA05 LM30490301980204AAA05	MSSP	9 days	Refer Table A7 L-3 MSS to L-2 MSS Crater Lake ROI 1in Appendix A.
Scene pair-6	LM20420361981074AAA03 LM30420361981083AAA03	MSSP	9 days	Refer Table A7 L-3 MSS to L-2 MSS Kelso Desert ROI 1-2 in Appendix A.
Scene pair-7	LM20400381981090AAA03 LM30400381981081AAA03	MSSP	9 days	Refer Table A7 L-3 MSS to L-2 MSS Near Sonoran Desert ROI 1-2 in Appendix A.
Scene pair-8	LM20400381981072AAA03 LM30400381981081AAA03	MSSP	9 days	Refer Table A7 L-3 MSS to L-2 MSS Near Sonoran Desert ROI 1-2 in Appendix A.
Scene pair-9	LM20420371981074AAA03 LM30420371981083AAA03	MSSP	9 days	Refer Table A7 L-3 MSS to L-2 MSS Algodones Dunes ROI 1-5 in Appendix A.
Scene pair-10	LM20360371980218AAA03 LM03603719800209AAA06	MSSP	9 days	Refer Table A7 L-3 MSS to L-2 MSS White Deserts ROI 1-4in Appendix A.

4.7.2 Results

The response of Landsat-3 MSS was plotted against Landsat-2 MSS for the best matching band pairs by accounting for their spectral difference and a linear regression line shown in orange was fitted to determine the cross-calibration gain and bias term as shown in Figure 4.15.

$$\text{X-Axis} = \text{SBAF}_{\frac{2M}{3M},\rho,\lambda,ROI} \cdot \rho_{3M,\lambda} \cdot \frac{d^2{}_{3M}}{d^2{}_{2M}} \cdot \frac{\cos\alpha_{2M}}{\cos\alpha_{3M}}$$

$$\text{Y-Axis} = DN_{2M,\lambda} = \left(\frac{\left(\frac{L_{2M,\lambda}}{G_{2M,\lambda,rad\_cross-cal} \cdot TDF_{\lambda}} \right)}{G_{2M,\lambda,absolute\ gains}} \right) - bias_{(5M,\lambda)}$$

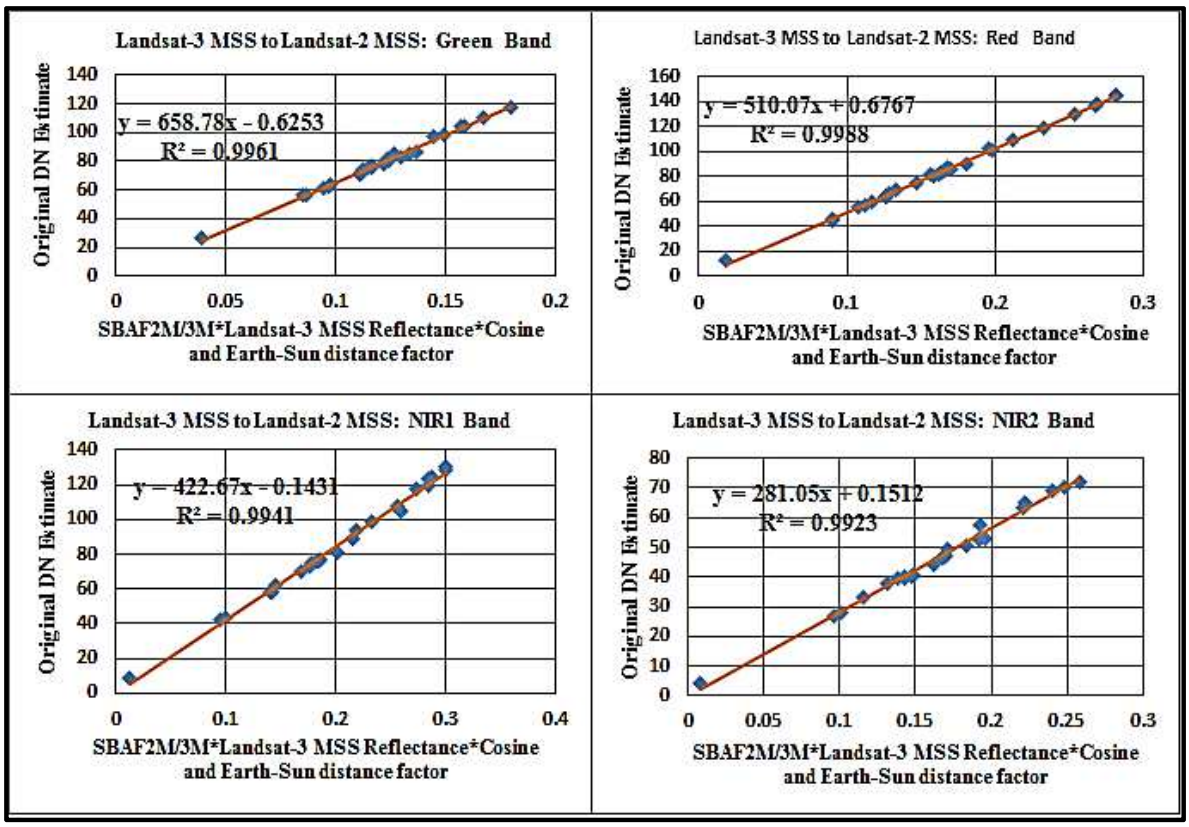

Figure 4.15. Cross-Calibration result for Landsat-3 MSS to Landsat -2 MSS .

In order to validate if the bias term is significant, a t-test was performed at a confidence interval of 95% and the results were shown in Table 4.20.

Table 4.20. Statistical t-test for cross-calibration of Landsat-3 MSS to Landsat-2 MSS.

		Green Band					Red band		
	Coefficients	Std Error	t Stat	P-value		Coefficients	Std Error	t Stat	P-value
Bias	-0.625	1.070	-0.584	0.565	Bias	0.677	0.623	1.086	0.287
Slope	658.785	8.566	76.906	0.000	Slope	510.065	3.469	147.015	0.000
		NIR1 Band					NIR2 Band		
	Coefficients	Std Error	t Stat	P-value		Coefficients	Std Error	t Stat	P-value
Bias	-0.143	1.469	-0.097	0.923	Bias	0.151	0.898	0.168	0.868
Slope	422.667	6.812	62.046	0.000	Slope	281.052	5.147	54.605	0.000

At a 95% confidence interval, the result of the test shows p-values for bias in all the bands are greater than a significance level of 0.05. Hence, bias was forced through zero to find the gains and the final equation is shown below with Gain and Bias values listed in Table 4.21.

$$DN_{2M,\lambda} = g_{2M,\rho,\lambda} \cdot \left(SBAF_{\frac{2M}{3M},\rho,\lambda,ROI} \cdot \rho_{3M,\lambda} \cdot \frac{d^2{}_{3M}}{d^2{}_{2M}} \cdot \frac{\cos\alpha_{2M}}{\cos\alpha_{3M}} \right) \quad (51)$$

Table 4.21. Reflectance cross-calibration coefficients from Landsat-3 MSS to Landsat-2 MSS after forcing bias through Zero.

Bands	Gain($g_{2M,\rho,\lambda}$)	Bias($b_{2M,\rho,\lambda}$)
Green	653.92	0
Red	513.59	0
NIR1	422.04	0
NIR2	281.88	0

These cross-calibration gains can be used to generate the TOA reflectance from Landsat-2 MSS 'DN'. The equation is shown below.

$$\rho_{2M,\lambda} = \frac{DN_{2M,\lambda + b_{2M,\rho,\lambda}}}{g_{2M,\rho,\lambda}} \quad (52)$$

4.8 Landsat-2 MSS to Landsat-1 MSS

Only MSS-WBVT data were used to cross-calibrate MSS2 to MSS1 as there is no other data type available during that time. An unequal number of ROIs was chosen for each band from 'non-stripy' regions as shown in Figure 4.16. Full ROI coordinates are given in appendix A. Spectral band

adjustment factors (SBAFs) were derived for the spectrally best matching bands of Landsat-2 MSS and Landsat-1 MSS. All the SBAFs are given in Appendix C.

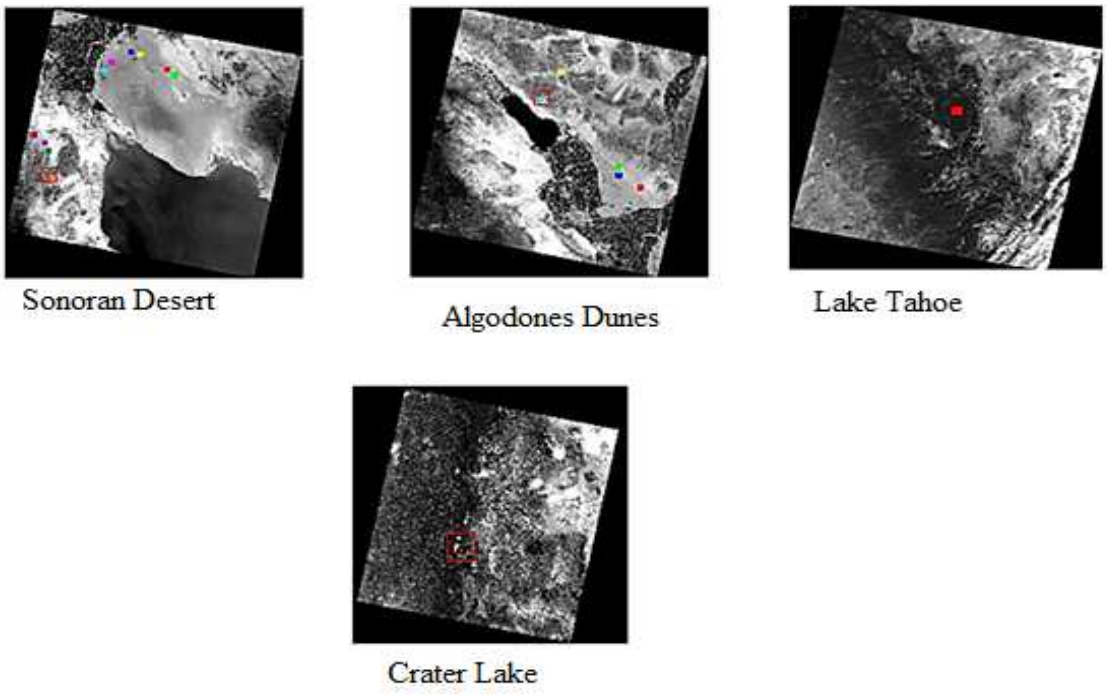

Figure 4.16. ROIs used in Landsat-2 MSS to Landsat-1 MSS cross-calibration.

4.8.1 Scene Pairs

After an exhaustive search, there were 29 scene pairs available from Landsat-2MSS to Landsat-1MSS. However, due to stripes, only nine scene pairs were used, all of them belong to MSS-WBVT data as shown in Table 4.22. All they are from the WRS1 path.

Table 4.22. Scene Pairs used in Landsat-2 MSS to Landsat-1 MSS cross-calibration.

Number of Scene pairs Used	Scene pair ID's	Data Type	Time Difference	ROI Info
Scene pair-1	LM10410381976217AAA03	MSSX-WBVT	9 days	Refer Table A8 L-2 MSS to L-1 MSS Sonoran Desert ROI 1-11 in Appendix A.
	LM20410381976226GDS02			
Scene pair-2	LM10410381977154GDS04			Refer Table A8 L-2 MSS to L-1 MSS Sonoran Desert ROI 1-11
	LM20410381977148GDS04			

		MSSX-WBVT	6 days	in Appendix A.
Scene pair-3	LM10410381977244GDS04			Refer Table A8 L-2 MSS to L-1 MSS Sonoran Desert ROI 1-11 in Appendix A
	LM20410381977238GDS03	MSSX-WBVT	6 days	
Scene pair-4	LM10490301975212GDS03			Refer Table A8 L-2 MSS to L-1 MSS Crater Lake ROI 1in Appendix A.
	LM20490301975221GDS03	MSSX-WBVT	9 days	
Scene pair-5	LM10490301976207GDS03			Refer Table A8 L-2 MSS to L-1 MSS Crater Lake ROI 1in Appendix A.
	LM20490301975198GDS03	MSSX-WBVT	9 days	
Scene pair-6	LM10410371975186AAA02			Refer Table A8 L-2 MSS to L-1 MSS Algodones Dunes ROI 1-4 in Appendix A.
	LM20410371975177AAA02	MSSX-WBVT	9 days	
Scene pair-7	LM10410371976289GDS03			Refer Table A8 L-2 MSS to L-1 MSS Algodones Dunes ROI 1-4 in Appendix A.
	LM20410371975280GDS02	MSSX-WBVT	9 days	
Scene pair-8	LM10410371976289GDS03			Refer Table A8 L-2 MSS to L-1 MSS Algodones Dunes ROI 1-4 in Appendix A.
	LM20410371975298GDS03	MSSX-WBVT	9 days	
Scene pair-9	LM10460331976204GDS03			Refer Table A8 L-2 MSS to L-1 MSS Lake Tahoe ROI 1 in Appendix A.
	LM20460331976195GDS03	MSSX-WBVT	9 days	

4.8.2 Results

The response of Landsat-2 MSS was plotted against Landsat-1 MSS for the best matching band pairs by accounting for their spectral differences and a linear regression line shown in orange was fitted to find the gain term as shown in Figure 4.17.

$$\text{X-Axis} = SBAF_{\frac{1M}{2M},\rho,\lambda,ROI} \cdot \rho_{2M,\lambda} \cdot \frac{d^2{}_{2M}}{d^2{}_{1M}} \cdot \frac{\cos\alpha_{1M}}{\cos\alpha_{2M}}$$

$$\text{Y-Axis} = DN_{1M,\lambda} = \left(\frac{\left(\frac{L_{1M,\lambda}}{G_{1M,\lambda,rad\_cross-cal} \cdot TDF_{\lambda}} \right)}{G_{1M,\lambda,absolute\ gains}} \right) - bias_{(5,\lambda)}$$

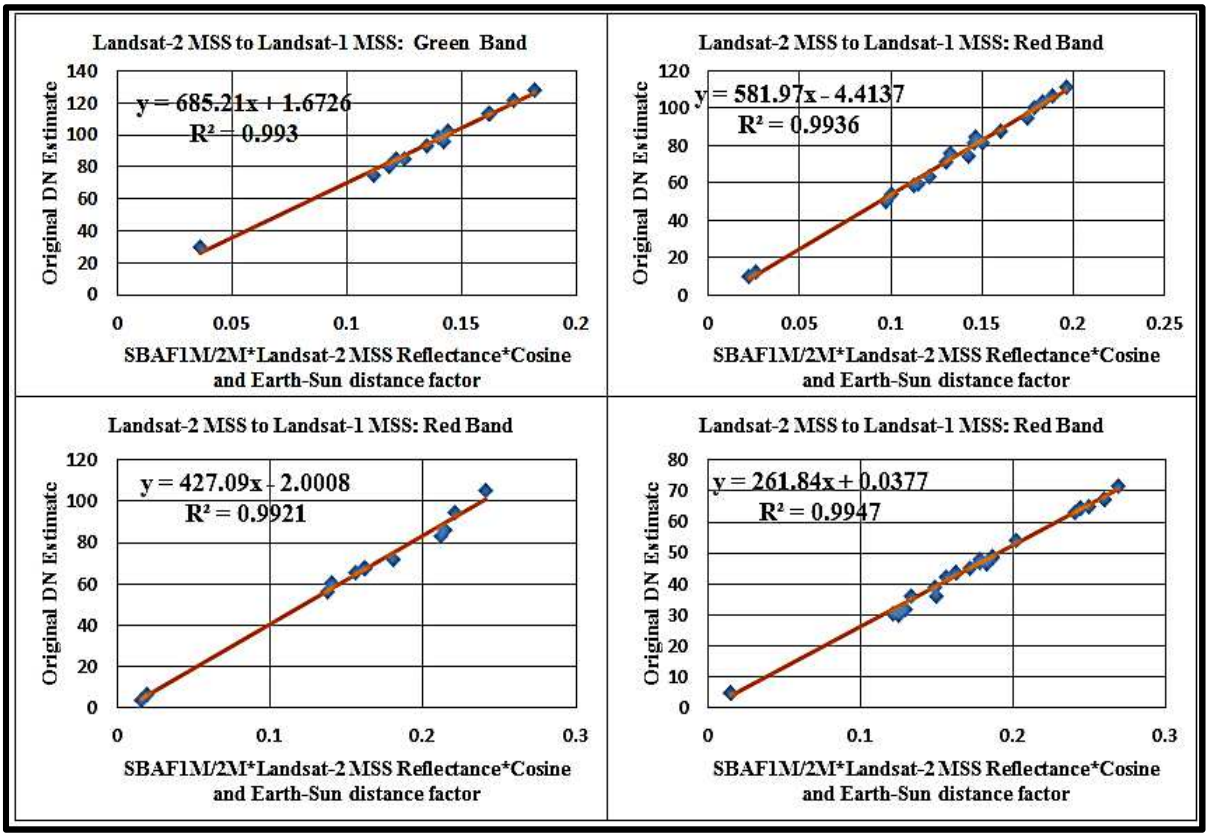

Figure 4.17. Cross-Calibration Result for Landsat-2 MSS and Landsat-1 MSS.

In order to validate if the bias term is significant, a t-test was performed at a confidence interval of 95% and the results were shown in Table 4.23.

Table 4.23. Statistical t-test for cross-calibration of Landsat-2 MSS to Landsat-1 MSS.

		Green Band					Red Band		
	Coefficients	Std Error	t Stat	P-value		Coefficients	Std Error	t Stat	P-value
Bias	1.673	2.417	0.692	0.503	Bias	-4.414	1.600	-2.758	0.013
slope	685.205	17.354	39.483	0.000	slope	581.966	11.370	51.183	0.000
		NIR1 Band					NIR2 Band		
	Coefficients	Std Error	t Stat	P-value		Coefficients	Std Error	t Stat	P-value
Bias	-2.001	2.049	-0.977	0.352	Bias	0.038	0.745	0.051	0.960
slope	427.093	12.078	35.363	0.000	slope	261.837	3.993	65.576	0.000

At a 95% confidence interval, except for red band, the result of the test shows p-values for other bands are greater than a significance level of 0.05. Hence, bias was forced through zero for all bands except 'red band' to find the gains shown in Table 4.24 and final equation is shown below.

$$DN_{1M,\lambda} = g_{1M,\rho,\lambda} \cdot \left(SBAF_{\frac{1M}{2M},\rho,\lambda,ROI} \cdot \rho_{2M,\lambda} \cdot \frac{d^2{}_{2M}}{d^2{}_{1M}} \cdot \frac{\cos\alpha_{1M}}{\cos\alpha_{2M}} \right) + b_{1M,\rho,\lambda} \quad (53)$$

Table 4.24. Reflectance cross-calibration coefficients from Landsat-2 MSS to Landsat-1 MSS after forcing bias through Zero.

Bands	Gain ($g_{1M,\rho,\lambda}$)	Bias ($b_{1M,\rho,\lambda}$)
Green	696.83	0
Red	581.97	-4.414
NIR1	416.32	0
NIR2	262.03	0

These cross-calibration gains can be used to generate the TOA reflectance from Landsat-1 MSS 'DN'. The equation is shown below.

$$\rho_{1M,\lambda} = \frac{DN_{1M,\lambda + b_{1M,\rho,\lambda}}}{g_{1M,\rho,\lambda}} \quad (54)$$

Chapter 5 Validation of cross-calibration gains and biases

The primary objective of this chapter to validate all the cross-calibration gains and biases, which have been calculated for the Landsat sensors. In order to verify the cross-calibration of gains and biases over the lifetime, trending of all sensors is required. The temporal reflectance of all sensors is plotted with respect to Landsat-8 OLI on the same radiometric scale. The idea is that if the region of interest is stable temporally and the data collected from that sensor are abundant, then any change observed in the sensor response over the long-term would be due to the degradation of the instrument itself [3]. Many studies have shown that bright sites like the Sonoran Desert, Algodones Dunes, Libya 4, etc., are very stable sites and usable for checking long-term trending of satellite sensors.

5.1 Validation using Algodones Dunes

In this work, the Algodones Dunes [41] [42] is used as a test site to validate the cross-calibration gains. Fortunately, there are different data formats of MSS available in the USGS archive for this site. The Algodones Dunes is situated 100 meters above sea level and centered at 32.94° latitude and -115.06° longitude. As discussed in Chapter 3 and Chapter 4, cross-calibration between each pair of sensors was done and the gain for each sensor and for each band was found through regression analysis. The gain terms of all sensors and bias term in Landsat-1 MSS can be validated by observing the effect after implementing it over the instrument's lifetime. The implementation was done for TOA reflectance for one of the PICS, i.e. Algodones Dunes [43], shown in Figure 5.1. In the final step, TOA reflectance of all sensors is plotted on the same scale against time. The data was plotted for the best matching spectral band between earlier sensors to the most recent sensors.

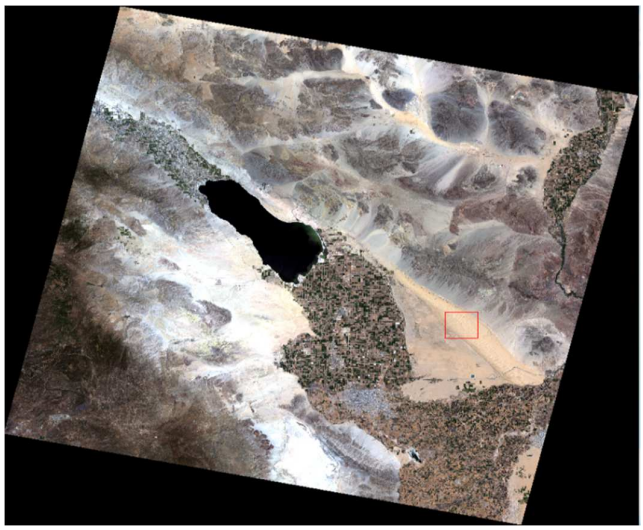

Figure 5.1. Algodones Dunes.

5.2 Statistical analysis using z-test

A z-test is performed to check if significant differences exist between TOA reflectance means of all sensors for each band. For a large dataset, according to the center limit theorem, the samples are considered to be normally distributed [44]. Suppose, if there are two populations where the first population has unknown mean μ_1 and known variance$\sigma_1{}^2$, and the second population has unknown mean μ_2 and unknown variance $\sigma_2{}^2$and if the assumption is that the two populations are normal, then the condition of the central limit theorem applies.

The two-sided hypothesis is given by

$$H_0: \mu_1 = \mu_2$$

$$H_1: \mu_1 \neq \mu_2$$

The test procedure is always based upon the distribution of the difference in the sample means $\bar{X}_1$-$\bar{X}_2$.The distribution of $\bar{X}_1$-$\bar{X}_2$ is normal with means $\mu_1 - \mu_2$ and variance $\frac{\sigma_1{}^2}{n1}+\frac{\sigma_2{}^2}{n2}$.

i.e. $\bar{X}_1$-$\bar{X}_2$~$\left(\mu_1 = \mu_2, \frac{\sigma_1{}^2}{n1} + \frac{\sigma_2{}^2}{n2}\right)$.

Hence, if the null hypothesis $H_0: \mu_1 = \mu_2$ is true, the test statistic will have a normal distribution. So, if both distributions have normal with known variance then the test statistics is given by equation (55). Z-test compares the means of two different distributions.

$$Z = \frac{\bar{x}_1 - \bar{x}_2}{\sqrt{\frac{{\sigma_1}^2}{n1} + \frac{{\sigma_2}^2}{n2}}} \tag{553}$$

The procedure for testing $H_0: \mu_1 = \mu_2$ is to calculate the value of the test statistic Z and reject the null hypothesis if

$$Z > Z_\alpha$$

Alternatively, the P value can also be found for the test and if any test value falls below the significance value of P then the null hypothesis is rejected.

5.3 Validation equations from Landsat-8 OLI to Landsat-7 ETM+

In order to validate gains and biases, systematic validation equations are required to observe the TOA reflectance that is generated by each sensor i.e. from Landsat-8 OLI to Landsat-1 MSS. This is done by dividing original DN estimates with cross-calibration gains that were shown in Chapter 3. Earth-Sun distance and Sun elevation angle correction factors were applied to all of these calculations. All of the Landsat data were converted to equivalent OLI values by applying the spectral band adjustment factor. Equations for each sensor to find TOA reflectance are given below.

For Landsat-8 OLI

$$\rho_{8,\lambda} = M_{8,\rho,\lambda} \cdot DN_{8,\lambda} + A_{8,\rho,\lambda} \tag{56}$$

For Landsat-7 ETM+

$$\rho_{7,\lambda} = \left(\frac{DN_{7,\lambda}}{G_{\frac{8,\lambda}{7,\lambda}}} \cdot \frac{{d^2}_7}{\cos\alpha_7} \right) \cdot SBAF_{\frac{8,\lambda}{7,\lambda}} \tag{57}$$

For Landsat-5 TM

$$\rho_{5,\lambda} = \left(\frac{DN_{5,\lambda}}{G_{\frac{7,\lambda}{5,\lambda}}} \cdot \frac{{d^2}_5}{\cos\alpha_5} \right) \cdot SBAF_{\frac{8,\lambda}{5,\lambda}} \tag{58}$$

For Landsat-4 TM

$$\rho_{4,\lambda} = \left(\frac{DN_{4,\lambda}}{G_{\frac{5,\lambda}{4,\lambda}}} \cdot \frac{d^2{}_4}{\cos\alpha_4} \right) \cdot SBAF_{\frac{8,\lambda}{4,\lambda}} \quad (59)$$

For Landsat-5 MSS

$$\rho_{5M,\lambda} = \left(\frac{DN_{5M,\lambda}}{G_{\frac{5,\lambda}{5M,\lambda}}} \cdot \frac{d^2{}_{5M}}{\cos\alpha_{5M}} \right) \cdot SBAF_{\frac{8,\lambda}{5M,\lambda}} \quad (60)$$

For Landsat-4 MSS

$$\rho_{4M,\lambda} = \left(\frac{DN_{4M,\lambda}}{G_{\frac{5M,\lambda}{4M,\lambda}}} \cdot \frac{d^2{}_{4M}}{\cos\alpha_{4M}} \right) \cdot SBAF_{\frac{8,\lambda}{4M,\lambda}} \quad (61)$$

For Landsat-3 MSS

$$\rho_{3M,\lambda} = \left(\frac{DN_{3M,\lambda}}{G_{\frac{4M,\lambda}{3M,\lambda}}} \cdot \frac{d^2{}_{3M}}{\cos\alpha_{3M}} \right) \cdot SBAF_{\frac{8,\lambda}{3M,\lambda}} \quad (62)$$

For Landsat-2 MSS

$$\rho_{2M,\lambda} = \left(\frac{DN_{2M,\lambda}}{G_{\frac{3M,\lambda}{2M,\lambda}}} \cdot \frac{d^2{}_{2M}}{\cos\alpha_{2M}} \right) \cdot SBAF_{\frac{8,\lambda}{2M,\lambda}} \quad (63)$$

For Landsat-1 MSS

$$\rho_{1M,\lambda} = \left(\frac{DN_{1M,\lambda} + b_{\frac{2M,\lambda}{1M,\lambda}}}{G_{\frac{2M,\lambda}{1M,\lambda}}} \cdot \frac{d^2{}_{1M}}{\cos\alpha_{1M}} \right) \cdot SBAF_{\frac{8,\lambda}{1M,\lambda}} \quad (64)$$

Each term used in the equations were already explained in Chapter 3. Lifetime trends against time of all sensors are plotted using these equations.

5.4 Lifetime trending of all sensors

Figure 5.3.1 shows temporal TOA reflectance from Algodones Dunes for Landsat-8 OLI, Landsat-7 ETM+, Landsat-5 TM and Landsat-4 TM in the blue band. The Standard deviation showed in the box represents that the data is having very less variance.

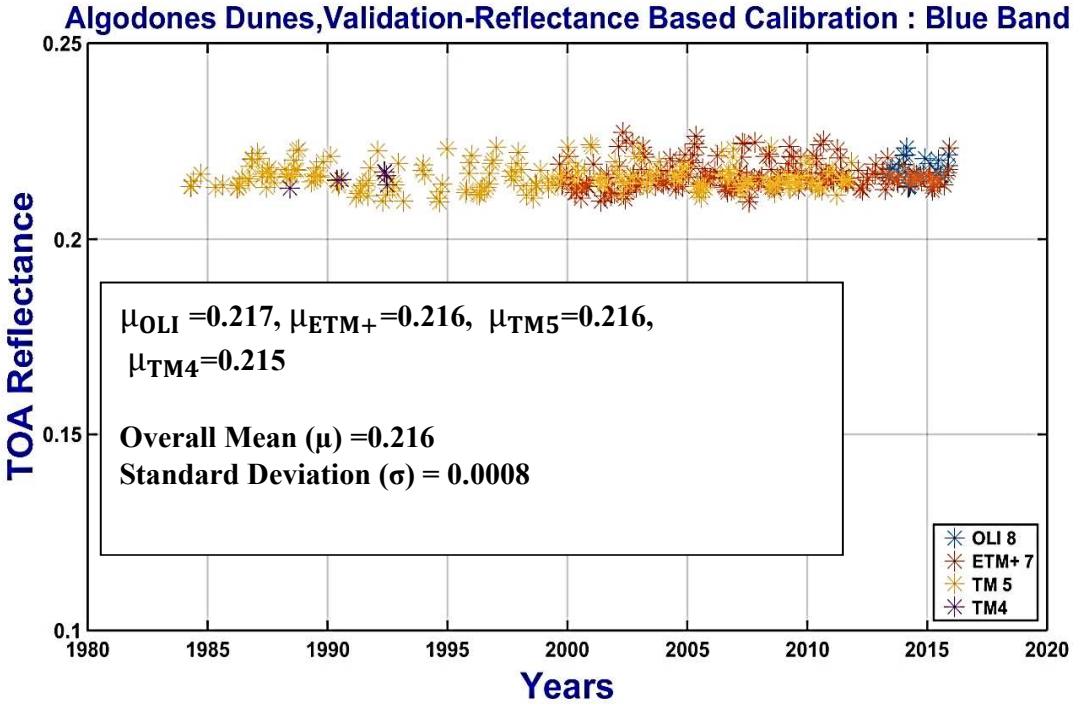

Figure 5.3.1 Consistent-Calibration of Landsat-8 OLI to Landsat-4 TM data in the blue band.

Table 5.3.1 shows the mean difference of TOA Reflectance before cross-calibration (calculated using ChKur solar model) and after cross-calibration (calculated using new cross-cal gains). A z test was performed to check the significant difference between the mean TOA reflectances calculated using new cross-cal gains for each pair of sensors.

Table 5.3.1 Percentage difference and z-test results for TOA reflectance between two successive sensors for the blue band.

Sensor Level	Mean differences after Cross_cal	Mean differences before Cross_cal	P-values from z test
OLI to ETM+	0.00059	0.0055	0.2
ETM+ to TM5	5.43E-05	0.0102	0.8
TM5 to TM4	0.00041	0.0061	0.6

Using a statistical z test 95% confidence level, the P-value for all bands is greater than 0.05 and thus the test showed there is no significant difference between sensors. Looking at Mean difference before cross-cal and after cross-cal, the results show a significant improvement in the Landsat archive after cross-calibration for the blue band.

Figure 5.3.2 shows temporal TOA reflectance from Algodones Dunes for all sensors in the green band. The Standard deviation showed in the box represents that the data is having very less variance.

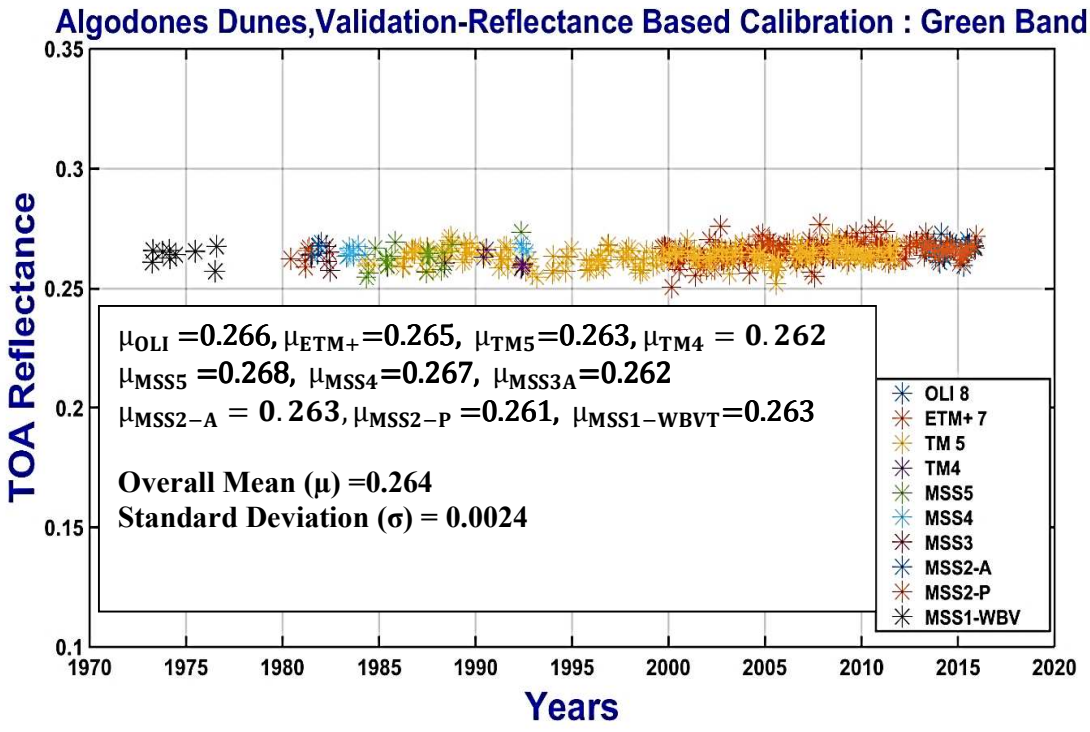

Figure 5.3.2 Consistent-Calibration of Landsat-8 OLI to Landsat-1 data in the green band.

Table 5.3.2 shows the mean difference before cross-calibration (calculated using ChKur solar model) and after cross-calibration (calculated using new cross-cal gains). A z test was performed to check the significant difference between the mean TOA reflectances calculated using new cross-calibration gains for each pair of sensors.

Table 5.3.2 Percentage difference and z-test results for TOA reflectance between two successive sensors for the green band.

Sensor Level	Mean differences after cross-cal	Mean differences before cross-cal	P-values from z-test
OLI to ETM+	0.0005	0.066	0.1
ETM+ to TM5	0.0002	0.0083	0.5
TM5 to TM4	0.0014	0.0451	0.3
TM5 to MSS5	0.0017	0.0432	0.1
MSS5 to MSS4	0.0006	0.0065	0.6
MSS4 to MSS3	0.0003	0.0105	0.8
MSS3 to MSS2	0.0002	0.009	0.2
MSS2 to MSS1	0.0008	0.010	0.3

Using a statistical z test 95% confidence level, the P-value for all bands is greater than 0.05 and thus the test showed there is no significant difference between sensors. Looking at Mean difference before cross-cal and after cross-cal, the results show a significant improvement in the Landsat archive after cross-calibration for the green band.

Figure 5.3.3 shows temporal TOA reflectance from Algodones Dunes for all sensors for the Red band. The Standard deviation showed in the box represents that the data is having very less variance.

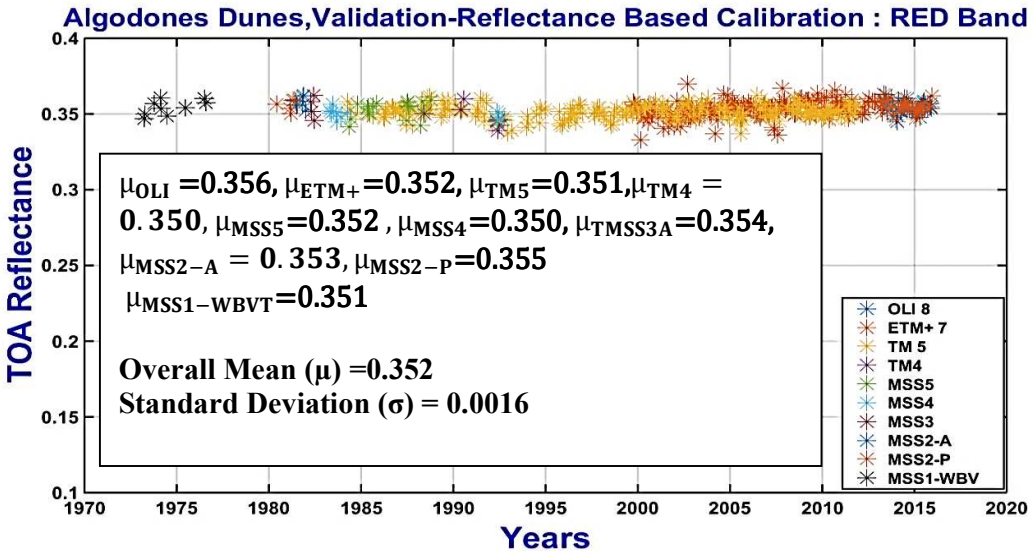

Figure 5.3.3. Consistent-Calibration of Landsat-8 OLI to Landsat-1 data in the red band.

Table 5.3.3 shows the mean difference of TOA Reflectance before cross-calibration (calculated using ChKur solar model) and after cross-calibration (calculated using new cross-cal gains). A z test was performed to check the significant difference between the mean TOA reflectances calculated using new cross-calibration gains for each pair of sensors.

Table 5.3.3. Percentage difference and z-test results for TOA reflectance between two successive sensors for red the band.

Sensor Level	Mean differences after cross-cal	Mean differences before cross-cal	P-values from z-test
OLI to ETM+	0.0020	0.0065	0.08
ETM+ to TM5	0.0009	0.0085	0.08
TM5 to TM4	0.0002	0.0008	0.9
TM5 to MSS5	0.0025	0.032	0.1
MSS5 to MSS4	0.0011	0.010	0.4
MSS4 to MSS3	0.0020	0.050	0.4
MSS3 to MSS2	0.0051	0.040	0.09
MSS2 to MSS1	0.0027	0.020	0.12

Using a statistical z test 95% confidence level, the P-value for all bands is greater than 0.05 and thus the test showed there is no significant difference between sensors. Looking at Mean difference before cross-cal and after cross-cal, the results show a significant improvement in the Landsat archive after cross-calibration for the red band.

Figure 5.3.4 shows temporal TOA reflectance from Algodones Dunes for all sensors for NIR band. The Standard deviation showed in the box represents that the data is having very less variance.

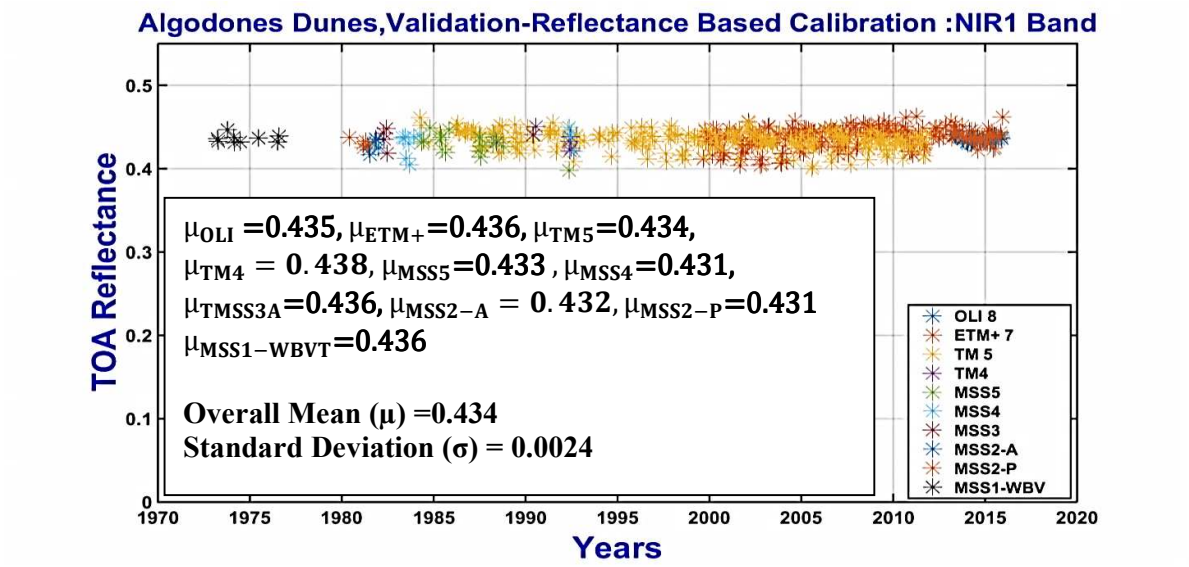

Figure 5.3.4. Consistent-Calibration of Landsat-8 OLI to Landsat-1 MSS data in the NIR1 band.

Table 5.3.4 shows the mean difference of TOA Reflectance before cross-calibration (calculated using ChKur solar model) and after cross-calibration(calculated using new cross-cal gains). A z test was performed to check the significant difference between the mean TOA reflectances calculated using new cross-calibration gains for each pair of sensors.

Table 5.3.4. Percentage difference and z-test results for reflectance between two successive sensors for the NIR1 band.

Sensor Level	Mean differences after cross-cal	Mean differences before cross-cal	P-value from z-test
OLI to ETM+	0.0005	0.017	0.6
ETM+ to TM5	0.0002	0.007	0.8
TM5 to TM4	0.0026	0.008	0.5
TM5 to MSS5	0.0031	0.025	0.2
MSS5 to MSS4	0.0010	0.020	0.6
MSS4 to MSS3	0.0020	0.019	0.6
MSS3 to MSS2	0.0130	0.080	0.68
MSS2 to MSS1	0.0020	0.020	0.13

Using a statistical z test 95% confidence level, the P-value for all bands is greater than 0.05 and thus the test showed there is no significant difference between sensors. Looking at Mean difference before cross-cal and after cross-cal, the results show a significant improvement in the Landsat archive after cross-calibration for the NIR1 band.

Figure 5.3.5 shows temporal TOA reflectance from Algodones Dunes for all sensors. The Standard deviation showed in the box represents that the data is having very less variance.

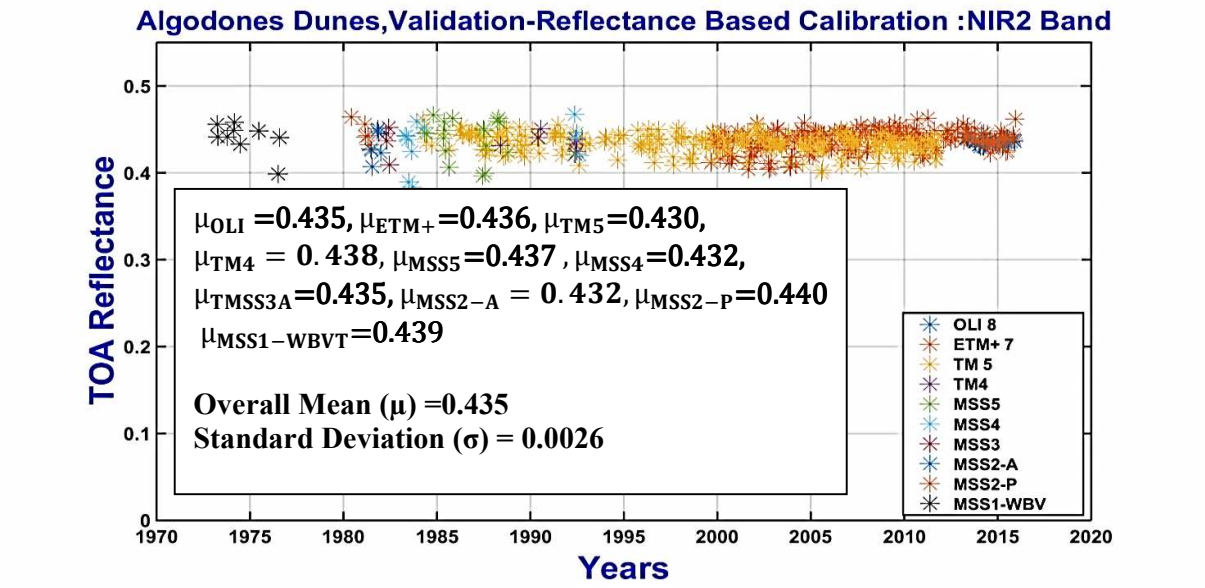

Figure 5.3.5. Consistent-Calibration of Landsat-8 OLI to Landsat-1 MSS data in the NIR2 band.

Table 5.3.5 shows the mean difference of TOA Reflectance before cross-calibration (calculated using ChKur solar model) and after cross-calibration (calculated using new cross-cal gains). A z test was performed to check the significant difference between the mean TOA reflectances calculated using new cross-calibration gains for each pair of sensors.

Table 5.3.5. Percentage difference and z-test results for TOA reflectance between two successive sensors for the NIR2 band.

Sensor Level	Mean differences after cross-cal	Mean differences before cross-cal	P-value from z-test
OLI to ETM+	0.0005	0.017	0.6
ETM+ to TM5	0.0002	0.007	0.8
TM5 to TM4	0.0020	0.008	0.5

TM5 to MSS5	0.0031	0.030	0.7
MSS5 to MSS4	0.0052	0.023	0.3
MSS4 to MSS3	0.0020	0.019	0.6
MSS3 to MSS2	0.0090	0.012	0.2
MSS2 to MSS1	0.0045	0.020	0.08

Using a statistical z test 95% confidence level, the P-value for all bands is greater than 0.05 and thus the test showed there is no significant difference between sensors. Looking at Mean difference before cross-cal and after cross cal, the results shows a significant improvement in the Landsat archive after cross-calibration for the NIR2 band.

Figure 5.3.6 shows temporal TOA reflectance from Algodones Dunes Landsat-8 OLI, Landsat-7 ETM+, Landsat-5 TM and Landsat-4 TM in the SWIR1 band.

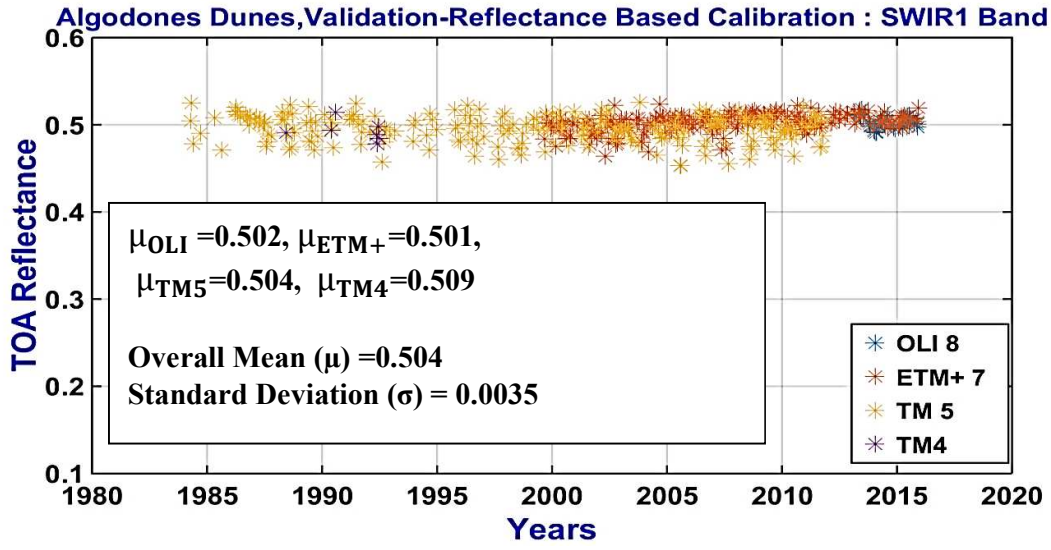

Figure 5.3.6. Consistent-Calibration of Landsat-8 OLI to Landsat-4 TM data in the SWIR1 band.

Table 5.3.6 shows the mean difference of TOA reflectance before cross-calibration (calculated using ChKur solar model) and after cross-calibration (calculated using new cross-cal gains). A z test was performed to check the significant difference between the mean TOA reflectances calculated using new cross-calibration gains for each pair of sensors.

Table 5.3.6 Percentage difference and z-test results for reflectance between two successive sensors for the SWIR1 band.

Sensor Level	Mean differences after cross-cal	Mean differences before cross-cal	P-value from z-test
OLI to ETM+	0.0010	0.009	0.2
ETM+ to TM5	0.0010	0.005	0.2
TM5 to TM4	0.0009	0.04	0.8

Using a statistical z test 95% confidence level, the P-value for all bands is greater than 0.05 and thus the test showed there is no significant difference between sensors. Looking at Mean difference before cross-cal and after cross cal, the results shows a significant improvement in the Landsat archive after cross-calibration for the SWIR1 band.

Figure 5.3.7 shows temporal TOA reflectance from Algodones Dunes for Landsat-8 OLI, Landsat-7 ETM+, Landsat-5 TM and Landsat-4 TM in the SWIR2 band.

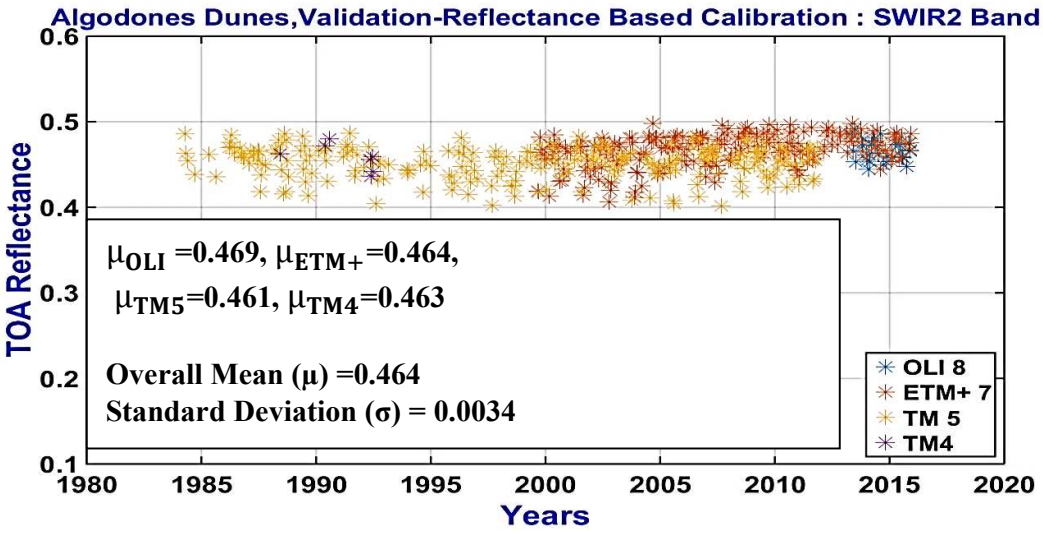

Figure 5.3.7. Consistent-Calibration of Landsat-8 OLI to Landsat-4 TM data in the SWIR2 band.

Table 5.3.7 shows the mean difference of TOA reflectance before cross-calibration (calculated using ChKur solar model) and after cross-calibration (calculated using new cross-cal gains). A z test was performed to check the significant difference between the mean TOA reflectances calculated using new cross-calibration gains for each pair of sensors.

Table 5.3.7. Percentage difference and z-test results for TOA reflectance between two successive sensors for the SWIR2 band.

Sensor Level	Mean differences after cross-cal	Mean differences before cross-cal	P-value from z-test
OLI to ETM+	0.005	0.010	0.07
ETM+ to TM5	0.005	0.0149	0.4
TM5 to TM4	0.001	0.009	0.6

Using a statistical z test 95% confidence level, the P-value for all bands is greater than 0.05 and thus the test showed there is no significant difference between sensors. Looking at Mean difference before cross-cal and after cross cal, the results shows a significant improvement in the Landsat archive after cross-calibration for the SWIR1 band.

Figure 5.3.8 shows temporal TOA reflectance from Algodones Dunes for Landsat-8 OLI and Landsat-7 ETM+ in the pan band.

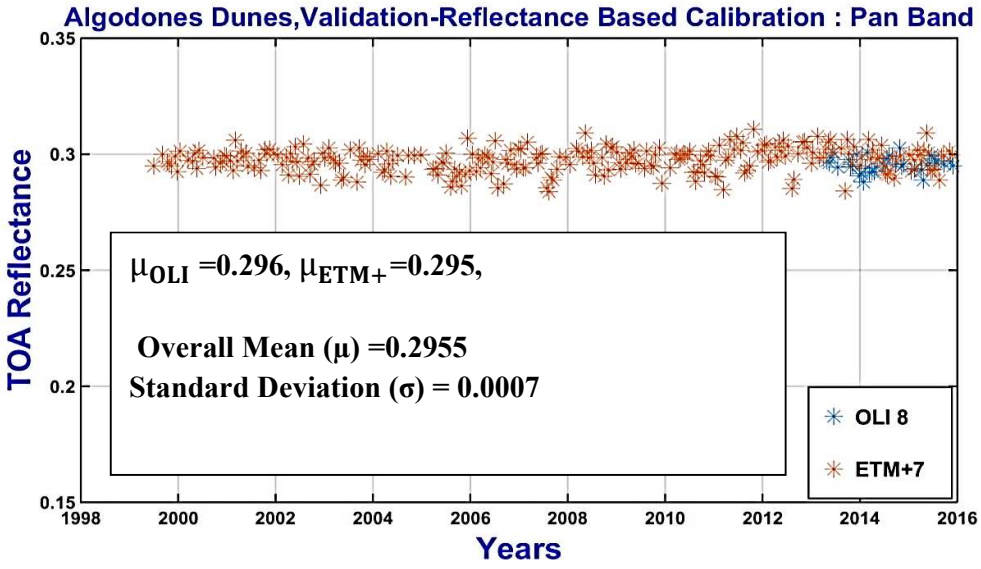

Figure 5.3.8 Consistent-Calibration of Landsat-8 OLI and Landsat-7 ETM+ in pan band.

Table 5.3.8. shows the mean difference of TOA reflectance before cross-calibration (calculated using ChKur solar model) and after cross-calibration (calculated using new cross-cal gains). A z test was performed to check the significant difference between the mean TOA reflectances calculated using new cross-calibration gains for each pair of sensors.

Table 5.3.8. Percentage difference and z-test results in TOA for reflectance between two successive sensors for the pan band.

Sensor Level	Mean differences after cross-cal	Mean differences before cross-cal	P-value from z-test
OLI to ETM+	5.44E-05	0.007	0.9

Using a statistical z test 95% confidence level, the P-value for all bands is greater than 0.05 and thus the test showed there is no significant difference between sensors. Looking at Mean difference before cross-cal and after cross cal, the results shows a significant improvement in the Landsat archive after cross-calibration for the pan band.

Chapter 6 Conclusion

The primary objective of the project–to consistently calibrate the entire Landsat series to a common reflectance–was achieved. Reflectance-based cross-calibration correction was performed from Landsat-8 OLI to Landsat-1 MSS using bright and dark targets. Consistent Landsat-8 reflectance-based equations were derived. Lifetime calibration of all Landsat data was verified using a pseudo-invariant calibration site (Algodones Dunes). This chapter summarizes the work and gives direction for future work.

6.1 Summary

The cross-calibration work is summarized as follows:

Landsat-8 OLI was cross-calibrated to Landsat-7 ETM+ using 12 good quality (i.e. cloud-free), and near-coincident scene pairs. Among these 12 scene pairs, eight were from the Sonoran Desert, and four were from Lake Tahoe.

Similarly, a cross-calibration between Landsat-7 ETM+ and Landsat-5 TM was performed using 11 good quality, cloud-free and near-coincident scene pairs. Among these 11 scene pairs, seven were from the Sonoran Desert, four from Lake Tahoe.

Landsat-5 TM was cross-calibrated to Landsat-4 TM. This was achieved using 32 good quality (i.e. cloud-free) and near-coincident scene pairs. Among these 32 scene pairs, four were from Ivanpah Playa, one from Makhtesh Ramon, nine from the Arabian Desert, four from Kelso Dunes, one from the Sonoran Desert, one from Algodones Dunes, two from Rock Springs, eight from near to the Sonoran Desert, and two from near the Algodones Dunes.

Landsat-5 TM to Landsat-5 MSS was cross-calibrated for best matching bands using 10 simultaneous scene pairs where seven were from the Sonoran Desert and three were from Lake Tahoe.

Landsat-5 MSS was cross-calibrated to the Landsat-4 MSS using eight simultaneous scene pairs. Among these eight scene pairs, one was from the Sonoran Desert, two from Lake Tahoe, two from Crater Lake, one from White Sands, and two were from Ivanpah Playa.

The cross-calibration from Landsat-4 MSS to Landsat-1 MSS was very difficult due to the presence of different data formats in the USGS archive. The cross-calibration chain was broken from Landsat-3 MSS because MSS-R data of Landsat-3 MSS had significant bias and stripes in MSS-X data. An in-depth study on MSS data revealed that MSS-A and MSS-P data is good for MSS3. Similarly, MSS-A, MSS-P, and MSSX-WBVT data are good for MSS2, but a few stripes have been seen in the MSS-R data of Landsat-2 MSS. MSSX-WBVT data is good for Landsat-1 MSS, and there are presently no other formats for Landsat-1 MSS in the USGS archive. Only MSS-A and MSS-P data were used to continue the calibration work from MSS3.

Cross-Calibration of the Landsat-4 MSS sensor to the Landsat-3 MSS sensor was accomplished by using six good quality, cloud-free scene pairs. Among these six scene pairs, one was from the Sonoran Desert having a time difference of 21 days. On January 20, 1983, both Landsat-3 MSS and Landsat-4 MSS followed nearly synchronous orbital paths with a difference of a few seconds. Among those scene pairs, two good quality scenes with no cloud cover were selected: a California scene with Path 043/Row 036 and a Florida scene with Path 017/Row 040. The remaining three scene pairs are simultaneous collections from Australia, which had a time difference of 10 minutes.

Similarly, the cross-calibration from Landsat-3 MSS to Landsat-2 MSS was accomplished by using 10 scene pairs. Among these 10 scene pairs, one was from the Sonoran Desert, one from Ivanpah Playa, two from Railroad valley, one from Crater Lake, one from Kelso Dunes, two near the Sonoran Desert, one from Algodones Dunes and, one from the White Desert.

To cross-calibrate Landsat-2 MSS to Landsat-1 MSS only the MSS1-WBVT data format was used. In total, nine scene pairs were used to calibrate the MSS1 sensor. Among them, three were from the Sonoran Desert, two from Crater Lake, three from Algodones Dunes, and one from Lake Tahoe. An unequal number of ROI's were used for all bands because some of the data is subjected to stripes and also green band data is unavailable after 1975 for Landsat -1 MSS. The cross-calibration gains and

bias calculated in Chapter 3, which are given here in Table 6.1, can place the entire Landsat data archive on a consistent reflectance scale.

Table 6.1. Cross-Calibration coefficients from Landsat-OLI 8 to Landsat-1 MSS.

Landsat-7 ETM				Landsat-5 TM		
Bands	Gain $(g_{7,\rho,\lambda})$	Bias $(b_{7,\rho,\lambda})$		Bands	Gain $(g_{5,\rho,\lambda})$	Bias $(b_{5,\rho,\lambda})$
BLUE	529.02	0		BLUE	775.30	0
GREEN	468.93	0		GREEN	370.59	0
RED	497.36	0		RED	434.08	0
NIR	339.86	0		NIR	358.43	0
SWIR1	356.88	0		SWIR1	547.57	0
SWIR2	376.37	0		SWIR2	384.66	0
PAN	415.13	0				
Landsat-4 TM				**Landsat-5 MSS**		
Bands	Gain $(g_{4,\rho,\lambda})$	Bias $(b_{4,\rho,\lambda})$		Bands	Gain $(g_{5M,\rho,\lambda})$	Bias $(b_{5M,\rho,\lambda})$
BLUE	924.32	0		GREEN	689.93	0
GREEN	405.93	0		RED	527.31	0
RED	456.06	0		NIR1	414.05	0
NIR	355.33	0		NIR2	277.73	0
SWIR1	545.07	0				
SWIR2	387.76	0				
Landsat-4 MSS				**Landsat-3 MSS**		
Bands	Gain $(g_{4M,\rho,\lambda})$	Bias $(b_{4M,\rho,\lambda})$		Bands	Gain $(g_{3M,\rho,\lambda})$	Bias $(b_{3M,\rho,\lambda})$
GREEN	586.08	0		GREEN	665.12	0
RED	476.03	0		RED	524.98	0
NIR1	377.94	0		NIR1	403.36	0
NIR2	258.77	0		NIR2	291.16	0
Landsat-2 MSS				**Landsat-1 MSS**		
Bands	Gain $(g_{2M,\rho,\lambda})$	Bias $(b_{2M,\rho,\lambda})$		Bands	Gain $(g_{1M,\rho,\lambda})$	Bias $(b_{1M,\rho,\lambda})$
GREEN	653.92	0		GREEN	696.83	0
RED	513.59	0		RED	581.97	-4.4137
NIR1	422.04	0		NIR1	416.32	0
NIR2	281.88	0		NIR2	262.03	0

The combined results of taking all sensors to Landsat-8 OLI were shown in Chapter 5. The DN from L1T product of particular sensor can be directly converted to its TOA reflectance using cross-cal gains showed in Table 6.1. The equations for each sensor are shown below.

For Landsat-8 OLI

$$\rho_{8,\lambda} = M_{8\rho,\lambda} \cdot DN_{8,\lambda} + A_{8,\rho,\lambda}$$

For Landsat-7 ETM+

$$\rho_{7,\lambda} = \frac{1}{g_{7,\rho,\lambda}} \cdot DN_{7,\lambda} + \frac{b_{7,\rho,\lambda}}{g_{7,\rho,\lambda}}$$

For Landsat-5 TM

$$\rho_{5,\lambda} = \frac{1}{g_{5,\rho,\lambda}} \cdot DN_{5,\lambda} + \frac{b_{5,\rho,\lambda}}{g_{5,\rho,\lambda}}$$

For Landsat-4 TM

$$\rho_{4,\lambda} = \frac{1}{g_{4,\rho,\lambda}} \cdot DN_{4,\lambda} + \frac{b_{4,\rho,\lambda}}{g_{4,\rho,\lambda}}$$

For Landsat-5 MSS

$$\rho_{5M,\lambda} = \frac{1}{g_{5M,\rho,\lambda}} \cdot DN_{5M,\lambda} + \frac{b_{5M,\rho,\lambda}}{g_{5M,\rho,\lambda}}$$

For Landsat-4 MSS

$$\rho_{4M,\lambda} = \frac{1}{g_{4M,\rho,\lambda}} \cdot DN_{4M,\lambda} + \frac{b_{4M,\rho,\lambda}}{g_{4M,\rho,\lambda}}$$

For Landsat-3 MSS

$$\rho_{3M,\lambda} = \frac{1}{g_{3M,\rho,\lambda}} \cdot DN_{3M,\lambda} + \frac{b_{3M,\rho,\lambda}}{g_{3M,\rho,\lambda}}$$

For Landsat-2 MSS

$$\rho_{2M,\lambda} = \frac{1}{g_{2M,\rho,\lambda}} \cdot DN_{2M,\lambda} + \frac{b_{2M,\rho,\lambda}}{g_{2M,\rho,\lambda}}$$

For Landsat-1 MSS

$$\rho_{1M,\lambda} = \frac{1}{g_{1M,\rho,\lambda}} \cdot DN_{1M,\lambda} + \frac{b_{1M,\rho,\lambda}}{g_{1M,\rho,\lambda}}$$

All terms used in the equations were already explained clearly in chapter 4.

6.2 Conclusions

The following conclusions were established, upon completion of this project**:-**

- The study suggested that the reflectance-based calibration is much better than the radiance-based calibration because of lower uncertainty. The results showed a significant improvement in reflectance calibration, and an overall uncertainty of sub ±3 % was seen for all the bands. There is a significant improvement in the TOA reflectance data for all sensors when compared to the previous data.
- After a consistent cross-calibration, it was observed the reflectance cross-calibration was stable within ±1-2% for blue band, ±3% for the green band, ±1-2% for red band, ±1-3% for NIR band, ±1-3% for SWIR bands and, ±1% for Pan band. The higher uncertainties from NIR band to SWIR band are due to the presence of atmospheric absorption features and low signal-to-noise ratio.
- This work also validated the consistent calibration across each Landsat MSS data formats MSS-P, MSS-A, and MSSX-WBVT. However, for some bands, uncertainty associated with MSS sensors was high, i.e. 3-4% when compared to modern Landsat sensors data. This is due to large atmospheric features in higher wavelengths.
- Previous MSS calibration indicated the need for a Time Dependent Factor (TDF). For MSS1 Green band, MSS2 Green band and Red band. TDF was derived during radiance calibration from a combination of MSSX, MSSA, and MSSP. However, MSSX-WBVT currently has a known calibration inconsistency. Therefore TDF is not required for MSS calibration.
- Statistical z-tests were performed at a 95% confidence interval to check if a significant difference existed between the mean TOA reflectance generated by different sensors. The results showed no significance difference between the sensors. Both TOA reflectance mean and the standard difference between pairs of sensors are very small.
- A new set of reflectance-based calibration equations were derived which eliminates the use of solar models to generate TOA reflectance for the Landsat L1T product.

6.3 Direction for Future Work

The older MSS data is imprecise and, had stripes and perhaps higher uncertainties. From Landsat-3 MSS to Landsat-1 MSS, striping was seen in the data and it was very difficult to choose proper ROIs for calibration. However, further analysis is required to understand the historical processing of MSS data to remove stripes from scenes. MSS-R data was not used from Landsat-5 MSS to Landsat-1 MSS during cross-calibration. When USGS generates new MSS-R data, which is reliable (i.e. no striping), the whole reflectance calibration must be transferred to MSS-R data (i.e. normalization of different data types to MSS-R data).

Further improvement of cross-calibration work can be done by using exact hyperspectral data acquired over the specific regions of interest for SBAF calculation. For example, as Hyperion data over Crater Lake is not available, the spectral signature of Lake Tahoe was used to calculate SBAF by assuming that both Crater Lake and Lake Tahoe have the same spectral profile.

In the entire project, atmospheric effects are not considered. As shown previously, some bands in MSS sensors exhibit large atmospheric effects due to various absorptions, and small inconsistencies may be reduced by considering this factor.

References

[1] Remote Sensing Definations. Available Online: http://www.amesremote.com/section1.htm. [Last Accessed 08-20-2016].

[2] X. M. Chen, "GIS and Remote Sensing in Environmental Risk Assesment," in *Green Technologies: Concept, Methodologies, Tools, and Applications*.

[3] D. L. Helder, S. Karki, R. Bhatt, E. Micijevic, D. Aaron, and B. Jasinski, "Radiometric Calibration of the Landsat MSS Sensor Series," in *IEEE Transactions on Geoscience and Remote Sensing*, vol. 50, no. 6, pp. 2380-2399, June 2012.

[4] The Landsat Program. Available Online: http://Landsat.gsfc.nasa.gov/. [Last Accessed 08-24-2016].

[5] Earth observation Resources. Available Online: https://directory.eoportal.org/web/eoportal/satellite-missions/l/landsat-1-3. [Last Accessed 08-24-2016].

[6] The Landsat Program. Available Online: http://landsat.gsfc.nasa.gov/?p=3227. [Last Accessed 09-03-2016].

[7] G. Chander, B.L.Markham, and D.L. Helder, "Summary of current radiometric calibration coefficients for Landsat MSS, TM, ETM+, and EO-1 ALI sensors," *Remote Sensing of Environment,* vol. 113, no. 5, pp. 893-903, 2009.

[8] EROS, "Landsat 1/5 Multispectral Scanner (MSS) Image Assessment system (IAS)," *Radiometric Algorithm Description Document (ADD),* June 2012. Available online: https://earth.esa.int/documents/700255/1834061/LS-IAS-07-MSS.pdf. [Last Accessed 09-04-2016].

[9] MSS Standard Interface Document. Available online: https://earth.esa.int/documents/700255/1834061/MSS_standard_ICD_1978. [Last Accessed 09-11-2016].

[10] EROS, "Landsat 4/5 Thematic Mapper (TM) Image Assessment System (IAS)," *Radiometric Algorithm Theoretical Basis Document (ATBD)*, July 2012. Available online: https://earth.esa.int/documents/700255/1834061/LS_IAS_03-TM.pdf. [Last Accessed 09-16-2016].

[11] National Aeronautics and Space Administration, "Landsat-7 Science Data Users Handbook". Available online: http://landsat.gsfc.nasa.gov/landsat-7-science-data-users-handbook. [Last Accessed 09-20-2016].

[12] Knight, Edward J., and Geir Kvaran. "Landsat-8 operational land imager design, characterization and performance. Remote Sensing 6.11 (2014): 10286-10305.

[13] D. L. Helder, B. L. Markham, K. J. Thome, J. A. Barsi, G. Chander and R. Malla, "Updated Radiometric Calibration for the Landsat-5 Thematic Mapper Reflective Bands," in *IEEE Transactions on Geoscience and Remote Sensing*, vol. 46, no. 10, pp. 3309-3325, Oct. 2008.

[14] S. Uprety, "Radiometric Stability Analysis of Landsat-1 through -5 MSS Sensors," *South Dakota State University- Thesis Dissertation,* 2009.

[15] Mishra, N., Haque, M. O., Leigh, L., Aaron, D., Helder, D., & Markham, B. (2014). Radiometric cross calibration of Landsat 8 operational land imager (OLI) and Landsat 7 enhanced thematic mapper plus (ETM+). Remote Sensing, 6(12), 12619-12638.

[16] "CEOS Cal/Val Portal," NASA, [Online]. Available online: http://calvalportal.ceos.org/cvp/web/guest/literature1. [Last Accessed 10-16-2016].

[17] G. Chander, et al. "Monitoring on-orbit calibration stability of the Terra MODIS and Landsat 7 ETM+ sensors using pseudo-invariant test sites." *Remote Sensing of Environment* 114.4 (2010): 925-939.

[18] B. L. Markham *et al*., "Landsat-7 ETM+: 12 Years On-Orbit Reflective-Band Radiometric Performance," in *IEEE Transactions on Geoscience and Remote Sensing*, vol. 50, no. 5, pp. 2056-2062, May 2012.

[19] B. L. Markham *et al*., "Landsat-7 ETM+ on-orbit reflective-band radiometric stability and absolute calibration," in *IEEE Transactions on Geoscience and Remote Sensing*, vol. 42, no. 12, pp. 2810-2820, Dec. 2004.

[20] P.M. Teillet, G. Fedosejevs, R.R. Irish, J.L. Barker, B.L. Markham, and J.C. Storey, "Radiometric Cross-calibration of the Landsat-7 ETM+ and Landsat-5 TM Sensors Based on Tandem Data Sets," *Remote Sensing of Environment,* vol. 78, no. 1-2, pp. 39-54, 2001.

[21] G. Chander and B. L. Markham, "Revised Landsat-5 TM radiometric calibration procedures and post calibration dynamic ranges," in *IEEE Transactions on Geoscience and Remote Sensing*, vol. 41, no. 11, pp. 2674-2677, Nov. 2003

[22] Micijevic, Esad, Md. Obaidul Haque, and Nischal Mishra. "Radiometric calibration updates to the Landsat collection." *SPIE Optical Engineering Applications*. International Society for Optics and Photonics, 2016.

[23] Metzler, M., & Malila, W. (1985). Characterization and comparison of Landsat-4 andLandsat-5 Thematic Mapper Data. *Photogrammetric Engineering and Remote Sensing,51*, 1315–1330.

[24] Cory Mettler and Dennis Helder. "Cross-Calibration of the Landsat-4 and Landsat-5 thematic mappers." Optics & Photonics 2005. International Society for Optics and Photonics, 2005.

[25] R. Malla and D. L. Helder, "Radiometric Calibration of Reflective Bands of Landsat 4 Thematic Mapper using Pseudo-Invariant Site Technique," *IGARSS 2008 - 2008 IEEE International Geoscience and Remote Sensing Symposium*, Boston, MA, 2008, pp. IV - 1344-IV - 1347.

[26] D. L. Helder, R. Malla, C. J. Mettler, B. L. Markham and E. Micijevic, "Landsat 4 Thematic Mapper Calibration Update," in *IEEE Transactions on Geoscience and Remote Sensing*, vol. 50, no. 6, pp. 2400-2408, June 2012.

[27] General Electric Company, "MSS Standard Interface Document," Goddard Space Flight Center, 15 July 1978.

[28] GSFC, NASA. "Landsat to ground station interface description." Goddard Space Flight Center, Greenbelt, MD*, Rev* 9 (1986).

[29] R.F. Nelson, "Sensor-induced temporal variability of Landsat MSS data," *Remote Sensing of Environment,* vol. 18, no. 1, pp. 35-48, 1985.

[30] B.L. Markham, J.L. barker, "Radiometric properties of U.S. processed Landsat MSS data," *Remote Sensing of Environment,* vol. 22, no. 1, pp. 39-71, 1987.

[31] Nelson, Janice S. *US Geological Survey (USGS) Earth Resources Observation and Science (EROS) Center-fiscal year 2010 annual report*. No. 2011-1057. US Geological Survey, 2011.

[32] B. L. Markham, and D. L. Helder, "Forty-year calibrated record of earth-reflected radiance from Landsat: A review," *Remote Sensing of Environment,* vol. 122, pp. 30-40, 2012.

[33] Morakot Kaewmanee, Chaichat Musanab and Panatda kietleadsereeb "The effect of Extraterresterial Solar model and Spectral differences on cross calibration" *Geo-Informatics and Space Technology Development Agency*. Available online:http://a-a-r-s.org/acrs/administrator/components/com_jresearch/files/publications/SC02-0257.pdf [Last Accessed 10-04-2016].

[34] B.Basnet, "Identification of Worldwide Optimal Pseudo-Invariant Calibration Sites for Post-Launch Radiometric Calibration of Earth Observation Satellite Sensors.," *South Dakota State University- Thesis Dissertation,* 2010.

[35] Cook, Monica, et al. "Spatial, Spectral, and Radiometric Characterization of Libyan and Sonoran Desert Calibration Sites in Support of GOES-R Vicarious Calibration." *Rochester Institute of Technology, College of Science, Center for Imaging Science, Rochester, New York* (2010).

[36] G. Chander *et al*., "Applications of Spectral Band Adjustment Factors (SBAF) for Cross-Calibration," in *IEEE Transactions on Geoscience and Remote Sensing*, vol. 51, no. 3, pp. 1267-1281, March 2013.

[37] Teillet, P. M., et al. "Impacts of spectral band difference effects on radiometric cross-calibration between satellite sensors in the solar-reflective spectral domain." *Remote Sensing of Environment* 110.3 (2007): 393-409.

[38] J. Pearlman, S. Carman, C. Segal, P. Jarecke, P. Clancy and W. Browne, "Overview of the Hyperion Imaging Spectrometer for the NASA EO-1 mission," *Geoscience and Remote Sensing Symposium, 2001. IGARSS '01. IEEE 2001 International*, Sydney, NSW, 2001, pp. 3036-3038 vol.7.

[39] Calibration Parameters Files (CPF). " Available online: http://landsat.usgs.gov/science_calibration.php. [Last Accessed 10-24-2016].

[40] D. L. Helder, B. L. Markham, K. J. Thome, J. A. Barsi, G. Chander, and R. Malla, "Updated Radiometric Calibration for the Landsat-5 Thematic Mapper Reflective Bands," in *IEEE Transactions on Geoscience and Remote Sensing*, vol. 46, no. 10, pp. 3309-3325, Oct. 2008.

[41] Nazeer, Majid, Janet E. Nichol, and Ying-Kit Yung. "Evaluation of atmospheric correction models and Landsat surface reflectance product in an urban coastal environment." *International Journal of Remote Sensing*35.16 (2014): 6271-6291.

[42] Pinto, Cibele, et al. "First in-Flight Radiometric Calibration of MUX and WFI on-Board CBERS-4." *Remote Sensing* 8.5 (2016): 405.

[43] Zimbelman, James R., and Steven H. Williams. "Eolian dunes and deposits in the western United States as analogs to wind-related features on Mars." *The Geology of Mars: Evidence from Earth-Based Analog* 1 (2007): 232.

[44] Paternoster, Raymond, et al. "Using the correct statistical test for the equality of regression coefficients." *Criminology* 36.4 (1998): 859-866.

Appendix A

Corner-Coordinates of all ROI's used in reflectance cross-calibration

Table A1. Landsat-8 OLI to Landsat-7 ETM+ cross-calibration ROI's corner-coordinates.

Locations	ROI's latitudes and Longitudes
Sonoran ROI1	ULX= -113.94118882,ULY= 31.78631241 URX= -113.90596823,URY= 31.78631241 LRX= -113.90596823,LRY= 31.76053818 LLX= -113.94118882,LLY= 31.76053818
Sonoran ROI2	ULX= -114.33230091,ULY= 32.27197199 URX= -114.30190129,URY= 32.27197199 LRX= -114.30190129, LRY= 32.24481538 LLX= -114.33230091, LLY= 32.24481538
Sonoran ROI3	ULX= -114.38621177,ULY= 32.27959248 URX= -114.35579275,URY= 32.27959248 LRX= -114.35579275,LRY= 32.25244791 LLX= -114.38621177,LLY= 32.25244791
Sonoran ROI4	ULX= -114.59441821,ULY= 32.40222851 URX= -114.47564530,URY= 32.40222851 LRX= -114.47564530,LRY= 32.33876515 LLX= -114.59441821,LLY= 32.33876515
Sonoran ROI5	ULX= -114.78201922,ULY= 32.29420369 URX= -114.72095513,URY= 32.29420369 LRX= -114.72095513,LRY= 32.23954652 LLX= -114.78201922,LLY= 32.23954652
Sonoran ROI6	ULX= -115.32426664,ULY= 31.55569363 URX= -114.72095513,URY= 31.55569363 LRX= -114.72095513,LRY= 31.51997663 LLX= -115.32426664,LLY= 31.51997663
Sonoran ROI7	ULX= -115.28327155,ULY= 31.55081970 URX= -115.24285912,URY= 31.55081970 LRX= -115.24285912,LRY= 31.51509034 LLX= -115.28327155,LLY= 31.51509034
Lake Tahoe ROI 1	ULX= -120.10042829,ULY= 39.15933860 URX= -120.10372711,URY= 39.15933860 LRX= -120.10372711,LRY= 39.07888180 LLX= -120.10042829,LLY= 39.07888180

Note: - ULX=Upper Left corner of X; ULY=Upper Left corner of Y; URX=Upper Right corner of X; URY=Upper Right corner of Y; LLX= Lower Left corner of X; LLY= Lower Left corner of Y; LRX= Lower Right corner of X; LRY= Lower Right corner of Y

Table A2. Landsat-7 ETM+ to Landsat-5 TM cross-calibration ROI's corner-coordinates.

Locations	ROIS latitudes and Longitudes
Sonoran ROI1	ULX= -113.94118882,ULY= 31.78631241 URX= -113.90596823,URY= 31.78631241 LRX= -113.90596823,LRY= 31.76053818 LLX= -113.94118882,LLY= 31.76053818
Sonoran ROI2	ULX= -114.33230091,ULY= 32.27197199 URX= -114.30190129,URY= 32.27197199 LRX= -114.30190129,LRY= 32.24481538 LLX= -114.33230091, LLY= 32.24481538
Sonoran ROI3	ULX= -114.38621177,ULY= 32.27959248 URX= -114.35579275,URY= 32.27959248 LRX= -114.35579275,LRY= 32.25244791 LLX= -114.38621177,LLY= 32.25244791
Sonoran ROI4	ULX= -114.59441821,ULY= 32.40222851 URX= -114.47564530,URY= 32.40222851 LRX= -114.47564530,LRY= 32.33876515 LLX= -114.59441821,LLY= 32.33876515
Sonoran ROI5	ULX= -114.78201922,ULY= 32.29420369 URX= -114.72095513,URY= 32.29420369 LRX= -114.72095513,LRY= 32.23954652 LLX= -114.78201922,LLY= 32.23954652
Sonoran ROI6	ULX= -115.32426664,ULY= 31.55569363 URX= -114.72095513,URY= 31.55569363 LRX= -114.72095513,LRY= 31.51997663 LLX= -115.32426664,LLY= 31.51997663
Sonoran ROI7	ULX= -115.28327155,ULY= 31.55081970 URX= -115.24285912,URY= 31.55081970 LRX= -115.24285912,LRY= 31.51509034 LLX= -115.28327155,LLY= 31.51509034

Lake Tahoe ROI 1	ULX= -120.10042829,ULY= 39.15933860 URX= -120.10372711,URY= 39.15933860 LRX= -120.10372711,LRY= 39.07888180 LLX= -120.10042829,LLY= 39.07888180

Table A3. Landsat-5 TM to Landsat-4 TM cross-calibration ROI's corner-coordinates.

Locations	**Longitudes and Latitudes of ROIS**
Sonoran Desert ROI1	ULX= -114.33151626,ULY= 32.27017809 URX= -115.24285912,URY= 32.27017809 LRX= -115.24285912,LRY= 32.24481538 LLX= -114.33151626, LLY= 32.24481538
Sonoran Desert ROI2	ULX= -114.38621177,ULY= 32.27959248 URX= -114.35579275,URY= 32.27959248 LRX= -114.35579275,LRY= 32.25244791 LLX= -114.38621177, LLY= 32.25244791
Sonoran Desert ROI3	ULX= -114.59441821,ULY= 32.40222851 URX= -114.47564530,URY= 32.40222851 LRX= -114.47564530,LRY= 32.33876515 LLX= -114.59441821, LLY= 32.33876515
Sonoran Desert ROI4	ULX= -114.53725405,ULY= 32.39354894 URX= -114.47564530,URY= 32.39354894 LRX= -114.47564530,LRY= 32.33876515 LLX= -114.53725405, LLY= 32.33876515
Sonoran Desert ROI5	ULX= -114.83920310,ULY= 32.30060698 URX= -114.77746250,URY= 32.30060698 LRX= -114.77746250,LRY= 32.24596463 LLX= -114.83920310, LLY= 32.24596463
Sonoran Desert ROI6	ULX= -114.78201922,ULY= 32.29420369 URX= -114.72095513,URY= 32.29420369 LRX= -114.72095513,LRY= 32.23954652 LLX= -114.78201922, LLY= 32.23954652
Sonoran Desert ROI7	ULX= -115.48799508,ULY= 31.74988072 URX= -115.41156302,URY= 31.74988072 LRX= -115.41156302,LRY= 31.73758462 LLX= -115.48799508, LLY= 31.73758462
Sonoran Desert ROI8	ULX= -115.38384959,ULY= 31.69231337 URX= -115.29960042,URY= 31.69231337 LRX= -115.29960042,LRY= 31.66090885 LLX= -115.38384959, LLY= 31.66090885
Sonoran Desert ROI9	ULX= -115.31828674,ULY= 31.67739353 URX= -115.29586394,URY= 31.67739353 LRX= -115.29586394,LRY= 31.65761161 LLX= -115.31828674, LLY= 31.65761161
	ULX= -115.32426664,ULY= 31.55569363 URX= -115.28383596,URY= 31.55569363

Sonoran Desert ROI10	LRX= -115.28383596,LRY= 31.51997663 LLX= -115.32426664, LLY= 31.51997663
Sonoran Desert ROI11	ULX= -115.28327155,ULY= 31.55081970 URX= -115.24285912,URY= 31.55081970 LRX= -115.24285912,LRY= 31.51509034 LLX= -115.28327155, LLY= 31.51509034
Algodones Dunes ROI1	ULX= -114.96446301,ULY= 32.82108048 URX= -114.92046642,URY= 32.82108048 LRX= -114.92046642,LRY= 32.78410383 LLX= -114.96446301, LLY= 32.78410383
Algodones Dunes ROI2	ULX= -115.11058515,ULY= 32.97163663 URX= -115.06950837,URY= 32.97163663 LRX= -115.06950837,LRY= 32.94178875 LLX= -115.11058515, LLY= 32.94178875
Algodones Dunes ROI3	ULX= -115.14095794,ULY= 32.99265471 URX= -115.09176362,URY= 32.99265471 LRX= -115.09176362,LRY= 32.95132952 LLX= -115.14095794, LLY= 32.95132952
Algodones Dunes ROI4	ULX= -115.58711210,ULY= 33.70886832 URX= -115.57370621,URY= 33.70886832 LRX= -115.57370621,LRY= 33.69735117 LLX= -115.58711210, LLY= 33.69735117
Algodones Dunes ROI5	ULX= -115.73758503,ULY= 33.49107354 URX= -115.72419124,URY= 33.49107354 LRX= -115.72419124,LRY= 33.47957263 LLX= -115.73758503, LLY= 33.47957263
Kelso Desert ROI1	ULX= -115.76574461,ULY= 34.96777457 URX= -115.75033128,URY= 34.96777457 LRX= -115.75033128,LRY= 34.95804204 LLX= -115.76574461, LLY= 34.95804204
Kelso Desert ROI2	ULX= -115.86229112,ULY= 34.84498731 URX= -115.85129428,URY= 34.84498731 LRX= -115.85129428,LRY= 34.83352243 LLX= -115.86229112, LLY= 34.83352243
Ivanpah Playa ROI1	ULX= -115.29339390,ULY= 35.98426755 URX= -115.27788308,URY= 35.98426755 LRX= -115.27788308,LRY= 35.97285395 LLX= -115.29339390, LLY= 35.97285395
Ivanpah Playa ROI2	ULX= -115.28699717,ULY= 35.98217949 URX= -115.27064853,URY= 35.98217949 LRX= -115.27064853,LRY= 35.96896368 LLX= -115.28699717, LLY= 35.96896368
Ivanpah Playa ROI3	ULX= -115.49562325,ULY= 35.75400831 URX= -115.46362428,URY= 35.75400831 LRX= -115.46362428,LRY= 35.72709874 LLX= -115.49562325, LLY= 35.72709874
Ivanpah Playa ROI4	ULX= -115.49200418,ULY= 35.74987544 URX= -115.45972834,URY= 35.74987544 LRX= -115.45972834,LRY= 35.72272156 LLX= -115.49200418,LLY= 35.72272156

Arabia 162/046 ROI1	ULX= 51.08714989,ULY= 20.53740692 URX= 51.10772810,URY= 20.53740692 LRX= 51.10772810,LRY= 20.51960914 LLX= 51.08714989, LLY= 20.51960914
Arabia 162/046 ROI2	ULX= 51.11208092,ULY= 20.57002620 URX= 51.12962635,URY= 20.57002620 LRX= 51.12962635,LRY= 20.55537598 LLX= 51.11208092, LLY= 20.55537598
Arabia 162/046 ROI3	ULX= 51.12597376,ULY= 20.66353647 URX= 51.14554076,URY= 20.66353647 LRX= 51.14554076,LRY= 20.64508827 LLX= 51.12597376, LLY= 20.64508827
Arabia 162/047 ROI1	ULX= 50.14523080,ULY= 18.40690015 URX= 50.16134958,URY= 18.40690015 LRX= 50.16134958,LRY= 18.39765952 LLX= 50.14523080, LLY= 18.39765952
Arabia 162/047 ROI2	ULX= 50.18272848,ULY= 18.55684250 URX= 50.19612017,URY= 18.55684250 LRX= 50.19612017,LRY= 18.54606453 LLX= 50.18272848, LLY= 18.54606453
Arabia 162/047 ROI3	ULX= 49.96785692,ULY= 19.21927275 URX= 49.97991211,URY= 19.21927275 LRX= 49.97991211,LRY= 19.20795486 LLX= 49.96785692, LLY= 19.20795486
Arabia 162/047 ROI4	ULX= 50.07036490,ULY= 19.30982197 URX= 50.08242937,URY= 19.30982197 LRX= 50.08242937,LRY= 19.29687095 LLX= 50.07036490, LLY= 19.29687095
Arabia 165/042 ROI1	ULX= 47.27566289,ULY= 26.15250625 URX= 47.29097354,URY= 26.15250625 LRX= 47.29097354,LRY= 26.14193885 LLX= 47.27566289, LLY= 26.14193885
Arabia 165/042 ROI2	ULX= 47.35304581,ULY= 25.65819260 URX= 47.36302363,URY= 25.65819260 LRX= 47.36302363,LRY= 25.64909643 LLX= 47.35304581,LLY= 25.64909643
Arabia 165/042 ROI3	ULX= 46.93038965,ULY= 25.40333803 URX= 46.94657633,URY= 25.40333803 LRX= 46.94657633,LRY= 25.39012567 LRX= 46.93038965,LRY= 25.39012567
Arabia 165/042 ROI3	ULX= 46.93038965,ULY= 25.40333803 URX= 46.94657633,URY= 25.40333803 LRX= 46.94657633,LRY= 25.39012567 LLX= 46.93038965,LLY= 25.39012567
Arabia 165/042 ROI4	ULX= 46.98797791,ULY= 25.47866653 URX= 47.00625499,URY= 25.47866653 LRX= 47.00625499,LRY= 25.46541918 LLX= 46.98797791,LLY= 25.46541918
	ULX= 44.72100057,ULY= 26.19676883 URX= 44.74114984,URY= 26.19676883

Arabia 167/042 ROI1	LRX= 44.74114984,LRY= 26.18051725 LLX= 44.72100057,LLY= 26.18051725
Arabia 167/042 ROI2	ULX= 44.65824808,ULY= 25.35953871 URX= 44.66841637,URY= 25.35953871 LRX= 44.66841637,LRY= 25.34818380 LLX= 44.65824808, LLY= 25.34818380
Arabia 167/042 ROI3	ULX= 44.06899835,ULY= 25.72186959 URX= 44.08373740,URY= 25.72186959 LRX= 44.08373740,LRY= 25.71058621 LLX= 44.06899835,LLY= 25.71058621
Makhtesh Ramon ROI1	ULX= 35.10690784,ULY= 29.96292863 URX= 35.12717576,URY= 29.96292863 LRX= 35.12717576,LRY= 29.94498050 LLX= 35.10690784,LLY= 29.94498050
Makhtesh Ramon ROI2	ULX= 35.12247004,ULY= 30.01596364 URX= 35.13890306,URY= 30.01596364 LRX= 35.13890306,LRY= 29.99918868 LLX= 35.12247004, LLY= 29.99918868
Makhtesh Ramon ROI3	ULX= 34.40815093,ULY= 29.75674987 URX= 35.04121707,URY= 29.75674987 LRX= 35.04121707,LRY= 29.73739842 LLX= 34.40815093, LLY= 29.73739842
Rock Springs 037/031	ULX= -109.92134330,ULY= 41.91224071 URX= -109.91134782,URY= 41.91224071 LRX= -109.91134782,LRY= 41.90751521 LLX= -109.92134330,LLY= 41.90751521
Rock Springs 037/031	ULX= -109.92538974,ULY= 41.88981424 URX= -109.91181570,URY= 41.88981424 LRX= -109.91181570,LRY= 41.87995916 LLX= -109.92538974,LLY= 41.87995916
Near to Sonoran 037/038	ULX= -113.53107847,ULY= 31.52455586 URX= -113.51567310,URY= 31.52455586 LRX= -113.51567310,LRY= 31.51314286 LLX= -113.53107847,LLY= 31.51314286
Near to Sonoran 037/038	ULX= -113.55332994,ULY= 31.64334332 URX= 113.54164196,URY= 31.64334332 LRX= -113.54164196,LRY= 31.63221359 LLX= -113.55332994,LLY= 31.63221359

Table A4. Landsat-5 TM to Landsat-5 MSS cross-calibration ROI's corner-coordinates.

Locations	ROIS latitudes and Longitudes
Sonoran ROI1	ULX= -113.94118882,ULY= 31.78631241 URX= -113.90596823,URY= 31.78631241 LRX= -113.90596823,LRY= 31.76053818 LLX= -113.94118882,LLY= 31.76053818
Sonoran ROI2	ULX= -114.33230091,ULY= 32.27197199 URX= -114.30190129,URY= 32.27197199 LRX= -114.30190129, LRY= 32.24481538 LLX= -114.33230091,LLY= 32.24481538
Sonoran ROI3	ULX= -114.38621177,ULY= 32.27959248 URX= -114.35579275,URY= 32.27959248 LRX= -114.35579275,LRY= 32.25244791 LLX= -114.38621177,LLY= 32.25244791
Sonoran ROI4	ULX= -114.59441821,ULY= 32.40222851 URX= -114.47564530,URY= 32.40222851 LRX= -114.47564530,LRY= 32.33876515 LLX= -114.59441821,LLY= 32.33876515
Sonoran ROI5	ULX= -115.32426664,ULY= 31.55569363 URX= -114.72095513,URY= 31.55569363 LRX= -114.72095513,LRY= 31.51997663 LLX= -115.32426664,LLY= 31.51997663
Sonoran ROI6	ULX= -115.28327155,ULY= 31.55081970 URX= -115.24285912,URY= 31.55081970 LRX= -115.24285912,LRY= 31.51509034 LLX= -115.28327155,LLY= 31.51509034
Lake Tahoe ROI1	ULX= -120.10042829,ULY= 39.15933860 URX= -120.10372711,URY= 39.15933860 LRX= -120.10372711,LRY= 39.07888180 LLX= -120.10042829,LLY= 39.07888180

Table A5. Landsat-5 MSS to Landsat-4 MSS cross-calibration ROI's corner-coordinates.

Locations	ROI's Latitudes and Longitudes
Sonoran Desert ROI 1	ULX= -114.33151626,ULY= 32.27017809 URX= -115.24285912,URY= 32.27017809 LRX= -115.24285912,LRY= 32.24481538 LLX= -114.33151626, LLY= 32.24481538
Sonoran Desert ROI 2	ULX= -114.38621177,ULY= 32.27959248 URX= -114.35579275,URY= 32.27959248 LRX= -114.35579275,LRY= 32.25244791 LLX= -114.38621177,LLY= 32.25244791
Sonoran Desert ROI 3	ULX= -114.59441821,ULY= 32.40222851 URX= -114.47564530,URY= 32.40222851 LRX= -114.47564530,LRY= 32.33876515 LLX= -114.59441821,LLY= 32.33876515
Sonoran Desert ROI 4	ULX= -114.53725405,ULY= 32.39354894 URX= -114.47564530,URY= 32.39354894 LRX= -114.47564530,LRY= 32.33876515 LLX= -114.53725405,LLY= 32.33876515
Sonoran Desert ROI 5	ULX= -114.83920310,ULY= 32.30060698 URX= -114.77746250,URY= 32.30060698 LRX= -114.77746250,LRY= 32.24596463 LLX= -114.83920310,LLY= 32.24596463
Sonoran Desert ROI 6	ULX= -114.78201922,ULY= 32.29420369 URX= -114.72095513,URY= 32.29420369 LRX= -114.72095513,LRY= 32.23954652 LLX= -114.78201922,LLY= 32.23954652
Sonoran Desert ROI 7	ULX= -115.48799508,ULY= 31.74988072 URX= -115.41156302,URY= 31.74988072 LRX= -115.41156302,LRY= 31.73758462 LLX= -115.48799508,LLY= 31.73758462
Sonoran Desert ROI 8	ULX= -115.38384959,ULY= 31.69231337 URX= -115.29960042,URY= 31.69231337 LRX= -115.29960042,LRY= 31.66090885 LLX= -115.38384959,LLY= 31.66090885
Sonoran Desert ROI 9	ULX= -115.31828674,ULY= 31.67739353 URX= -115.29586394,URY= 31.67739353 LRX= -115.29586394,LRY= 31.65761161 LLX= -115.31828674,LLY= 31.65761161
Sonoran Desert ROI 10	ULX= -115.32426664,ULY= 31.55569363 URX= -115.28383596,URY= 31.55569363 LRX= -115.28383596,LRY= 31.51997663 LLX= -115.32426664,LLY= 31.51997663
Sonoran Desert ROI 11	ULX= -115.28327155,ULY= 31.55081970 URX= -115.24285912,URY= 31.55081970 LRX= -115.24285912,LRY= 31.51509034 LLX= -115.28327155,LLY= 31.51509034
	ULX= -120.10042829,ULY= 39.15933860 URX= -120.10372711,URY= 39.15933860

Lake Tahoe ROI 1	LRX= -120.10372711,LRY= 39.07888180 LLX= -120.10042829,LLY= 39.07888180
Crater Lake ROI 1	ULX= -122.13615386,ULY= 42.96571952 URX= -122.07321381,URY= 42.96571952 LRX= -122.07321381,LRY= 42.92213736 LLX= -122.13615386,LLY= 42.92213736
White Sands ROI 1	ULX= -107.26213746,ULY= 33.26393800 URX= -107.21321439,URY= 33.26481887 LRX= -107.21238264,LRY= 33.23183031 LLX= -107.26128737,LLY= 33.23095053
White Sands ROI 2	ULX= -107.32723702,ULY= 33.02251892 URX= -107.30284374,URY= 33.02297167 LRX= -107.30235158,LRY= 33.00404426 LLX= -107.32673965,LLY= 33.00359184
White Sands ROI 3	ULX= -107.04839617,ULY= 33.01821138 URX= -107.02528361,URY= 33.01858873 LRX= -107.02487554,LRY= 33.00073960 LLX= -107.04798345,LLY= 33.00036250
White Sands ROI 4	ULX= -107.33444174,ULY= 32.97910121 URX= -107.31070215,URY= 32.97954295 LRX= -107.31022321,LRY= 32.96115630 LLX= -107.33395788,LLY= 32.96071486
Ivanpah Playa ROI 1	ULX= -115.29339390,ULY= 35.98426755 URX= -115.27788308,URY= 35.98426755 LRX= -115.27788308,LRY= 35.97285395 LLX= -115.29339390,LLY= 35.97285395
Ivanpah Playa ROI 2	ULX= -115.28699717,ULY= 35.98217949 URX= -115.27064853,URY= 35.98217949 LRX= -115.27064853,LRY= 35.96896368 LLX= -115.28699717,LLY= 35.96896368
Ivanpah Playa ROI 3	ULX= -115.49562325,ULY= 35.75400831 URX= -115.46362428,URY= 35.75400831 LRX= -115.46362428,LRY= 35.72709874 LLX= -115.49562325,LLY= 35.72709874
Ivanpah Playa ROI 4	ULX= -115.49200418,ULY= 35.74987544 URX= -115.45972834,URY= 35.74987544 LRX= -115.45972834,LRY= 35.72272156 LLX= -115.49200418,LLY= 35.72272156

Table A6. Landsat-4 MSS to Landsat-3 MSS cross-calibration ROI's corner-coordinates.

Locations	ROI's Latitudes and Longitudes
Sonoran Desert ROI1	ULX= -114.33151626,ULY= 32.27017809 URX= -115.24285912,URY= 32.27017809 LRX= -115.24285912,LRY= 32.24481538 LLX= -114.33151626,LLY= 32.24481538
Sonoran Desert ROI2	ULX= -114.38621177,ULY= 32.27959248 URX= -114.35579275,URY= 32.27959248 LRX= -114.35579275,LRY= 32.25244791 LLX= -114.38621177,LLY= 32.25244791
Sonoran Desert ROI3	ULX= -114.59441821,ULY= 32.40222851 URX= -114.47564530,URY= 32.40222851 LRX= -114.47564530,LRY= 32.33876515 LLX= -114.59441821,LLY= 32.33876515
Sonoran Desert ROI4	ULX= -114.53725405,ULY= 32.39354894 URX= -114.47564530,URY= 32.39354894 LRX= -114.47564530,LRY= 32.33876515 LLX= -114.53725405,LLY= 32.33876515
Sonoran Desert ROI5	ULX= -114.83920310,ULY= 32.30060698 URX= -114.77746250,URY= 32.30060698 LRX= -114.77746250,LRY= 32.24596463 LLX= -114.83920310,LLY= 32.24596463
Sonoran Desert ROI6	ULX= -114.78201922,ULY= 32.29420369 URX= -114.72095513,URY= 32.29420369 LRX= -114.72095513,LRY= 32.23954652 LLX= -114.78201922,LLY= 32.23954652
Sonoran Desert ROI7	ULX= -115.48799508,ULY= 31.74988072 URX= -115.41156302,URY= 31.74988072 LRX= -115.41156302,LRY= 31.73758462 LLX= -115.48799508,LLY= 31.73758462
Sonoran Desert ROI8	ULX= -115.38384959,ULY= 31.69231337 URX= -115.29960042,URY= 31.69231337 LRX= -115.29960042,LRY= 31.66090885 LLX= -115.38384959,LLY= 31.66090885
Sonoran Desert ROI9	ULX= -115.31828674,ULY= 31.67739353 URX= -115.29586394,URY= 31.67739353 LRX= -115.29586394,LRY= 31.65761161 LLX= -115.31828674,LLY= 31.65761161
Sonoran Desert ROI10	ULX= -115.32426664,ULY= 31.55569363 URX= -115.28383596,URY= 31.55569363 LRX= -115.28383596,LRY= 31.51997663 LLX= -115.32426664,LLY= 31.51997663
Sonoran Desert ROI11	ULX= -115.28327155,ULY= 31.55081970 URX= -115.24285912,URY= 31.55081970 LRX= -115.24285912,LRY= 31.51509034 LLX= -115.28327155,LLY= 31.51509034
	ULX= -116.16099508,ULY= 34.94737136 URX= -116.13162834,URY= 34.94737136

California ROI1	LRX= -116.13162834,LRY= 34.92822884 LLX= -116.16099508,LLY= 34.92822884
California ROI2	ULX= -116.29728091,ULY= 34.60629022 URX= -116.26153572,URY= 34.60629022 LRX= -116.26153572,LRY= 34.57848460 LLX= -116.29728091,LLY= 34.57848460
California ROI3	ULX= -117.15230714,ULY= 35.16821348 URX= -117.12064284,URY= 35.16821348 LRX= -117.12064284,LRY= 35.14227952 LLX= -117.15230714,LLY= 35.14227952
California ROI4	ULX= -116.11608664,ULY= 34.59970144 URX= -116.08300412,URY= 34.59970144 LRX= -116.08300412,LRY= 34.57348640 LLX= -116.11608664,LLY= 34.57348640
Florida ROI 1	ULX= -81.30405581,ULY= 28.30863744 URX= -81.26244104,URY= 28.30872378 LRX= -81.26236400,LRY= 28.27731046 LLX= -81.30396655,LLY= 28.27722423
Australia 112/078 , 119/078 ROI1	ULX= 118.75046695,ULY= -26.71161049 URX= 118.76866261,URY= -26.71161049 LRX= 118.76866261,LRY= -26.72323013 LLX= 118.75046695,LLY= -26.72323013
Australia 112/079 , 119/079 ROI1	ULX= 118.11074261,ULY= -28.12357492 URX= 118.12853606,URY= -28.12357492 LRX= 118.12853606,LRY = -28.13742670 LLX= 118.11074261,LLY= -28.13742670
Australia 112/079 , 119/079 ROI2	ULX= 118.72438651,ULY= -26.78659882 URX= 118.75615971,URY= -26.78659882 LRX= 118.75615971,LRY= -26.81220381 LLX= 118.72438651,LLY= -26.81220381

Table A7. Landsat-3 MSS to Landsat-2 MSS cross-calibration ROI's corner-coordinates.

Locations	**ROI's Latitudes and Longitudes**
Sonoran Desert ROI1	ULX= -114.33151626,ULY= 32.27017809 URX= -115.24285912,URY= 32.27017809 LRX= -115.24285912,LRY= 32.24481538 LLX= -114.33151626,LLY= 32.24481538
Sonoran Desert ROI2	ULX= -114.38621177,ULY= 32.27959248 URX= -114.35579275,URY= 32.27959248 LRX= -114.35579275,LRY= 32.25244791 LLX= -114.38621177,LLY= 32.25244791
Sonoran Desert ROI3	ULX= -114.59441821,ULY= 32.40222851 URX= -114.47564530,URY= 32.40222851 LRX= -114.47564530,LRY= 32.33876515 LLX= -114.59441821, LLY= 32.33876515
	ULX= -114.53725405,ULY= 32.39354894 URX= -114.47564530,URY= 32.39354894

Sonoran Desert ROI4	LRX= -114.47564530,LRY= 32.33876515 LLX= -114.53725405,LLY= 32.33876515
Sonoran Desert ROI5	ULX= -114.83920310,ULY= 32.30060698 URX= -114.77746250,URY= 32.30060698 LRX= -114.77746250,LRY= 32.24596463 LLX= -114.83920310,LLY= 32.24596463
Sonoran Desert ROI6	ULX= -114.78201922,ULY= 32.29420369 URX= -114.72095513,URY= 32.29420369 LRX= -114.72095513,LRY= 32.23954652 LLX= -114.78201922,LLY= 32.23954652
Sonoran Desert ROI7	ULX= -115.48799508,ULY= 31.74988072 URX= -115.41156302,URY= 31.74988072 LRX= -115.41156302,LRY= 31.73758462 LRX= -115.48799508,LRY= 31.73758462
Sonoran Desert ROI8	ULX= -115.38384959,ULY= 31.69231337 URX= -115.29960042,URY= 31.69231337 LRX= -115.29960042,LRY= 31.66090885 LLX= -115.38384959,LLY= 31.66090885
Sonoran Desert ROI9	ULX= -115.31828674,ULY= 31.67739353 URX= -115.29586394,URY= 31.67739353 LRX= -115.29586394,LRY= 31.65761161 LLX= -115.31828674,LLY= 31.65761161
Sonoran Desert ROI10	ULX= -115.32426664,ULY= 31.55569363 URX= -115.28383596,URY= 31.55569363 LRX= -115.28383596,LRY= 31.51997663 LLX= -115.32426664,LLY= 31.51997663
Sonoran Desert ROI11	ULX= -115.28327155,ULY= 31.55081970 URX= -115.24285912,URY= 31.55081970 LRX= -115.24285912,LRY= 31.51509034 LLX= -115.28327155,LLY= 31.51509034
Ivanpah Playa ROI1	ULX= -115.29339390,ULY= 35.98426755 URX= -115.27788308,URY= 35.98426755 LRX= -115.27788308,LRY= 35.97285395 LLX= -115.29339390,LLY= 35.97285395
Ivanpah Playa ROI2	ULX= -115.28699717,ULY= 35.98217949 URX= -115.27064853,URY= 35.98217949 LRX= -115.27064853,LRY= 35.96896368 LLX= -115.28699717,LLY= 35.96896368
Ivanpah Playa ROI3	ULX= -115.49562325,ULY= 35.75400831 URX= -115.46362428,URY= 35.75400831 LRX= -115.46362428,LRY= 35.72709874 LLX= -115.49562325,LLY= 35.72709874
Ivanpah Playa ROI4	ULX= -115.49200418,ULY= 35.74987544 URX= -115.45972834,URY= 35.74987544 LRX= -115.45972834,LRY= 35.72272156 LLX= =-115.49200418,LLY= 35.72272156
Crater Lake	ULX= -122.13615386,ULY= 42.96571952 URX= -122.07321381,URY= 42.96571952 LRX= -122.07321381,LRY= 42.92213736 LLX= -122.13615386,LLY= 42.92213736

Near to Sonoran 037/038	ULX= -113.53107847,ULY= 31.52455586 URX= -113.51567310,URY= 31.52455586 LRX= -113.51567310,LRY= 31.51314286 LLX= -113.53107847,LLY= 31.51314286
Near to Sonoran 037/038	ULX= -113.55332994,ULY= 31.64334332 URX= 113.54164196,URY= 31.64334332 LRX= -113.54164196,LRY= 31.63221359 LLX= -113.55332994,LLY= 31.63221359
Algodones Dunes ROI1	ULX= -114.96446301,ULY= 32.82108048 URX= -114.92046642,URY= 32.82108048 LRX= -114.92046642,LRY= 32.78410383 LLX= -114.96446301,LLY= 32.78410383
Algodones Dunes ROI2	ULX= -115.11058515,ULY= 32.97163663 URX= -115.06950837,URY= 32.97163663 LRX= -115.06950837, LLY= 32.94178875 LLX= -115.11058515,LLY= 32.94178875
Algodones Dunes ROI3	ULX= -115.14095794,ULY= 32.99265471 URX= -115.09176362,URY= 32.99265471 LRX= -115.09176362,LRY= 32.95132952 LLX= -115.14095794,LLY= 32.95132952
Algodones Dunes ROI4	ULX= -115.58711210,ULY= 33.70886832 URX= -115.57370621,URY= 33.70886832 LRX= -115.57370621,LRY= 33.69735117 LLX= -115.58711210,LLY= 33.69735117
Algodones Dunes ROI5	ULX= -115.73758503,ULY= 33.49107354 URX= -115.72419124,URY= 33.49107354 LRX= -115.72419124,LRY= 33.47957263 LLX= -115.73758503,LLY= 33.47957263
Kelso Desert ROI1	ULX= -115.76574461,ULY= 34.96777457 URX= -115.75033128,URY= 34.96777457 LRX= -115.75033128,LRY= 34.95804204 LLX= -115.76574461,LLY= 34.95804204
Kelso Desert ROI2	ULX= -115.86229112,ULY= 34.84498731 URX= -115.85129428,URY= 34.84498731 LRX= -115.85129428,LRY= 34.83352243 LLX= -115.86229112,LLY= 34.83352243
Railroad Valley ROI1	ULX= -115.72743540,ULY= 38.74501551 URX= -115.71198281,URY= 38.74501551 LRX= -115.71198281,LRY= 38.73366799 LLX= -115.72743540,LLY= 38.73366799
Railroad Valley ROI2	ULX= -115.86552222,ULY= 38.80230352 URX= -115.83210295,URY= 38.80230352 LRX= -115.83210295,LRY= 38.77548099 LLX= -115.86552222,LLY= 38.77548099
Railroad Valley ROI3	ULX= -115.78274095,ULY= 38.79444158 URX= -115.74935692,URY= 38.79444158 LRX= -115.74935692,LRY= 38.76759589 LLX= -115.78274095,LLY= 38.76759589
	ULX= -115.70420712,ULY= 38.82008987 URX= -115.68786164,URY= 38.82008987

Railroad Valley ROI4	LRX= -115.68786164,LRY= 38.80693133 LLX= -115.70420712,LLY= 38.80693133
Railroad Valley ROI5	ULX= -115.81829125,ULY= 38.77534213 URX= -115.78490234,URY= 38.77534213 LRX= -115.78490234,LRY= 38.74850645 LLX= -115.81829125,LLY= 38.74850645
White sands ROI1	ULX= -107.50592324,ULY= 33.32147519 URX= -107.48800664,URY= 33.32147519 LRX= -107.48800664,LRY= 33.30691260 LLX= -107.50592324,LLY= 33.30691260
White sands ROI2	ULX= -107.44677193,ULY= 33.07563873 URX= -107.42574455,URY= 33.07563873 LRX= -107.42574455,LRY= 33.05873709 LLX= -107.44677193,LLY= 33.05873709
White sands ROI3	ULX= -107.56499499,ULY= 33.31778885 URX= -107.54388509,URY= 33.31778885 LRX= -107.54388509,LRY= 33.30091163 LLX= -107.56499499,LLY= 33.30091163
White sands ROI4	ULX= -107.33061870,ULY= 33.15469183 URX= -107.52382753,URY= 33.15469183 LRX= -107.52382753, LRY= 33.13361237 LLX= -107.33061870, LLY= 33.13361237

Table A8. Landsat-2 MSS to Landsat-1 MSS cross-calibration ROI's corner-coordinates.

Locations	**ROI's Latitudes and Longitudes**
Sonoran Desert ROI1	ULX= -114.33151626,ULY= 32.27017809 URX= -115.24285912,URY= 32.27017809 LRX= -115.24285912,LRY= 32.24481538 LLX= -114.33151626, LLY= 32.24481538
Sonoran Desert ROI2	ULX= -114.38621177,ULY= 32.27959248 URX= -114.35579275,URY= 32.27959248 LRX= -114.35579275,LRY= 32.25244791 LLX= -114.38621177,LLY= 32.25244791
Sonoran Desert ROI3	ULX= -114.59441821,ULY= 32.40222851 URX= -114.47564530,URY= 32.40222851 LRX= -114.47564530,LRY= 32.33876515 LLX= -114.59441821,LLY= 32.33876515
Sonoran Desert ROI4	ULX= -114.53725405,ULY= 32.39354894 URX= -114.47564530,URY= 32.39354894 LRX= -114.47564530,LRY= 32.33876515 LLX= -114.53725405,LLY= 32.33876515
Sonoran Desert ROI5	ULX= -114.83920310,ULY= 32.30060698 URX= -114.77746250,URY= 32.30060698 LRX= -114.77746250,LRY= 32.24596463 LLX= -114.83920310,LLY= 32.24596463
Sonoran Desert ROI6	ULX= -114.78201922,ULY= 32.29420369 URX= -114.72095513,URY= 32.29420369 LRX= -114.72095513,LRY= 32.23954652

	LLX= -114.78201922,LLY= 32.23954652
Sonoran Desert ROI7	ULX= -115.48799508,ULY= 31.74988072 URX= -115.41156302,URY= 31.74988072 LRX= -115.41156302,LRY= 31.73758462 LLX= -115.48799508,LLY= 31.73758462
Sonoran Desert ROI8	ULX= -115.38384959,ULY= 31.69231337 URX= -115.29960042,URY= 31.69231337 LRX= -115.29960042,LRY= 31.66090885 LLX= -115.38384959,LLY= 31.66090885
Sonoran Desert ROI9	ULX= -115.31828674,ULY= 31.67739353 URX= -115.29586394,URY= 31.67739353 LRX= -115.29586394,LRY= 31.65761161 LLX= -115.31828674,LLY= 31.65761161
Sonoran Desert ROI10	ULX= -115.32426664,ULY= 31.55569363 URX= -115.28383596,URY= 31.55569363 LRX= -115.28383596,LRY= 31.51997663 LLX= -115.32426664,LLY= 31.51997663
Sonoran Desert ROI11	ULX= -115.28327155,ULY= 31.55081970 URX= -115.24285912,URY= 31.55081970 LRX= -115.24285912,LRY= 31.51509034 LLX= -115.28327155,LLY= 31.51509034
Crater Lake ROI 1	ULX= -122.13615386,ULY= 42.96571952 URX= -122.07321381,URY= 42.96571952 LRX= -122.07321381,LRY= 42.92213736 LLX= -122.13615386,LLY= 42.92213736
Algodones Dunes ROI1	ULX= -114.96446301,ULY= 32.82108048 URX= -114.92046642,URY= 32.82108048 LRX= -114.92046642,LRY= 32.78410383 LLX= -114.96446301,LLY= 32.78410383
Algodones Dunes ROI2	ULX= -115.11058515,ULY= 32.97163663 URX= -115.06950837,URY= 32.97163663 LRX= -115.06950837,LRY= 32.94178875 LLX= -115.11058515,LLY= 32.94178875
Algodones Dunes ROI3	ULX= -115.14095794,ULY= 32.99265471 URX= -115.09176362,URY= 32.99265471 LRX= -115.09176362,LRY= 32.95132952 LLX= -115.14095794,LLY= 32.95132952
Algodones Dunes ROI4	ULX= -115.58711210,ULY= 33.70886832 URX= -115.57370621,URY= 33.70886832 LRX= -115.57370621,LRY= 33.69735117 LLX= -115.58711210,LLY= 33.69735117
Lake Tahoe ROI1	ULX= -120.10042829,ULY= 39.15933860 URX= -120.10372711,URY= 39.15933860 LRX= -120.10372711,LRY= 39.07888180 LLX= -120.10042829,LLY= 39.07888180

Appendix B

Relative Spectral Responses between each pair of sensors

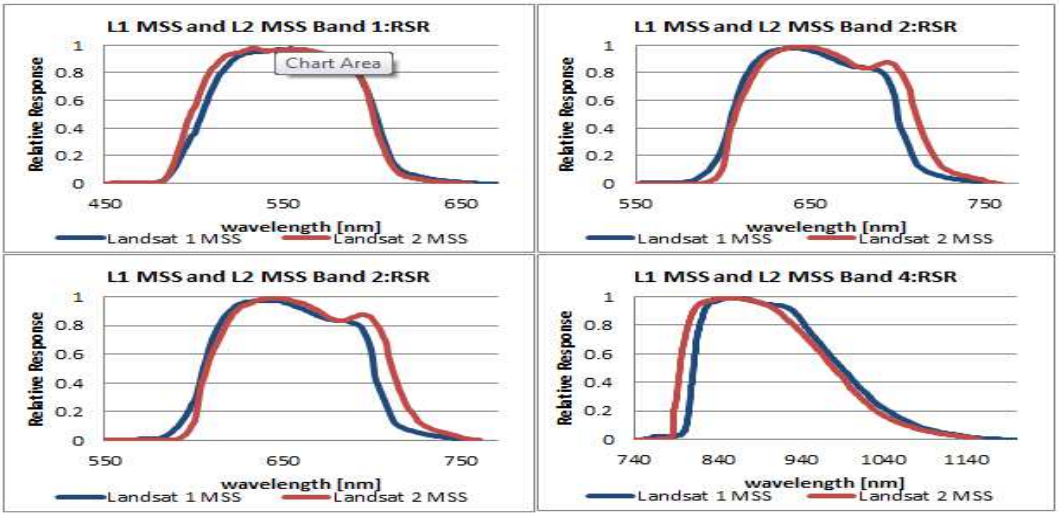

Figure A1. Relative spectral response functions of Landsat-1 MSS and Landsat-2 MSS sensor.

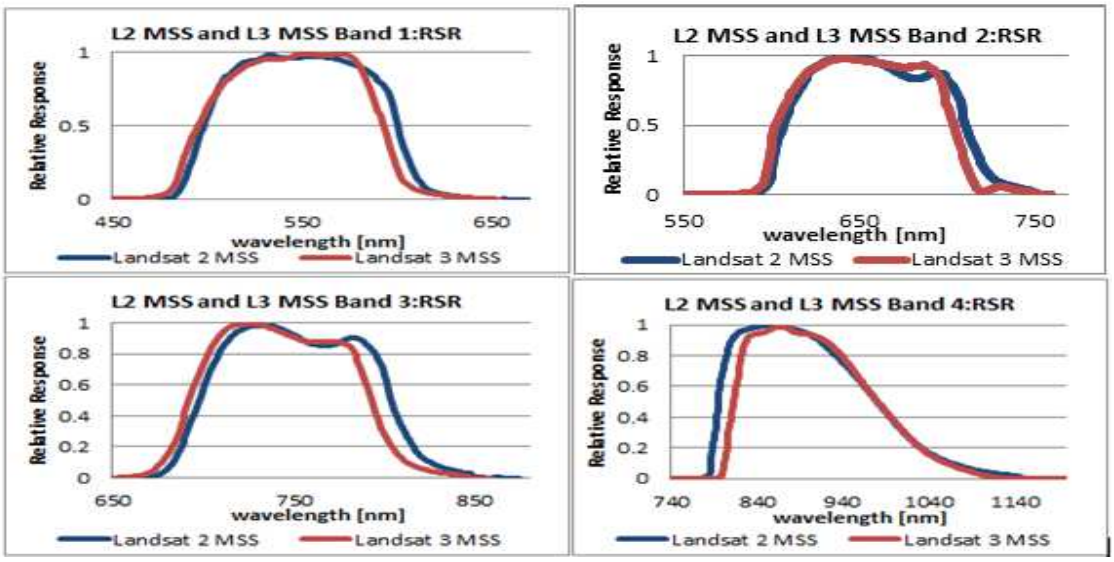

Figure A2. Relative spectral response functions of Landsat-2 MSS and Landsat-3 MSS sensor.

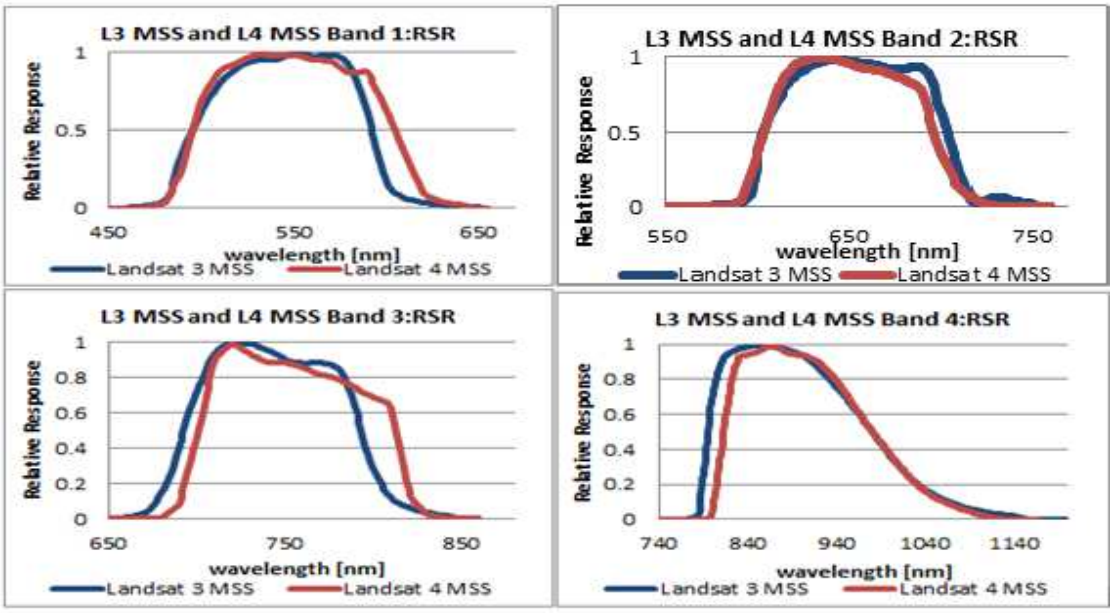

Figure A3 Relative spectral response function of Landsat-3 MSS and Landsat-4 MSS sensor.

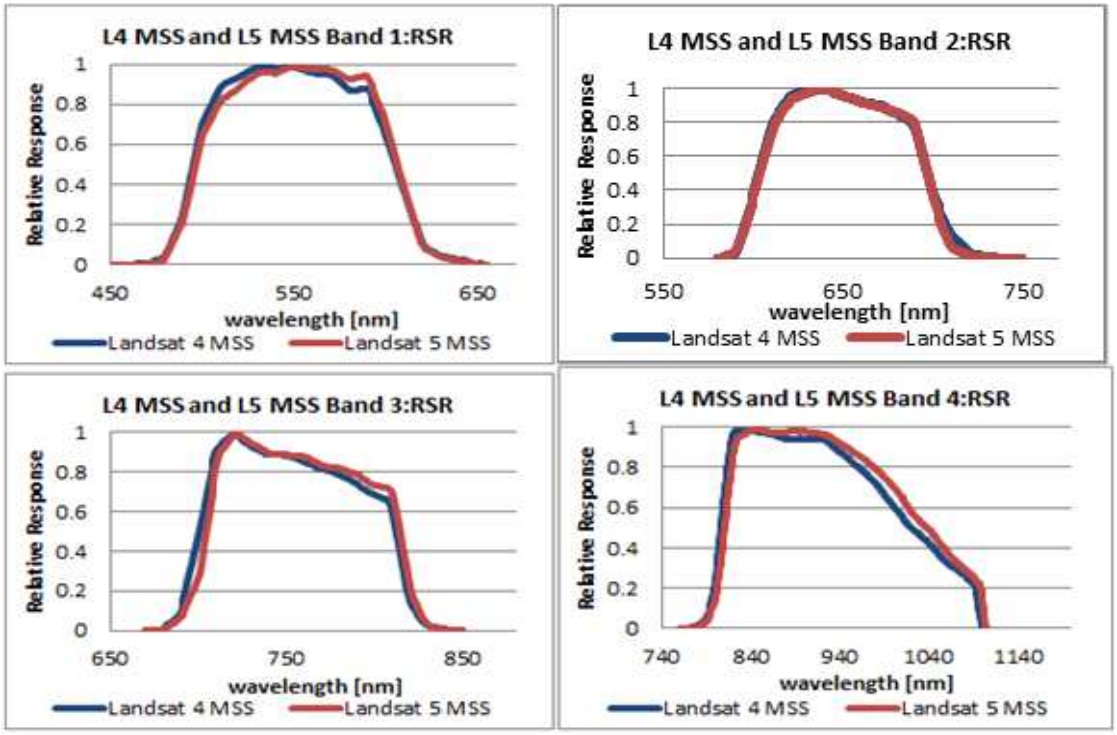

Figure A4. Relative spectral response functions of Landsat-4 MSS and Landsat-5 MSS sensor.

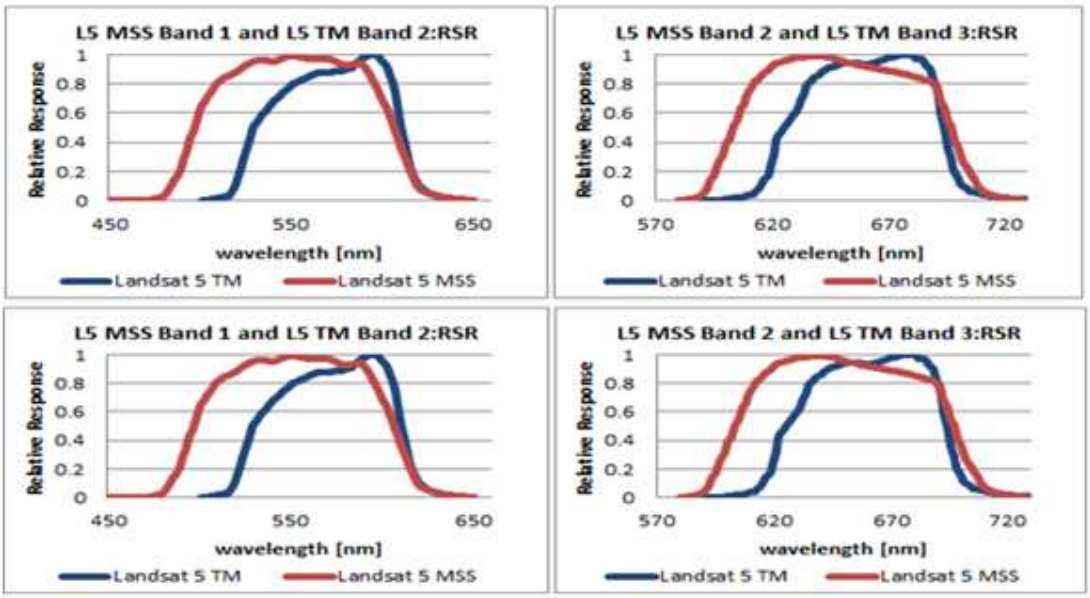

Figure A5. Relative spectral response functions of Landsat-5 TM and Landsat-5 MSS sensor.

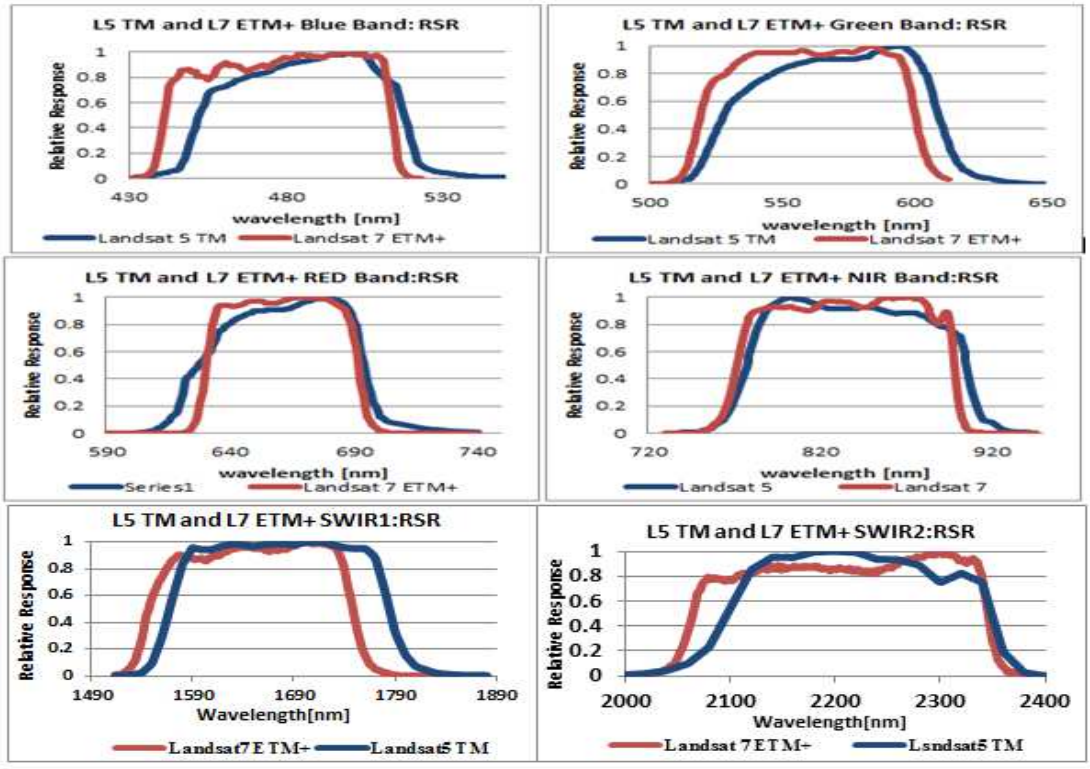

Figure A6. Relative spectral response functions of Landsat-5 TM and Landsat-7 ETM+ sensor

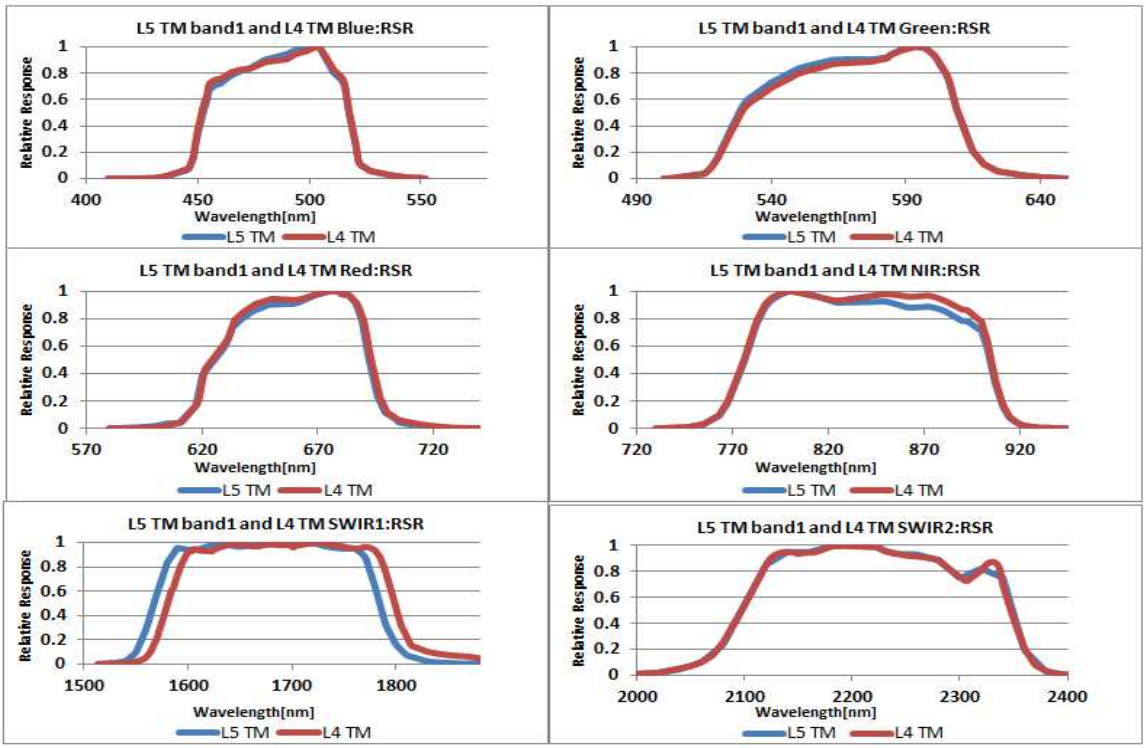

Figure A7. Relative spectral response functions of Landsat-5 TM and Landsat-4 TM sensor

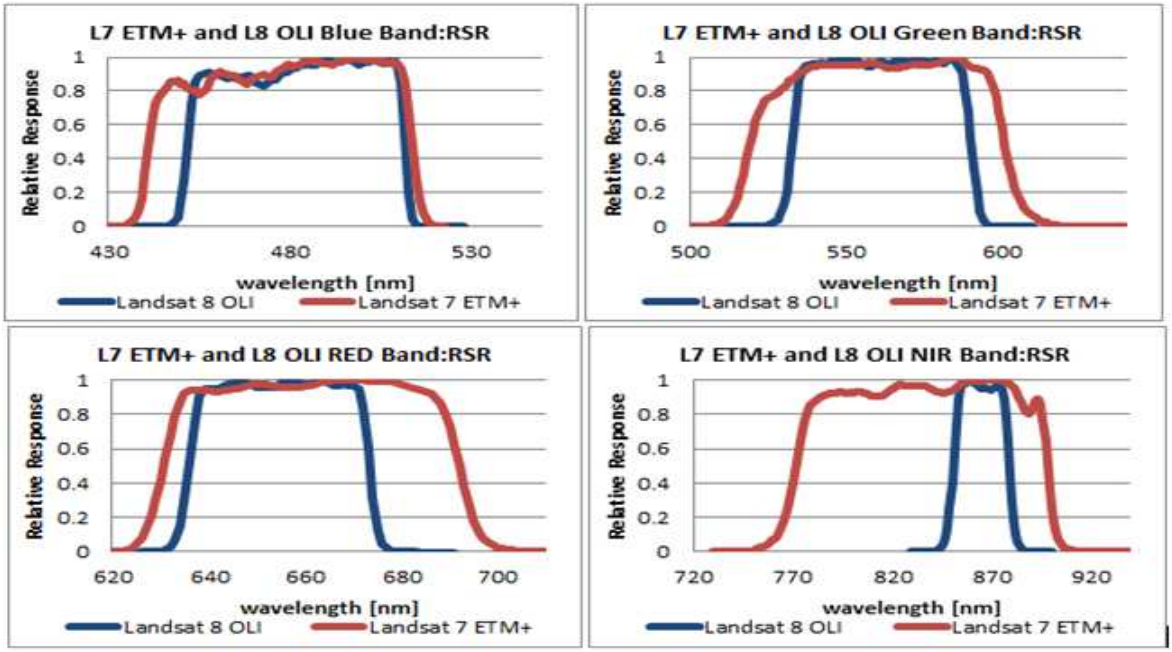

Figure A8. Relative spectral response functions of Landsat-7 ETM+ and Landsat-8 OLI sensor

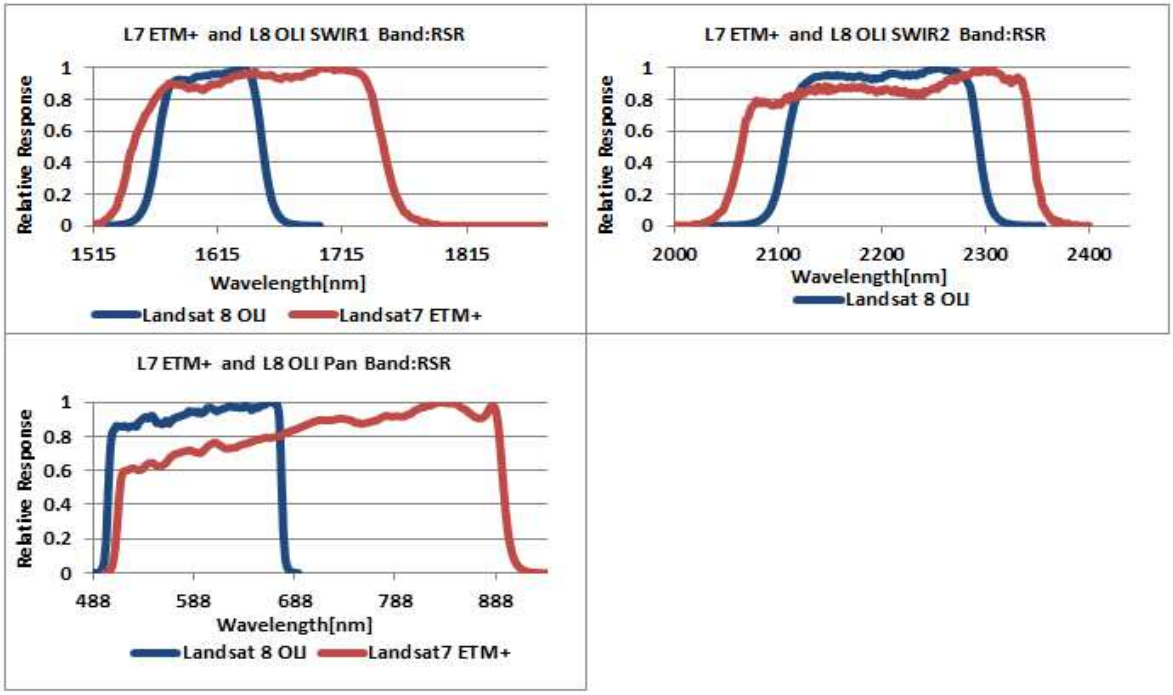

Figure A9. Relative spectral response functions of Landsat-7 ETM+ and Landsat-8 OLI sensor.

Appendix C

Spectral band adjustment factors for each pair of sensors

Table C1. SBAF from Landsat-8 OLI to Landsat-7 ETM+: Sonoran Desert.

Dates		BLUE	GREEN	RED	NIR	SWIR1	SWIR2	PAN
10/1/2012		0.990	1.005	1.010	0.916	0.985	0.945	1.254
12/24/2012		0.991	1.005	1.011	0.908	0.985	0.936	1.254
4/16/2013		0.990	1.006	1.010	0.933	0.999	0.952	1.281
	Average	0.990	1.005	1.010	0.919	0.990	0.944	1.263
	Std dev	0.001	0.001	0.001	0.013	0.008	0.008	0.016
	COV	0.06%	0.06%	0.06%	1.39%	0.82%	0.85%	1.23%

Table C2. SBAF from Landsat-8 OLI to Landsat-7 ETM+: Lake Tahoe.

Dates		BLUE	GREEN	RED	NIR	SWIR1	SWIR2	PAN
9/10/2002		1.018	1.017	0.976	1.065	0.954	1.016	0.55
11/29/2002		1.016	1.023	0.974	1.113	0.981	1.065	0.542
	Average	1.017	1.020	0.975	1.089	0.968	1.041	0.546
	Std dev	0.001	0.004	0.001	0.034	0.019	0.035	0.006
	COV	0.14%	0.42%	0.15%	3.12%	1.97%	3.33%	1.04%

Table C3. SBAF from Landsat-7 ETM+ to Landsat-5 TM: Sonoran Desert.

Dates		BLUE	GREEN	RED	NIR	SWIR1	SWIR2
10/1/2012		1.019	1.046	0.995	0.991	0.935	1.009
12/24/2012		1.017	1.041	0.994	0.989	0.933	1.013
4/16/2013		1.020	1.048	0.995	0.955	0.950	1.008
	Average	1.019	1.045	0.995	0.978	0.939	1.010
	Std dev	0.002	0.004	0.001	0.020	0.009	0.003
	COV	0.15%	0.35%	0.06%	2.07%	0.99%	0.26%

Table C4. SBAF from Landsat-7 ETM+ to Landsat-5 TM: Lake Tahoe.

Dates		BLUE	GREEN	RED	NIR	SWIR1	SWIR2
9/10/2002		0.963	0.931	1.006	0.997	0.960	1.026
11/29/2002		0.966	0.933	1.003	1.001	0.971	1.020
	Average	0.965	0.932	1.005	0.999	0.966	1.023
	Std dev	0.002	0.001	0.002	0.003	0.008	0.004
	COV	0.22%	0.15%	0.21%	0.28%	0.81%	0.41%

Table C5. SBAF from Landsat-5 TM to Landsat-4 TM: Makhtesh Ramon.

Dates		BLUE	GREEN	RED	NIR	SWIR1	SWIR2
9/15/2005		0.999	1.003	0.998	1.001	0.998	1.001

Table C6. SBAF from Landsat-5 TM to Landsat-4 TM: Ivanpah Playa.

Dates		BLUE	GREEN	RED	NIR	SWIR1	SWIR2
11/14/2001		0.999	1.001	0.999	1.001	0.999	1.001
3/22/2002		0.999	1.002	0.999	1.001	0.999	1.001
	Average	0.999	1.002	0.999	1.001	0.999	1.001
	Std dev	0.000	0.001	0.000	0.000	0.000	0.000
	COV	0.00%	0.07%	0.00%	0.00%	0.00%	0.00%

Table C7. SBAF from Landsat-5 TM to Landsat-4 TM: Arabian Deserts 162/046.

Dates		BLUE	GREEN	RED	NIR	SWIR1	SWIR2
6/27/2003		0.999	1.002	0.998	1.001	0.998	1.008
11/18/2003		0.999	1.003	0.998	1.001	0.998	1.009
	Average	0.999	1.003	0.998	1.001	0.998	1.009
	Std dev	0.000	0.001	0.000	0.000	0.000	0.001
	COV	0.00%	0.07%	0.00%	0.00%	0.00%	0.07%

Table C8. SBAF from Landsat-5 TM to Landsat-4 TM: Sonoran Deserts.

Dates		BLUE	GREEN	RED	NIR	SWIR1	SWIR2
10/1/2012		0.999	1.003	0.998	1.001	0.998	1.001
12/24/2012		0.999	1.003	0.998	1.001	0.998	1.001
4/16/2013		0.999	1.003	0.998	1.001	0.998	1.001
	Average	0.999	1.003	0.998	1.001	0.998	1.001
	Std dev	0.000	0.000	0.000	0.000	0.000	0.000
	COV	0.00%	0.00%	0.00%	0.00%	0.00%	0.00%

Table C9. SBAF from Landsat-5 TM to Landsat-4 TM: Arabian3 desert 161/045.

Dates	BLUE	GREEN	RED	NIR	SWIR1	SWIR2
8/7/2003	0.999	1.003	0.998	1.002	0.998	1.001

Table C10. SBAF from Landsat-5 TM to Landsat-4 TM: Algodones Dunes.

Dates		BLUE	GREEN	RED	NIR	SWIR1	SWIR2
1/1/2012		0.999	1.003	0.999	1.000	0.999	1.001
3/14/2012		0.999	1.002	0.998	1.000	0.999	1.001
2/12/2013		0.999	1.002	0.998	1.000	0.999	1.001
	Average	0.999	1.002	0.998	1.000	0.999	1.001
	Std dev	0.000	0.001	0.001	0.000	0.000	0.000
	COV	0.00%	0.06%	0.06%	0.00%	0.00%	0.00%

Table C11. SBAF from Landsat-5 TM to Landsat-4 TM: kelso Dunes.

Dates		BLUE	GREEN	RED	NIR	SWIR1	SWIR2
8/27/2003		0.999	1.001	0.998	1.001	0.998	1.000
10/028/2003		0.999	1.001	0.998	1.000	0.998	1.000
	Average	0.999	1.001	0.998	1.001	0.998	1.000
	Std dev	0.000	0.000	0.000	0.001	0.000	0.000
	COV	0.00%	0.00%	0.00%	0.07%	0.00%	0.00%

Table C12. SBAF from Landsat-5 TM to Landsat-4 TM: Arabian Deserts.

Dates		BLUE	GREEN	RED	NIR	SWIR1	SWIR2
9/28/2002		0.999	1.003	0.998	1.001	0.998	1.000
10/14/2002		0.999	1.003	0.997	1.001	0.998	1.000
	Average	0.999	1.003	0.998	1.001	0.998	1.000
	Std dev	0.000	0.000	0.001	0.000	0.000	0.000
	COV	0.00%	0.00%	0.07%	0.00%	0.00%	0.00%

Table C13. SBAF from Landsat-5 TM to Landsat-4 TM: Arabian Deserts 165/042.

Dates		BLUE	GREEN	RED	NIR	SWIR1	SWIR2
9/28/2002		0.999	1.003	0.998	1.001	0.998	1.000
10/14/2002		0.999	1.003	0.997	1.001	0.998	1.000
	Average	0.999	1.003	0.998	1.001	0.998	1.000
	Std dev	0.000	0.000	0.001	0.000	0.000	0.000
	COV	0.00%	0.00%	0.07%	0.00%	0.00%	0.00%

Table C14. SBAF from Landsat-5 TM to Landsat-4 TM: Rock Springs.

Dates		BLUE	GREEN	RED	NIR	SWIR1	SWIR2
7/22/2012		0.999	1.000	0.998	1.001	0.998	1.000
8/25/2012		0.999	1.000	0.998	1.000	0.998	1.000
	Average	0.999	1.000	0.998	1.001	0.998	1.000
	Std dev	0.000	0.000	0.000	0.001	0.000	0.000
	COV	0.00%	0.00%	0.00%	0.07%	0.00%	0.00%

Table C15. SBAF from Landsat-5 TM to Landsat-4 TM: Near to Sonoran.

Dates		BLUE	GREEN	RED	NIR	SWIR1	SWIR2
11/20/2005		0.999	1.000	0.997	1.002	0.997	1.000
11/27/2005		0.999	1.000	0.997	1.000	0.997	1.000
	Average	0.999	1.000	0.997	1.001	0.997	1.000
	Std dev	0.000	0.000	0.000	0.001	0.000	0.000
	COV	0.00%	0.00%	0.00%	0.14%	0.00%	0.00%

Table C16. SBAF from Landsat-5 TM to Landsat-5 MSS: Sonoran Desert.

Dates		GREEN	RED	NIR1	NIR2
10/1/2012		0.937	0.978	0.945	0.96
12/24/2012		0.933	0.978	0.946	0.994
4/16/2013		0.936	0.979	0.948	0.94
	Average	0.935	0.978	0.946	0.965
	Std dev	0.002	0.001	0.002	0.027
	COV	0.22%	0.06%	0.16%	2.83%

Table C17. SBAF from Landsat-5 TM to Landsat-5 MSS: Lake Tahoe.

Dates		GREEN	RED	NIR1	NIR2
9/10/2002		1.169	1.051	1.24	0.981
11/29/2002		1.153	1.049	1.232	0.989
	Average	1.161	1.05	1.236	0.985
	Std dev	0.011	0.001	0.006	0.006
	COV	0.95%	0.14%	0.46%	0.59%

Table C18. SBAF from Landsat-5 MSS to Landsat-4 MSS: Lake Tahoe: Sonoran Deserts.

Dates		GREEN	RED	NIR1	NIR2
10/1/2012		0.993	1.000	0.999	0.993
12/24/2012		0.994	1.000	0.999	0.994
4/16/2013		0.993	1.000	0.998	0.994
	Average	0.993	1.000	0.999	0.994
	Std dev	0.001	0.000	0.001	0.001
	COV	0.06%	0.00%	0.06%	0.06%

Table C19. SBAF from Landsat-5 MSS to Landsat-4 MSS: Lake Tahoe: Lake Tahoe.

Dates		GREEN	Red	NIR1	NIR2
9/10/2002		1.013	0.998	1.011	1.003
11/29/2002		1.013	0.997	1.016	1.01
	Average	1.013	0.998	1.014	1.007
	Std dev	0.000	0.001	0.004	0.005
	COV	0.00%	0.07%	0.35%	0.49%

Table C20. SBAF from Landsat-5 MSS to Landsat-4 MSS: Lake Tahoe: Ivanpah Playa.

Dates		GREEN	RED	NIR1	NIR2
7/9/2001		0.996	1.000	0.998	0.993
8/10/2001		0.996	1.000	0.998	0.994
9/11/2001		0.997	1.000	0.997	0.995
	Average	0.996	1.000	0.998	0.994
	Std dev	0.001	0.000	0.001	0.001
	COV	0.06%	0.00%	0.06%	0.10%

Table C21. SBAF from Landsat-5 MSS to Landsat-4 MSS: White Sands.

Dates		GREEN	RED	NIR1	NIR2
3/8/2015		0.996	1.000	0.997	0.992
4/1/2015		0.996	1.000	0.997	0.992
4/28/2015		0.996	1.001	0.995	0.992
	Average	0.996	1.000	0.996	0.992
	Std dev	0.000	0.001	0.001	0.000
	COV	0.00%	0.06%	0.12%	0.00%

Table C22. SBAF from Landsat-4 MSS to Landsat-3 MSS: Sonoran Deserts.

Dates		GREEN	RED	NIR1	NIR2
10/1/2012		0.970	1.007	0.993	0.965
12/24/2012		0.968	1.009	0.992	0.972
4/16/2013		0.970	1.006	0.997	0.959
	Average	0.969	1.007	0.994	0.965
	Std dev	0.001	0.002	0.003	0.007
	COV	0.12%	0.15%	0.27%	0.67%

Table C23. SBAF from Landsat-4 MSS to Landsat-3 MSS: Lake Tahoe.

Dates		GREEN	RED	NIR1	NIR2
9/10/2002		1.014	0.978	1.039	1.036
11/29/2002		1.031	0.979	1.025	1.025
	Average	1.023	0.979	1.032	1.031
	Std dev	0.012	0.001	0.01	0.008
	COV	1.18%	0.07%	0.96%	0.75%

Table C24. SBAF from Landsat-4 MSS to Landsat-3 MSS: California.

Dates		GREEN	RED	NIR1	NIR2
8/7/2006		0.982	1.006	0.994	0.981
8/12/2006		0.986	1.005	0.993	0.979
	Average	0.948	1.006	0.993	0.98
	Std dev	0.003	0.001	0.001	0.001
	COV	1.18%	0.07%	0.07%	0.14%

Table C25. SBAF from Landsat-4 MSS to Landsat-3 MSS: California.

Dates		GREEN	RED	NIR1	NIR2
12/26/2002		0.965	1.009	0.992	0.936
2/12/2003		0.966	1.009	0.992	0.938
1/30/2004		0.959	1.012	0.991	0.938
	Average	0.963	1.010	0.992	0.937
	Std dev	0.004	0.002	0.001	0.001
	COV	0.39%	0.17%	0.06%	0.12%

Table C26. SBAF from Landsat-3 MSS to Landsat-2 MSS: Sonoran Desert.

Dates		GREEN	RED	NIR1	NIR2
10/1/2012		1.021	1.007	1.009	1.002
12/24/2012		1.019	1.007	1.010	1.003
4/16/2013		1.023	1.010	1.010	1.001
	Average	1.021	1.008	1.010	1.002
	Std dev	0.002	0.002	0.000	0.001
	COV	0.22%	0.19%	0.04%	0.11%

Table C27. SBAF from Landsat-3 MSS to Landsat-2 MSS: Ivanpah Playa.

Dates		GREEN	RED	NIR1	NIR2
11/14/2001		1.012	1.006	1.008	1.001
3/22/2002		1.015	1.007	1.009	1.001
	Average	1.014	1.007	1.009	1.001
	Std dev	0.002	0.001	0.000	0.000
	COV	0.17%	0.05%	0.04%	0.03%

Table C28. SBAF from Landsat-3 MSS to Landsat-2 MSS: Railroad Valley.

Dates		GREEN	RED	NIR1	NIR2
9/10/2002		1.008	1.005	1.005	0.998
11/29/2002		1.008	1.004	1.004	0.998
	Average	1.008	1.005	1.005	0.998
	Std dev	0.000	0.000	0.000	0.000
	COV	0.03%	0.04%	0.05%	0.04%

Table C29. SBAF from Landsat-3 MSS to Landsat-2 MSS: Kelso Dunes.

Dates		GREEN	RED	NIR1	NIR2
8/7/2003		1.005	1.001	1.007	1.001
10/28/2003		1.008	1.004	1.01	1.002
	Average	1.006	1.002	1.009	1.002
	Std dev	0.002	0.002	0.002	0.000
	COV	0.20%	0.21%	0.18%	0.00%

Table C30. SBAF from Landsat-3 MSS to Landsat-2 MSS: Algodones Dunes.

Dates		GREEN	RED	NIR1	NIR2
1/1/2012		1.014	1.004	1.009	1.002
3/14/2012		1.017	1.008	1.010	1.001
2/12/2013		1.016	1.007	1.011	1.001
	Average	1.016	1.006	1.010	1.001
	Std dev	0.002	0.002	0.001	0.001
	COV	0.15%	0.21%	0.10%	0.01%

Table C31. SBAF from Landsat-3 MSS to Landsat-2 MSS: Lake Tahoe.

Dates		GREEN	RED	NIR1	NIR2
9/10/2002		1.028	1.019	1.015	1.010
11/29/2002		1.027	1.011	1.012	1.011
	Average	1.028	1.015	1.014	1.011
	Std dev	0.001	0.006	0.002	0.001
	COV	0.07%	0.56%	0.21%	0.01%

Table C32. SBAF from Landsat-3 MSS to Landsat-2 MSS: White deserts.

Dates		GREEN	RED	NIR1	NIR2
3/8/2015		1.015	1.013	1.013	1.003
4/1/2015		1.015	1.012	1.013	1.003
4/28/2015		1.016	1.016	1.017	1.003
	Average	1.015	1.013	1.014	1.003
	Std dev	0.002	0.002	0.002	0.000
	COV	0.15%	0.22%	0.21%	0.00%

Table C33. SBAF from Landsat-2 MSS to Landsat-1 MSS: Sonoran Deserts.

Dates		GREEN	RED	NIR1	NIR2
10/1/2012		1.012	0.988	0.997	0.999
12/24/2012		1.010	0.988	0.997	0.998
4/16/2013		1.013	0.984	0.996	0.999
	Average	1.012	0.987	0.997	0.999
	Std dev	0.002	0.002	0.001	0.001
	COV	0.15%	0.23%	0.06%	0.06%

Table C34. SBAF from Landsat-2 MSS to Landsat-1 MSS: Lake Tahoe.

Dates		GREEN	RED	NIR1	NIR2
9/10/2002		0.975	1.041	1.010	0.998
11/29/2002		0.976	1.04	1.014	1.000
	Average	0.976	1.041	1.012	0.999
	Std dev	0.001	0.001	0.003	0.001
	COV	0.07%	0.07%	0.28%	0.14%

Table C35. SBAF from Landsat-2 MSS to Landsat-1 MSS: Algodones Dunes.

Dates		GREEN	RED	NIR1	NIR2
1/1/2012		1.008	0.992	0.998	0.999
3/14/2012		1.010	0.988	0.997	0.999
2/12/2013		1.009	0.986	0.993	0.997
	Average	1.009	0.989	0.996	0.998
	Std dev	0.001	0.003	0.002	0.001
	COV	0.085%	0.299%	0.230%	0.092%

Table C36. SBAF from Landsat-2 MSS to Landsat-1 MSS: White Deserts.

Dates		GREEN	RED	NIR1	NIR2
1/1/2012		1.008	0.992	0.998	0.999
3/14/2012		1.01	0.988	0.997	0.999
2/12/2013		1.008	0.986	0.995	0.999
	Average	0.976	0.989	0.997	0.999
	Std dev	0.001	0.003	0.003	0.000
	COV	0.10%	0.31%	0.14%	0.00%